

**COMPUTATIONAL STUDY OF
WIND FLOW AND POLLUTANT
DISPERSION NEAR TREE
CANOPIES**

Salim Mohamed Salim, BEng, AMIMechE

**Thesis submitted to the University of Nottingham
for the degree of Doctor of Philosophy**

June 2011

ABSTRACT

Air quality in urban and industrial complexes is of great importance owing to the many implications on human and environmental health. Air pollution in built-up areas is typically associated with traffic exhaust emissions. High pedestrian level concentrations are the result of a non trivial combination of pollutant sources, climate and city morphological configurations. The increase of urbanisation puts a strain on city resources, resulting in increased use of transport and a denser and more compact urban fabric. The consequence of such a change in city morphology exacerbates current human air pollution exposure.

There have been several Computational Fluid Dynamics (CFD) studies on air pollution problems in urban areas, which have largely centred on employing the conventional Reynolds-Averaged Navier-Stokes (RANS) approach, and in all of these investigations, the RANS models have been reported to numerically overpredict pollutant concentration levels when compared to wind tunnel (WT) measurements.

In addition, the majority of previous investigations have failed to account for the aerodynamic effects of trees, which can occupy a significant portion of typical urban street canyons. The presence of trees aggravates the pollutant concentration at pedestrian level by altering the air circulation and ventilation. Trees act as obstacles to the airflow, reducing wind velocity within street canyons and restricting air exchange with the above-roof flow. As a result fewer pollutants are dispersed out of the canyon.

To address shortcomings of previous numerical investigations, the work undertaken in this project has two main objectives. The study first aims to implement Large Eddy Simulation (LES) to improve the flow and concentration predictions, and second to demonstrate the aerodynamic impacts of trees.

A wall y^+ approach is used to determine the computational grid configuration and corresponding RANS turbulence model. The approach is evaluated in the present numerical study and is found to be exceptionally useful in resolving flow structures near shear zones, particularly in tree-lined canyons. This allows for the appropriate mesh resolution to be selected, when taking into account a compromise between prediction accuracy and computational cost.

In part one of the project, the prediction accuracy of the pollutant dispersion within tree-free urban street canyons of width to height ratios $W/H = 1$ and $W/H=2$, are examined using two steady-state RANS turbulence closure models - the standard $k-\varepsilon$ and Reynolds Stress Model (RSM) and LES coupled with the advection-diffusion method for species transport. The numerical results, which include the statistical properties of pollutant dispersion, e.g. the mean concentration distributions, the time-evolution and three-dimensional spreads of the pollutant, are then compared to WT measurements available from the online database (CODASC, 2008) www.codasc.de. The accuracy and computational cost of both numerical approaches are compared.

The time-evolution of the pollutant concentration (for LES only) and the mean values are presented. It is observed that amongst the two RANS models, RSM performs better than standard $k-\varepsilon$ except at the centreline of the canyon walls. However, LES, although more computationally expensive, does better than RANS.

A supplementary investigation is performed to illustrate that unsteady RANS (URANS) is not a suitable replacement for LES when wishing to resolve the internally induced fluctuations of flow and concentration fields. URANS fails to capture the transient mixing process.

Part two of the research extends the study from the tree-free street canyons by investigating the aerodynamic influence of tree plantings. Configurations of $W/H=1$ with single row of trees and $W/H=2$ with two rows of trees are simulated. In both cases, two tree crown porosities are studied, one for a loosely ($P_{vol} = 97.5\%$) and another for a densely ($P_{vol} = 96\%$) packed tree

crown, corresponding to pressure loss coefficients $\lambda = 80 \text{ m}^{-1}$ and $\lambda = 200 \text{ m}^{-1}$, respectively.

Results of the tree-lined cases are then compared to the tree-free street canyons from the previous investigation. It is observed that the presence of trees reduces the in-canyon circulation and air exchange, thus increasing the overall concentration levels. Similar to the tree-free cases, LES performs better than RANS.

In addition, it is shown that a wider street $W/H = 2$ with two rows of trees promotes better air ventilation and circulation with lower pollutant accumulation at pedestrian level, as opposed to a narrow street $W/H = 1$ with one row of trees. This is also true for tree-free cases.

PUBLISHED WORK

Journal Publication

S.M. Salim, S.C. Cheah (2009), Wall y^+ Strategy for Dealing with Wall-bounded Turbulent Flows, *Lecture Notes in Engineering and Computer Science*, Volume 2175 (1), pp. 2165-2170.

S.M. Salim, M. Ariff, S.C. Cheah (2010), Wall y^+ Approach for Dealing with Turbulent Flows over a Wall Mounted Cube, *Progress in Computational Fluid Dynamics*, Volume 10 (5-6), pp. 341-351.

C.Y. Lee, S.M. Salim, A. Chan, S.C. Cheah (2010), CFD Study of Flow over Parallel Ridges with Varying Height and Spacing, *Lecture Notes in Engineering and Computer Science*, Volume 2184 (1), pp. 1206-1211.

S.M. Salim, R. Buccolieri, A. Chan, S. Di Sabatino (2011), Numerical Simulation of Atmospheric Pollutant Dispersion in an Urban Street Canyon: Comparison between RANS and LES, *Journal of Wind Engineering and Industrial Aerodynamics*, Volume 99 (2-3), pp. 103-113.

S.M. Salim, R. Buccolieri, A. Chan, S. Di Sabatino, S.C. Cheah (2011), Large Eddy Simulation of the Aerodynamic Effects of Trees on Pollutant Concentration in Street Canyons, *Procedia Environmental Sciences*. (In Press)

R. Buccolieri, S.M. Salim, L. S. Leo, S. Di Sabatino, A. Chan, G. L. Gennaro, C. Gromke (2011), Analysis of Local Scale Tree-Atmosphere Interaction on Pollutant Concentration in Idealized Street Canyons and Application to a Real Urban Junction, *Atmospheric Environment*, Volume 45 (9), pp. 1702-1713.

S.M. Salim, A. Chan, S.C. Cheah, Numerical Simulation of Atmospheric Pollutant Dispersion in Tree-lined Street Canyons: Comparison

between RANS and LES, *Journal of Building and Environment*,
doi:10.1016/j.buildenv.2011.01.032.

Conference Proceedings

S.M. Salim, S.C. Cheah (2009), Wall y^+ Strategy for Dealing with Wall-bounded Turbulent Flows, *Proceedings of the International MultiConference of Engineers and Computer Scientists*, IMECS 2009, Hong Kong, March 2009.

M. Al-Sammarraee, A. Chan, S.M. Salim, P.L. Lau, Large-Eddy Simulations of Sedimentation Process and Particle Dynamics in a Longitudinal Sedimentation Basin of a Water Treatment Plant, *The 2009 Joint ASCE-ASME-SES Conference on Mechanics and Materials*, Blacksburg, VA, USA, June 2009.

S.M. Salim, R. Buccolieri, A. Chan, S. Di Sabatino, C. Gromke, Urban Air Quality Management: Effect of Trees on Air Pollution Concentrations in Urban Street Canyons, *Proceedings of the Universitas 21 International Graduate Research Conference: Sustainable Cities for the Future*, University of Melbourne & University of Queensland, Australia, Dec 2009.

M. Ariff, S.M. Salim, S.C. Cheah, Wall y^+ Approach for Dealing with Turbulent Flow over a Surface Mounted Cube: Part 1- Low Reynolds Number, *Seventh International Conference on CFD in the Mineral and Process Industries*, CSIRO, Melbourne, Australia, Dec 2009.

M. Ariff, S.M. Salim, S.C. Cheah, Wall y^+ Approach for Dealing with Turbulent Flow over a Surface Mounted Cube: Part 2- High Reynolds Number, *Seventh International Conference on CFD in the Mineral and Process Industries*, CSIRO, Melbourne, Australia, Dec 2009.

R. Buccolieri, S.M. Salim, S. Di Sabatino, A. Chan, P. Ielpo, G. de Gennaro, C.M. Placentino, M. Caselli, C. Gromke, Study of tree-atmosphere interaction and assessment of air quality in real city neighbourhoods,

13th International Conference on Harmonization within Atmospheric Dispersion Modelling for Regulatory Purposes, Paris, June 2010.

S.M. Salim, A. Chan, R. Buccolieri, S. Di Sabatino S.C. Cheah, Large eddy simulation of the aerodynamic effects of trees on pollutant concentration in street canyons, *Urban Environmental Pollution*, Boston, USA, June 2010.

C.Y. Lee, S.M. Salim, A. Chan, S.C. Cheah (2010), CFD Study of Flow over Parallel Ridges with Varying Height and Spacing, *Proceedings of the World Congress on Engineering*, WCE 2010, London, UK, June – July 2010.

Book Chapter

S.M. Salim, A. Chan, R. Buccolieri, S. Di Sabatino, Numerical Simulation of Atmospheric Pollutant Dispersion in Urban Street Canyons and the Aerodynamic Effects of Trees, *CFD Applications in Energy and Environmental Sectors* by the International Energy and Environmental Foundation. (In Press)

ACKNOWLEDGEMENT

The author wishes to thank God Almighty for the strength, wisdom, knowledge, health and opportunity bestowed upon him. The author expresses his deepest gratitude to Prof. Andy Chan and Dr. Cheah Siew Cheong for their guidance and invaluable advice and to Dr. Silvana Di Sabatino and Dr. Riccardo Buccolieri for their collaboration and support during his research visit in Italy. All their interest for this work has been a constant source of motivation.

The author is also indebted to his family, particularly Mum and Dad; and friends for their support, encouragement and unwavering patience.

Lastly, the author would like to thank the University of Nottingham for the PhD Scholarship, the Graduate School for the Universitas21 and Building Experience and Skills Travel (BEST) Scholarships, and the Institution of Mechanical Engineer UK (IMechE) for the Environmental Issues Award.

NOMENCLATURE

Italicised Alphabets

C	measured concentration
C^+	normalised concentration
C_s	Smagorinsky constant
D	molecular diffusion coefficient
D_t	turbulent diffusivity
f_i	body forces [tensor form]
h	enthalpy (J)
H	building height (m)
I	turbulence intensity (%)
J	mass diffusion
k	kinetic energy (m^2s^{-2})
L	length of building in span-wise direction (m)
L_s	mixing length
p	pressure (Pa)
p_{stat}	static pressure (Pa)
\bar{p}	mean component of pressure (Pa)
p'	fluctuating component of pressure (Pa)
P_{vol}	pore volume (%)
Q	emission rate (gs^{-1})
Re	Reynolds number
Re_H	Reynolds number based on cube height
t	time (s)
t_c	turnover time of primary circulation (s)
T	temperature (K)
T_f	flow-through time
T_b	bulk turnover time (s)
S_{ij}	rate-of-strain tensor (s^{-1})
Sc_t	turbulent Schmidt number
u_i	velocity [tensor form](ms^{-1})

\bar{u}_i	mean component of velocity [tensor form](ms^{-1})
u_i'	fluctuating component of velocity [tensor form](ms^{-1})
u_*	friction velocity (ms^{-1})
u_H	flow velocity at building height (ms^{-1})
U_c	velocity scale of mean wind in the canyon (ms^{-1})
U_b	bulk velocity (ms^{-1})
W	street canyon width (m)
w^+	normalised vertical velocity
x	stream-wise distance (m)
x_i	distance [tensor form] (m)
y	vertical distance (m)
y^+	wall dimensionless unit
Y	mass fraction
z	span-wise distance (m)

Greek Letters

δ	boundary layer thickness (m)
ε	dissipation rate of turbulent kinetic energy (m^2s^{-3})
Φ_{ij}	pressure strain (Pa)
ρ	air density (kgm^{-3})
τ_{ij}	Reynolds Stress tensor (Pa)
τ_w	wall shear stress (Pa)
κ	von Kármán constant (0.4)
ν	kinematic viscosity (m^2s^{-1})
μ	dynamic viscosity ($\text{kgm}^{-1}\text{s}^{-1}$)
μ_t	dynamic turbulent viscosity ($\text{kgm}^{-1}\text{s}^{-1}$)
ω	specific dissipation rate ($=\varepsilon/k$) (s^{-1})
ν	turbulent velocity scale (ms^{-1})
ν_τ	kinematic turbulent viscosity (m^2s^{-1})
λ	pressure loss coefficient (m^{-1})
Δt	time-step size

Common Abbreviations

CFD	Computational Fluid Dynamics
DES	Detached Eddy Simulation
DNS	Direct Numerical Simulation
LES	Large Eddy Simulation
RANS	Reynolds-averaged Navier-Stokes
RSM	Reynolds Stress Model
SGS	Sub-grid scale
SWF	Standard Wall Function
UDF	User Defined Function
URANS	Unsteady Reynolds-averaged Navier-Stokes
WT	Wind tunnel
2D	Two Dimensional
3D	Three Dimensional

TABLE OF CONTENTS

ABSTRACT	i
PUBLISHED WORK	iv
Journal Publication	iv
Conference Proceedings	v
Book Chapter	vi
ACKNOWLEDGEMENT	vii
NOMENCLATURE	viii
Italicised Alphabets	viii
Greek Letters	ix
Common Abbreviations.....	x
TABLE OF FIGURES.....	xiv
1 INTRODUCTION	1
1.1 Background to the Problem.....	1
1.2 Scope of Present Study	2
1.2.1 Literature Review	2
1.2.2 Problem Specification.....	6
1.2.3 Research Objectives.....	8
1.2.4 Significance of Research	9
1.3 Research Outline	11
1.4 Report Organization.....	12
2 STUDYING TURBULENCE THROUGH COMPUTATIONAL FLUID DYNAMICS	15
2.1 Turbulence	15
2.1.1 Turbulence Modelling	16
2.2 Numerical Methods.....	22

2.2.1	Reynolds-averaged Navier-Stokes.....	22
2.2.2	Large Eddy Simulation.....	24
2.3	Summary.....	27
3	WALL y^+ APPROACH.....	28
3.1	Motivation for the Wall y^+ Approach.....	28
3.2	Near-wall Treatment.....	30
3.3	The Wall y^+ Approach.....	32
3.3.1	Low Reynolds Number.....	33
3.3.2	High Reynolds Number.....	33
3.4	Example on Reynolds number $Re_H = 40,000$	34
3.4.1	Model Description.....	34
3.4.2	Results.....	36
3.5	Conclusion.....	42
4	WIND TUNNEL EXPERIMENT.....	43
4.1	Experimental Setup.....	43
4.2	Experimental Tree Crown Modelling.....	48
5	SIMULATION SETUP.....	50
5.1	Computational Domain and Boundary Conditions.....	50
5.1.1	Geometry and Mesh Setup.....	50
5.1.2	Inlet Boundary Condition.....	54
5.1.3	Wall Roughness.....	57
5.2	Flow Simulation.....	61
5.3	Dispersion Modelling.....	63
5.4	Tree Crown Modelling.....	64
6	TREE-FREE STREET CANYONS.....	67
6.1	Comparison between LES and RANS.....	67
6.2	$W/H = 1$ vs. $W/H = 2$	73

6.3	Instantaneous Solution	76
6.4	LES vs. URANS	79
6.5	Conclusion	82
7	TREE-LINED STREET CANYONS	83
7.1	Comparison between LES and RANS	83
7.2	$W/H = 1$ (single row of trees) vs. $W/H = 2$ (two rows of trees)	89
7.3	Instantaneous Solution	92
7.4	Effect of Trees (Tree-free vs. Tree-lined)	92
7.5	Conclusion	98
8	CONCLUSIONS	99
8.1	Numerical Approach	99
8.2	Wall y^+ Approach	100
8.3	Wall Roughness	101
8.4	Aerodynamic Effects of Trees	101
8.5	Influence of Tree Crown Porosity	102
8.6	Street Canyon Aspect Ratio	102
8.7	Direction of Future Research	103
	REFERENCES	105
	APPENDICES	115
	APPENDIX A – CODASC Database	115
	APPENDIX B – Mesh Configuration	116
	APPENDIX C – Mesh Independence Study	118
	APPENDIX D – User Defined Function for Inlet Profiles	121
	APPENDIX E – In-Canyon Velocity Vectors relationship to Velocity Contours	123

TABLE OF FIGURES

Figure 2.1 Structure of turbulence	15
Figure 2.2 The energy cascade of turbulence	17
Figure 2.3 (a) Time history of velocity in a turbulent flow (b) Fluctuating component (c) Square of the fluctuating component. Dashed lines represent the time averages (Bhaskaran and Collins, 2002)	18
Figure 2.4 Spatial-filtering in Large Eddy Simulation (LES)	21
Figure 2.5 Prediction methods in CFD (FLUENT, 2005b)	27
Figure 3.1 Near-wall region (FLUENT, 2005a)	30
Figure 3.2 The sub-divisions of the near-wall region (FLUENT, 2005a)	31
Figure 3.3 Near-wall treatments in FLUENT (FLUENT, 2005a)	32
Figure 3.4 Computational geometry of studied case replicating experimental investigation of Martinuzzi and Tropea (1993)	34
Figure 3.5 Computational grid (Mesh 1)	35
Figure 3.6 Computational grid (Mesh 2)	35
Figure 3.7 Computational grid (Mesh 3)	36
Figure 3.8 Wall y^+ of the considered meshes	36
Figure 3.9 Comparison of mean streamwise velocity profiles in the symmetry line $x/H = 0.5$ using Standard $k-\varepsilon$	38
Figure 3.10 Comparison of mean streamwise velocity profiles in the symmetry line $x/H = 0.5$ using RSM	38

Figure 3.11 Comparison of the mean streamwise velocity profiles of Mesh 3 in the symmetry line (a) $x/H = -1.0$, (b) $x/H = 0.5$ (c) $x/H = 1.0$, (d) $x/H = 1.5$, (e) $x/H = 2.5$ and (f) $x/H = 4.0$. Legends are the same in all plots.....	39
Figure 3.12 Comparison of streamlines in symmetry plane $z/H = 0$ (left) and first cell from bottom wall (right).....	41
Figure 4.1 Schematic of wind tunnel experimental setup showing the fetch and test sections (CODASC, 2008).....	45
Figure 4.2 Real-life street canyons with single row of trees (left) and double row of trees (right).....	46
Figure 4.3 The wind tunnel experimental setup with a) $W/H = 1$ for tree-free street canyon, b) $W/H = 2$ for tree-free street canyon, c) $W/H = 1$ with single row of trees and d) $W/H = 2$ with two rows of trees (CODASC, 2008).....	47
Figure 4.4 Close-up of wind tunnel tree crown model (for $W/H = 1$) (CODASC, 2008).....	48
Figure 5.1 Computational domain and boundary conditions for the CFD simulation setup.....	51
Figure 5.2 Wall y^+ for the generated meshes (shown for Mesh B).....	53
Figure 5.3 Velocity and turbulent kinetic energy (TKE) profiles for the inlet boundary condition comparing UDF and experimental profiles.....	55
Figure 5.4 Velocity vectors coloured by magnitude.....	55
Figure 5.5 Contours of turbulent kinetic energy, k	56
Figure 5.6 Contours of turbulent dissipation rate, ε	56
Figure 5.7 Horizontal homogeneity between a smooth and rough wall performed using RSM. Legends are same in both graphs.....	59

Figure 5.8 Comparison of pollutant prediction at Wall A (leeward) and Wall B (windward) between a smooth and rough wall for the RANS simulations against WT data	60
Figure 5.9 Positions of line source and tree planting shown for the WT experiment (CODASC, 2008) and present computational domain for $W/H = 1$	66
Figure 5.10 Positions of line source and tree planting shown for the WT experiment (CODASC, 2008) and present computational domain for $W/H = 2$	66
Figure 6.1 Mean normalised concentration data on Wall A (leeward) and Wall B (windward) showing comparison between a) WT data (CODASC, 2008) and numerical results performed with b) standard $k-\varepsilon$, c) RSM and d) LES ($W/H = 1$).....	68
Figure 6.2 Mean normalised concentration data on Wall A (leeward) and Wall B (windward) showing comparison between WT data (CODASC, 2008) and numerical results performed with standard $k-\varepsilon$, RSM and LES ($W/H = 2$)	69
Figure 6.3 Mean concentration profiles at three different locations on a) Wall A (leeward) and b) Wall B (windward) to compare the different numerical results to experimental data ($W/H = 1$). Legends and axis title are the same for all graphs.....	70
Figure 6.4 Mean concentration profiles at three different locations on a) Wall A (leeward) and b) Wall B (windward) to compare the different numerical results to experimental data ($W/H = 2$).....	71
Figure 6.5 a) Mean normalised vertical velocity contours, w^+ and b) corresponding mean normalised concentration contours, C^+ at the mid plane of the street canyon (that is $y/H = 0$ for $x/H = 9$ to 10) comparing standard $k-\varepsilon$, RSM and LES ($W/H = 1$).....	74
Figure 6.6 a) Mean normalised vertical velocity contours, w^+ and b) corresponding mean normalised concentration contours, C^+ at the mid plane of	

the street canyon (that is $y/H = 0$ for $x/H = 9$ to 11) comparing standard $k-\varepsilon$, RSM and LES ($W/H = 2$).....	75
Figure 6.7 Instantaneous normalised concentration data on Wall A (leeward) and Wall B (windward) for different time instances obtained by LES compared to mean data from WT and LES ($W/H = 1$).....	77
Figure 6.8 a) Instantaneous normalised vertical velocity contours, w^+ and b) corresponding instantaneous normalised concentration contours, C^+ at mid plane of the canyon (that is $y/H=0$ from $x/H=9$ to 10) obtained using LES showing the time-evolution ($t = 10, 20, 30$ and 40 s) and mean results ($W/H = 1$).....	78
Figure 6.9 URANS against LES for unsteady simulations at $t = 10, 20$ and 30 s showing the mid-plane normalised vertical velocities, w^+ (a and c) and corresponding normalised concentrations, C^+ (b and d) ($W/H = 1$)	80
Figure 6.10 URANS against LES for unsteady simulation at $t = 10, 20$ and 30 s showing the wall concentration levels at Wall A (leeward) and Wall B (windward) against WT data (CODASC, 2008) ($W/H = 1$)	81
Figure 7.1 Mean concentration data on Wall A (leeward) and Wall B (windward) comparing between WT (CODASC, 2008) and numerical results performed with standard $k-\varepsilon$, RSM and LES for tree crowns with porosity $\lambda = 80 \text{ m}^{-1}$ and $\lambda = 200 \text{ m}^{-1}$ ($W/H = 1$)	84
Figure 7.2 Mean concentration data on Wall A (leeward) and Wall B (windward) comparing between WT (CODASC, 2008) and numerical results performed with standard $k-\varepsilon$, RSM and LES for tree crowns with porosity $\lambda = 80 \text{ m}^{-1}$ and $\lambda = 200 \text{ m}^{-1}$ ($W/H = 2$)	85
Figure 7.3 Mean concentration profiles at three different locations on a) Wall A (leeward) and b) Wall B (windward) comparing numerical results against WT data for tree crowns with porosity $\lambda = 80 \text{ m}^{-1}$ and $\lambda = 200 \text{ m}^{-1}$ ($W/H = 1$)	87

Figure 7.4 Mean concentration profiles at three different locations on a) Wall A (leeward) and b) Wall B (windward) comparing the numerical results against WT data for tree crowns with porosity $\lambda = 200 \text{ m}^{-1}$ ($W/H = 2$)88

Figure 7.5 a) Mean normalised vertical velocity contours, w^+ and b) corresponding mean normalised concentration contours, C^+ at the mid plane of the street canyon ($y/H = 0$ for $x/H = 9$ to 10) comparing standard $k-\varepsilon$, RSM and LES for tree crown with porosity $\lambda = 80 \text{ m}^{-1}$ and $\lambda = 200 \text{ m}^{-1}$ ($W/H = 1$)90

Figure 7.6 a) Mean normalised vertical velocity contours, w^+ and b) corresponding mean normalised concentration contours, C^+ at the mid plane of the street canyon ($y/H = 0$ for $x/H = 9$ to 11), comparing standard $k-\varepsilon$, RSM and LES for tree crown with porosity $\lambda = 200 \text{ m}^{-1}$ ($W/H = 2$).....91

Figure 7.7 Instantaneous normalised concentration data on Wall A (leeward) and Wall B (windward) for different time instances obtained by LES compared against mean data from WT and LES, for tree crown with porosity $\lambda = 200 \text{ m}^{-1}$ ($W/H = 1$)93

Figure 7.8 a) Instantaneous normalised vertical velocity contours, w^+ and b) corresponding instantaneous normalised concentration contours, C^+ at mid plane of the canyon ($y/H = 0$ from $x/H = 9$ to 10) obtained using LES showing the time-evolution ($t = 10, 20, 30$ and 40 s) and the mean results for tree crown with porosity $\lambda = 200 \text{ m}^{-1}$ ($W/H = 1$)94

Figure 7.9 Mean normalised concentration data on Wall A (leeward) and Wall B (windward) comparing tree-free to tree-lined canyons, for WT and LES time-averaged results ($W/H = 1$).....96

Figure 7.10 Mean normalised vertical velocity contours, w^+ and b) corresponding mean normalised concentration contours, C^+ at mid plane of the canyon ($y/H = 0$ from $x/H = 9$ to 10) obtained using LES comparing tree-free to tree-lined canyons ($W/H = 1$)97

1 INTRODUCTION

1.1 Background to the Problem

Atmospheric boundary-layer flows and their interactions with obstacles, particularly in relation to urban air quality, have been widely researched by academics, and government establishments alike due to their importance in many aspects of meteorology, wind engineering and environmental science. Health risks associated with exposure to traffic exhaust emissions in built-up areas have resulted in increased research to enable regulators and urban planners to mitigate air pollution problems. Similarly, emergency authorities require operational modelling tools that would assist in developing evacuation plans following accidental or deliberate release of hazardous airborne matter.

The flow patterns that develop around individual buildings govern the flow distribution and pollutant dispersion about single buildings. The superposition and interaction of flow patterns associated with adjacent buildings govern the final distribution of façade pressures and the movement of pollutants in urban and industrial complexes (Chang, 2006). This then raises the question to what extent would the presence of trees, which can occupy a significant portion of the urban street canyons, further impact the flow pattern.

Most cities sustainable initiative to solving the problem of urban air pollution is based on increasing the amount of greenery, with roadside tree plantings taking the lead, and it is widely championed that vegetation have socio-economic, environmental and aesthetic benefits (Price, 2003).

According to Coder (1996), trees contribute to remove air pollutants, release oxygen, offset the communities carbon footprint, reduce storm water runoff, save energy, provide wildlife habitats, manage the micro-climate and strengthen the sense of community within a given region.

On the other hand, it has been discovered that the planting of trees, especially in dense built-up areas, may amplify pollutant concentration levels at street level due to the trapping of traffic emissions when compared to their tree-free counterparts. This is attributed to less ventilation, reduced dispersion and dilution, and increased blockage on already restricted air circulation and ventilation within urban canyons (Gromke and Ruck, 2007).

A better understanding is required of what role and to what degree trees play in changing the quality of urban life, before promoting tree planting as a green strategy. Although many metropoli have extensive plans on tree planting, there is little information available of what and how trees should be planted, especially in relation to air quality improvement, aside from city beautification. Apart from a few studies, there have not been too many scientific literatures addressing the role of trees in reducing air pollution in urban and industrial complexes.

At the micro-scale, the Computational Fluid Dynamics (CFD) technique is the preferred way of investigation (Britter and Hanna, 2003, Britter and Schatzmann, 2007). CFD is also favoured against the traditional experimental investigations due to the huge savings in cost and time, and the richness of detail that can be obtained by CFD (Tominaga and Stathopoulos, 2009).

1.2 Scope of Present Study

Issues that have not yet been fully addressed in the literature and objectives of the present study are identified, and the significances of the research are outlined.

1.2.1 Literature Review

A number of studies have been performed for the flow and transport of pollutants released about a single building and a cluster of buildings (Li and Stathopoulos, 1997, Meroney et al., 1999, Blocken et al., 2008, Shi et al., 2008, Tominaga and Stathopoulos, 2009) but the street canyon remains the most widely examined configuration in urban air quality problems. Street

sections flanked with buildings promote the accumulation of traffic-induced pollutants, since the air exchange is restricted as a result of the isolation effect of the buildings to the airflow. Numerous experimental and numerical studies on street canyons, ranging from small to large scale, have been performed and the flow and transport mechanism is well understood. Comprehensive reviews are available in the literature (Vardoulakis et al., 2003, Ahmad et al., 2005, Li et al., 2006). All these studies deal with prevailing atmospheric wind directed perpendicular to the street length axis, since this wind regime is determined to be the most critical for pollutant accumulation in street canyons.

Earlier studies on the prediction of flow and pollutant dispersion within street canyons were performed using two-dimensional steady-state Reynolds-averaged Navier-Stokes (RANS) equations and their corresponding turbulence closure schemes (Baik and Kim, 1999, Chan et al., 2002, Assimakopoulos et al., 2003). Subsequent to these initial studies, the investigations were extended to three-dimensional modelling in order to capture the inherent nature of turbulence, and improved predictions were observed (Hsieh et al., 2007, Di Sabatino et al., 2008, Xie et al., 2006). Recently, an interest has risen in employing Large Eddy Simulation (LES) to address the shortcomings of RANS, i.e. its inability to capture the unsteady and inherent fluctuations of the flow field within the street canyon on which the dispersion of pollutants depends (So et al., 2005, Cai et al., 2008, Letzel et al., 2008, Tominaga and Stathopoulos, 2010).

Steady-state RANS, which is the most widely used approach in industry for the modelling of turbulent flows, assumes that non-convective transport in a turbulent flow is governed by stochastic three-dimensional turbulence possessing a broadband spectrum with no distinct frequencies and, therefore, models the entire range of eddy length scales. This approach has obvious weaknesses and poses serious uncertainties in flows for which large scale organised structures dominate, such as flows around buildings and within canyons. In addition, RANS models often assume gradient transport, which may not be the case for pollutant exchange at the roof level of a street canyon. LES, although computationally more expensive, has an advantage over RANS

in that it explicitly resolves the majority of the energy carrying eddies and the internally or externally induced periodicity involved, whereas only the universally small scale eddies are modelled (Cheng et al., 2003).

Another important aspect that has been absent in most investigations dealing with air quality problems in urban and industrial complexes is the aerodynamic impact of other large obstacles. Air exchange between street level and the above-roof airflow is limited in street canyons situated in dense built-up areas. Near ground traffic-released emissions are not effectively diluted and removed, but remain trapped at street-level resulting in high pollutant concentrations (Gromke et al., 2008).

This brings to question what would be the effect of tree planting in street canyons and to what extent would they affect the pollutant dispersion and air exchange processes. Tree crowns can occupy a considerable fraction of street canyons separating the lower street level from the upper roof level and may have significant effects on the natural ventilation and traffic exhaust dispersion.

Previously, only a few studies have addressed pollutant dispersion in street canyons with tree planting. Gross (1997) studied the impact of two rows of avenue-like trees planted along the street next to the building walls by means of a two-equation k - ε turbulence closure scheme. Tree crown porosities were accounted for by additional vegetation terms in the conservation equations, based on the characteristic tree aerodynamical parameters like the leaf drag, the distribution of leaves within the crown and the tree stand density.

Increased pollutant concentration levels and decelerated flow were found near the building walls when compared to tree-free street canyons. Ries and Eichhorn (2001) found that the local pollutant concentration increased at the leeward wall and that the flow velocity within the canyon was reduced for a similar configuration of trees. They employed a one equation k - ε turbulence model based on a differential equation for the turbulent kinetic energy, k including an additional term accounting for the increased generation of k

within porous tree crowns. For the dissipation rate ε , an algebraic relation based on the Blackadar mixing length (Blackadar, 1962) formula was used.

Gayev and Savory (1999) studied a two-dimensional cavity with regular arrays of vertical standing cylinders occupying a volume fraction of 3.2% and found that for a perpendicular approach flow, the flow field in the cavity was considerably modified by the cylinders. A decrease in the volume flow rate of the recirculating fluid of 44% and an average increase in turbulence intensity of 67% with local increases of up to 200% were observed.

In all these studies, a common conclusion is drawn on the influence of tree planting in street canyons, where a lower flow velocity and higher pollutant concentration levels are observed. However, all the aforementioned numerical studies on the aerodynamic effects of trees in street canyons were performed for a two-dimensional (2D) domain, thus, they neither accounted for the inherent three-dimensional (3D) nature of microscale turbulence nor for the 3D flow field in real street canyons. Furthermore, no variation in the tree planting configuration and crown porosity were investigated.

Mochida et al. (2008) and Mochida and Lun (2008) reviewed recent achievements in the field of canopy flows and concluded that the presence of trees aerodynamically decreases the wind velocity and increases turbulence. The same observations were made in the extensive 3D experimental and numerical studies by Gromke and Ruck (2007, 2009), Gromke et al. (2007, 2008), Buccolieri et al. (2009, 2011) and Balczó et al. (2009). The reports demonstrated that in the presence of trees, both wind tunnel (WT) measurements and numerical results showed reduced flow velocities and larger overall pollutant concentration levels when compared to their tree-free counterparts.

In other words, entrainment conditions and thus air exchange mechanisms were altered significantly by the trees, resulting in lower velocity fields and an overall increase in pollutant concentration within the canyon as compared to a tree-free configuration. They attributed these observations mainly to the trees' blockage effect on the air circulation within the canyons. This reduces the air

exchange and less pollutant is dispersed out of the canyons. For all their numerical simulations they employed steady-state RANS and acknowledged that although the computational results had good qualitative agreement with WT measurements, the quantitative agreement was considerably poor and cited the failure for RANS to capture the transient mixing process within the canyons as one of the causes for the discrepancy.

1.2.2 Problem Specification

Some of the shortcomings in published work are discussed and presented in this section.

- a) In the various 3D numerical analyses (Buccolieri et al., 2009, 2011, Gromke et al., 2007, 2008, and Balczó et al., 2009) of street canyons with tree planting, steady-state RANS equations such as RSM and standard $k-\varepsilon$ have been employed. The steady-state simulations did not predict the transient nature of the mixing process in the street canyons, ensuing in lower volume fluxes in the canyon and consequently overpredicting the concentration levels. As a result the numerical predictions were poor in comparison to WT measurement data.
- b) It has been identified that the discrepancies between the wind tunnel and numerical flow results are due to the poor prediction of the turbulence kinetic energy in the street canyon – roof top interface, which is lower than in the WT experiments. The vertical momentum exchange from the above-roof flow downward to the street canyon is too small, resulting in reduced shear force driving the canyon vertex which is consequently weaker than in experimental observations. As less air rotates within the street canyon, less pollutant gets drawn out resulting in larger concentration predictions. The RANS turbulence models employed and assumption of steady-state solution in the numerical analyses are responsible for this (Gromke et al., 2008).
- c) In the CFD study of Gromke et al. (2008, 2009), Buccolieri et al. (2009, 2011) and Balczó et al. (2009), the modelling of the rough boundary layer

was not appropriately accounted for. It was assumed that the sand grain roughness K_s was equal to the aerodynamic roughness length z_0 . Gao and Chow (2005) and Blocken et al. (2007a, 2007b) separately investigated the wall function problem associated with horizontal homogeneity over roughness terrain and showed that the vertical profiles of mean wind speed and turbulence quantities had to be maintained along the downstream distance to improve predictions.

- d) Up to now, limited work has been done to check the performance of CFD models for routine air pollution studies. At present there is still no standardisation of modelling practice for atmospheric applications. This is part of the ongoing research performed within the COST (European Cooperation in Science and Technology) Action 732: Quality assurance and improvement of micro-scale meteorological models. <http://www.mi.uni-hamburg.de/Home.484.0.html> (2005-2009).
- e) Most of the published work focused on presenting the mean pollutant concentration and/or flow field data in the mid stream-wise direction preventing a detailed evaluation of the spatial and temporal performances of the numerical techniques used (i.e. they did not show the distribution along the façades of the buildings). It is also known that WT experiments usually provide data for limited number of measurement locations (Buccolieri et al., 2009).
- f) Although a few comparative studies between steady-state RANS modelling and LES techniques exist for turbulent flows over building-like obstacles (Rodi, 1997, Cheng et al., 2003, and Tominaga and Stathopoulos, 2010), little has been performed in relation to the prediction of pollutant dispersion within urban street canyons, and specifically for street canyons lined with trees. Similarly, none has been performed comparing unsteady RANS (URANS) against LES.

1.2.3 Research Objectives

In light of the identified shortcomings with respect to the problem, the present study aims to:

- a) Implement the porous media model in FLUENT to represent the tree crown in the numerical simulations and investigate its effects on the flow and pollutant concentration field.
- b) Demonstrate the influence of tree plantings on the airflow and transport of airborne materials by comparing between tree-free and tree-lined canyons. The study also involves examining two street canyon aspect ratios (i.e. $W/H=1$ and $W/H=2$) with two different tree planting configurations (single row and two rows of trees, respectively) and two crown porosities one for a loosely ($P_{vol} = 97.5\%$) and another for a densely ($P_{vol} = 96\%$) packed tree crown, corresponding to pressure loss coefficients of $\lambda = 80 \text{ m}^{-1}$ and $\lambda = 200 \text{ m}^{-1}$, respectively. This would allow a comprehensive conclusion to be drawn regarding the impact of trees and provide recommendations on the appropriate configurations to optimize air circulation and ventilation in new urban developments.
- c) Employ LES using the commercial CFD code FLUENT to account for the unsteady mixing process and validate the numerical results against WT experimental data. The results will also be compared to previously used steady-state RANS turbulence models in order to determine to what extent the flow field and pollutant concentration predictions have improved and at what computational cost. Since LES resolves the majority of the energy containing eddies unlike RANS which models all the turbulent length scales, it is envisioned that the turbulent kinetic energy will be accounted for appropriately resulting in an improvement in the numerical prediction, in response to identified shortcoming (Point (b) of Section 1.2.1).
- d) Determine whether the implementation of Blocken et al. (2007a, 2007b) recommendations on dealing with rough boundary layers would be of significance on the numerical prediction, and examine the wall function

problem in relation to horizontal homogeneity. This is done in comparison to the aforementioned studies by Gromke et al. (2008, 2009) and Buccolieri et al. (2009, 2011) which assumed the sand grain height, K_s to be equal to the aerodynamic roughness, z_0 .

- e) Implement and evaluate the wall y^+ approach in determining the most suitable mesh resolution and RANS turbulence model. This is complemented with a grid independence study to verify that the wall y^+ approach does indeed guide in the selection of an appropriate grid configuration for any generic study on wall-bounded turbulent flows.
- f) Finally, to illustrate that unsteady RANS (URANS), albeit resolving unsteadiness, is not a direct replacement to LES, because URANS only captures the externally induced fluctuations and not necessarily the inherent randomness within the flow field. Such comparison in relation to airflow and pollutant dispersion within urban street canyons has not been performed previously.

1.2.4 Significance of Research

As mentioned in the introduction, a concerted effort by different academic institutions, research agencies and governmental organisations are being made to understand the impact of large numbers of discrete bluff obstacles (buildings, vegetation, traffic, etc) on the atmospheric boundary-layer flow because of its importance in many aspects of meteorology, wind engineering, and environmental science.

Initially these studies were focused on single objects e.g. wall-mounted cube in turbulent flows (Ferziger, 1993, Iaccarino et al., 2003, Martinuzzi and Tropea, 1993, Shah and Ferziger, 1997, Yakhot et al., 2006, Meinders et al., 1991, Hussein and Martinuzzi, 1996, Gao and Chow, 2005, Seeta Ratnam and Vengadesan, 2008, Meinders and Hanjalić, 2002). Later, research was extended to cover the study of airflow and pollutant dispersion in a cluster of buildings (Baik and Kim, 1999, Chang and Meroney, 2003, Eliasson et al., 2006, Gerdes and Olivari, 1999, Hanna et al., 2002, Kastner-Klein et al., 2001,

Kastner-Klein and Plate, 1999, Pavageau and Schatzmann, 1999, Di Sabatino et al., 2008, So et al., 2005).

Part of many cities' sustainable initiative is to increase the amount of greenery for community and socio-economic benefits. But on the other hand, trees may also increase the amount of pollutant concentration trapped at street level when compared to tree-free streets.

It is imperative that proper strategies are developed to reduce this negative effect of tree planting in street canyons by studying different configurations, aspect ratios, tree crown porosities, amongst others. This is the focus of the present research work utilising CFD, specifically LES, as its main tool.

The field of study focusing on the aerodynamic influences of trees on the pollutant concentration in urban street canyons is in its teething stage with the potential for further improvements in its modelling.

This would contribute to the ongoing research of improving and assuring the quality of CFD models for predicting flow and transport processes in urban and industrial environments as undertaken under the COST Action 732 (COST, 2005-2009).

The LES viscous model is expected to improve computational flow predictions due to its transient nature and resolution of the large scales of motion, unlike RANS which models the entire range of eddy length scale. A number of studies have been published on flow structures and dispersion in street canyons using LES (Li et al., 2009, Letzel et al., 2008, So et al., 2005, Cai et al., 2008, Shi et al., 2008, Xie and Castro, 2009) but none have included the influence of trees which this project hopes to address. In addition, it is verified that for typical urban airflow problems, URANS is not a suitable replacement for LES because the former is unable to capture the internally induced fluctuations, although both solves for unsteadiness.

The findings would equip regulators, policy makers and urban planners with better understanding and implementation of CFD tools to mitigate air pollution problems, and provide emergency authorities assistance in developing

evacuation plans following accidental or deliberate release of hazardous airborne materials. Development of more accurate numerical predictions and generation of a larger pool of data demonstrating LES consistency and reliability would translate to more confidence in the industry in using CFD as a stand-alone tool and reduce dependency on costly experimental investigations. With enhanced practices and better policies implemented by local councils as a result of the research, air quality and pedestrian comfort would improve significantly, thus, benefiting urban dwellers. In addition, better modelling of atmospheric boundary layer flows could result in improvements in urban designs relating to ventilation and thermal control, assisting in carbon footprint mitigation measures.

The study will provide invaluable information that helps to understand air pollution problems in urban areas and rectification through tree plantation. The results produced will serve as an additional scientific resource to urban planners, environmental engineers and developers for environmental consideration. The fundamental knowledge about trees and winds are novel and are valuable to the study of wind aerodynamics, urban meteorology and arboriculture.

1.3 Research Outline

In the present work, the influence of trees and the numerical performances between RAN and LES are evaluated for the flow field and pollutant dispersion within street canyons of the following configurations:

- $W/H = 1$ without trees.
- $W/H = 1$ lined with single row of trees.
- $W/H = 2$ without trees.
- $W/H = 2$ lined with two rows of trees.

The CFD code FLUENT is used and the advection-diffusion method is employed for dispersion modelling while the tree crowns are represented as porous bodies and line sources replicate traffic exhaust emissions. The relative benefits and drawbacks of the two numerical approaches are assessed and the

computational results are compared to concentration measurement data from WT experiments carried out at the Karlsruhe Institute of Technology, Germany www.codasc.de (CODASC, 2008). Two cases of tree crown porosities are investigated, one for a loosely ($P_{vol} = 97.5\%$) and another for a densely ($P_{vol} = 96\%$) packed model, resulting in pressure loss coefficients of $\lambda = 80 \text{ m}^{-1}$ and $\lambda = 200 \text{ m}^{-1}$, respectively. Finally, numerical results of tree-lined cases are compared to tree-free scenarios to demonstrate the aerodynamic effects of trees on the flow field and pollutant dispersion.

The wall y^+ approach is implemented in determining the best mesh configuration and corresponding turbulence model and near-wall function.

In the RANS simulation the two-equation standard $k-\varepsilon$ and seven-equation RSM turbulence models are employed with second order upwind scheme, whereas for LES, the dynamic Smagorinsky-Lilly sub-grid scale (SGS) model is implemented.

Finally, an unsteady RANS (URANS) simulation is conducted to verify that it is not a suitable replacement for LES, as the former is incapable of capturing the internally induced fluctuations in the flow field development.

1.4 Report Organization

Chapter 1 discusses the basis of the project by outlining the background and motivation of the present study, reviewing the literature, iterating what has been done, identifying the shortcomings of previous research and proposing the contributions that the present study can make to the body of work undertaken in the field of atmospheric boundary layer flow, pollutant transport and urban air quality. The objectives and significance of the research are also discussed.

Chapter 2 introduces the concept of Turbulence in the context of Computational Fluid Dynamics (CFD) and discusses the different numerical approaches available for solving the conservation equations of continuity, momentum and energy, namely Direct Numerical Simulation (DNS),

Reynolds-averaged Navier-Stokes (RANS) and Large Eddy Simulation (LES). Two of the turbulence models that are used in the present study, i.e. RANS and LES, are described in detail in the second subsection under Numerical Methods.

Chapter 3 examines the concept of the wall y^+ approach in providing guidance for selection of an appropriate grid configuration and corresponding turbulence model in CFD investigations of wall-bounded turbulent flows. A case study on flow over a cube is performed to demonstrate its applicability with validation against experimental data. The wall y^+ approach is used in the present study to identify the right grid resolution, resulting in a balance between computational cost and prediction accuracy.

Chapter 4 describes the wind tunnel (WT) experimental investigations on aerodynamic studies of the influence of trees on airflow and pollution dispersion processes in urban street canyons performed at the Laboratory of Building and Environmental Aerodynamics, Karlsruhe Institute of Technology, Germany. Concentration measurement data are available to the scientific community via an online data base www.codasc.de. A section describing the modelling of trees is presented, formulating the porosity of the tree crowns in terms of the pressure loss coefficient λ [m^{-1}] evaluated in forced convection, and the choices of two pore volumes P_{vol} representing the majority of real tree canopies.

Chapter 5 outlines the numerical modelling approach performed in FLUENT. This includes defining the computational domain of the flow problem, setting boundary conditions and establishing the approach to model the flow, turbulence, pollutant emission and dispersion, and tree crown porosities.

The wall y^+ approach described in **Chapter 3** is used in selecting the appropriate mesh configuration. Treatment of wall roughness is examined. A User Defined Function (UDF) is programmed in C Language and implemented in the simulation to describe the inlet boundary conditions and is presented in **Appendix D**.

Chapter 6 presents and discusses results of two cases of tree-free street canyons i.e. $W/H = 1$ and $W/H = 2$ without trees. The prediction accuracy between RANS and LES are compared against WT data. Both wall concentration levels and mid-plane contours are presented to illustrate the relative performances. The instantaneous solutions at different time instances obtained by LES are illustrated.

In addition, unsteady-state RANS (i.e. URANS) is performed to assess whether it is able to capture the inherent fluctuations of the flow field within the urban street canyon and is shown to fail. Finally, it is determined that LES ability to resolve the transient mixing process by resolving the unsteady fluctuation field within the urban street enables it to produce accurate results.

Chapter 7 presents and discusses the results of two cases of tree-lined street canyons, $W/H = 1$ and $W/H = 2$, with single row and two rows of trees respectively. Two different tree crown porosities are examined to determine the aerodynamic effects of trees.

Chapter 8 concludes the entire project and deliberates on future research directions. These include conclusions on the numerical approach, wall roughness, wall y^+ approach, aerodynamic effects of trees, influence of tree crown porosity and finally street canyon aspect ratio.

2 STUDYING TURBULENCE **THROUGH COMPUTATIONAL** **FLUID DYNAMICS**

The chapter is divided into two sub-sections; the first gives a condensed theoretic background on turbulence in the context of CFD. This is followed by description of the numerical methods employed in the present research work. Comprehensive literature can be found in a wide range of recommended texts (Chung, 2002, Anderson and Wendt, 2009, Pope, 2005, Wilcox, 2006, Versteeg and Malalasekera, 2007).

2.1 Turbulence

Turbulent flows are three-dimensional, unsteady, rotational, viscous and chaotic fluid motion as portrayed by Figure 2.1. They are characterized by low momentum diffusion, high momentum convection and rapid variation of pressure and velocity (Versteeg and Malalasekera, 2007). As the Reynolds number exceeds a critical limit, the Navier-Stokes equations become unstable, due to the inherent non-linearity which exerts its effects when Reynolds number is large. This results in the irregularity of turbulent flows.

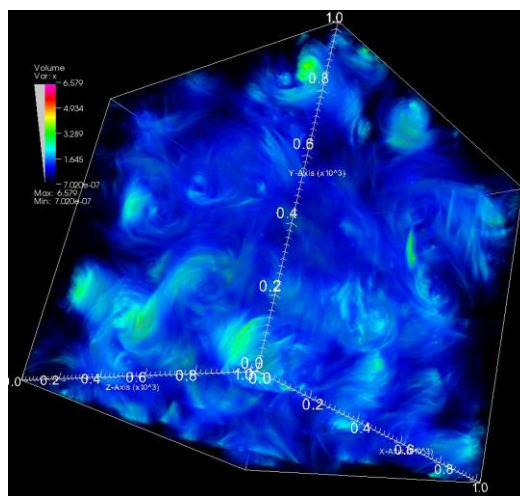


Figure 2.1 Structure of turbulence

The characteristics of turbulence can be summarized as:

- Unsteady, irregular (aperiodic) motion in which transported quantities (mass, momentum, scalar species) fluctuate in time and space.
- Fluid properties exhibit random variations: statistical averaging results in accountable, turbulence related transport mechanisms.
- Contains a wide range of eddy sizes (scales): typical identifiable swirling patterns, where large eddies 'carry' small eddies.

The effects of turbulence are present in virtually every sphere of engineering consequence: the design of tall structures, drag reduction techniques in aircrafts and automobiles, urban air pollution, weather forecast, sports performance, power production and cooling of microchips; among others. Yet its phenomenon is not completely understood.

Due to the vast engineering significance, it is important to form both a conceptual understanding and quantitative description of turbulent flows and also have access to viable tools that are capable of representing the effects of turbulence while keeping in mind the computational cost.

2.1.1 Turbulence Modelling

Turbulence causes the formation of eddies of many different length scales as noted by Richardson (1922). Larger eddies contain most of the kinetic energy which they derive from the main flow. The kinetic energy from the larger eddies then gets transferred to the smaller eddies via vortex stretching in what is known as the energy cascade. The process continues creating smaller and smaller structures producing a hierarchy of eddies. Eventually, the structures get small enough that molecular diffusion becomes important and the smallest eddies at the Kolmogorov length scales (Kolmogorov, 1941) convert their kinetic energy into thermal energy via viscous dissipation. The energy cascade is illustrated in Figure 2.2.

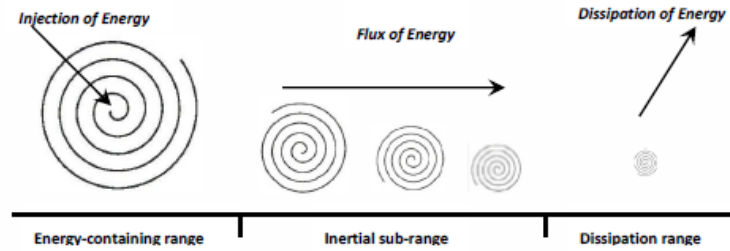


Figure 2.2 The energy cascade of turbulence

2.1.1.1 Direct Numerical Simulation

Direct Numerical Simulation (DNS) of turbulent flow takes the set of Navier-Stokes equations as a starting point and develops a transient solution on a sufficiently fine spatial mesh with sufficiently small time steps to resolve even the smallest turbulent eddies and the fastest fluctuations. In other words, DNS is the solution of the time-dependent Navier-Stokes equations without recourse to modelling but is not suitable for practical industrial application due to the huge computational demand. It is feasible only as a research tool for simple geometries and low turbulent Reynolds number (Versteeg and Malalasekera, 2007).

This leads to the developments of two other numerical approaches that eliminate the need to resolve small scales.

2.1.1.2 Reynolds-averaged Navier-Stokes Modelling (Time-averaging)

The flow properties are disintegrated into their mean and fluctuating components (Figure 2.3) by Reynolds decomposition and substituted into the Navier-Stokes equations, which on time-averaging yields the Reynolds-averaged Navier-Stokes equations (RANS),

$$u = \bar{u} + u' : \bar{u} = \frac{1}{t} \int_0^t u dt, t$$

The Navier-Stokes equations of motion for an incompressible Newtonian fluid are the Continuity equation,

$$\frac{\partial u_i}{\partial x_i} = 0,$$

and Momentum equations,

$$\frac{\partial u_i}{\partial t} + u_j \frac{\partial u_i}{\partial x_j} = f_i - \frac{1}{\rho} \frac{\partial p}{\partial x_i} + \nu \frac{\partial^2 u_i}{\partial x_j^2}.$$

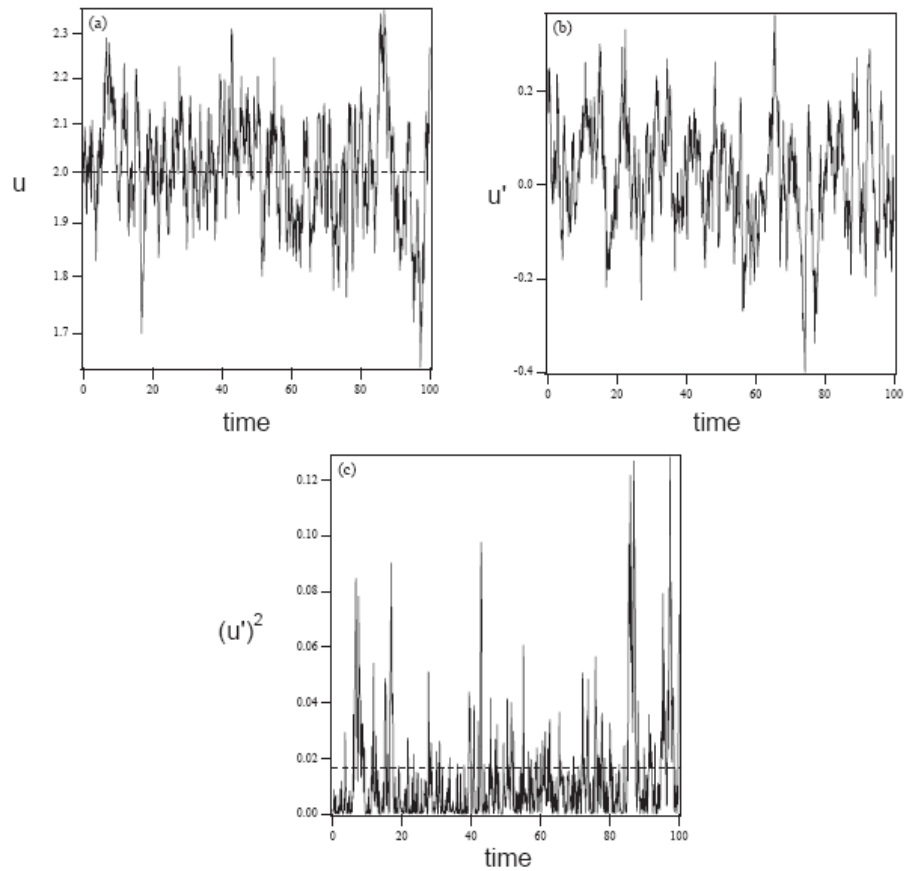


Figure 2.3 (a) Time history of velocity in a turbulent flow (b) Fluctuating component (c) Square of the fluctuating component. Dashed lines represent the time averages (Bhaskaran and Collins, 2002)

Substituting $u_i = \bar{u}_i + u'_i$, $p = \bar{p} + p'$, etc, where the bar donates the mean value and the prime denotes the fluctuating part and taking a time-averaging of the equations above yields the Reynolds Averaged Navier-Stokes Equations (RANS) for the mean variables,

Continuity

$$\frac{\partial \bar{u}_i}{\partial x_i} = 0,$$

and Momentum

$$\frac{\partial \bar{u}_i}{\partial t} + \bar{u}_j \frac{\partial \bar{u}_i}{\partial x_j} + \overline{u_j' \frac{\partial u_i'}{\partial x_j}} = \bar{f}_i - \frac{1}{\rho} \frac{\partial \bar{p}}{\partial x_i} + \nu \frac{\partial^2 \bar{u}_i}{\partial x_j^2}.$$

Where the Reynolds stresses are given by $R_{ij} = -\rho \overline{u_i' u_j'}$.

These are mean flow equations which can be evaluated using numerical analysis to determine time-averaged solutions to the Navier-Stokes equations as long as the Reynolds stresses are modelled properly. They are sufficient for most engineering problems, because they can supply adequate information about the turbulent processes, without the need to predict the effect of each and every eddy in the flow (Versteeg and Malalasekera, 2007).

Appearance of the fluctuations associated with turbulence have consequences on the time-averaged Navier-Stokes equations where the velocity fluctuations give rise to additional stresses in the fluid, the so called Reynolds stresses which need to be modelled in order to mathematically close the problem and solve it. Different RANS turbulence models exist and those that are available in the commercial CFD package FLUENT include: Spalart-Allmaras, $k-\varepsilon$ and its variants, $k-\omega$ and its variants and RSM. Further details on the models can be found in the reference texts (FLUENT, 2005a, Versteeg and Malalasekera, 2007, Pope, 2005).

2.1.1.3 Large Eddy Simulation (Spatial-filtering)

In RANS modelling discussed in the previous section, all turbulence scales are modelled on time-averaging. In Large Eddy Simulation (LES), the transport equations are filtered such that only the larger eddies need be resolved, whereas the smaller eddies are modelled. It is difficult to model the larger eddies due to the fact that they are anisotropic (i.e. they vary in different directions), are subjected to history effects and dependent upon flow

configuration, boundary conditions, disturbances, etc. On the other hand, smaller eddies are typically isotropic as postulated by Kolmogorov (1941) and so are amenable to modelling.

A spatial filtering operation is used to separate the larger and smaller eddies of the flow, giving rise to a resolved scale (larger eddies) and sub-grid scale (smaller eddies) that is modelled.

A spatial filtering operation by means of a filter function $G(x, x', \Delta)$ is performed,

$$\bar{\phi}(x, t) \equiv \iiint_{-\infty}^{\infty} G(x, x', \Delta) \phi(x', t) dx'$$

where $\bar{\phi}(x, t)$ = filtered function

and $\phi(x', t)$ = original (unfiltered) function

and Δ = cut-off width which is determined by grid resolution.

In this section, the overbar indicates spatial filtering, not time-averaging as in RANS. The top-hat (box filter), Gaussian filter and spectral cut-off are the commonest forms of the filtering function in 3D LES computations (Versteeg and Malalasekera, 2007).

Using the top-hat filter,

$$G(x, x') = \begin{cases} \frac{1}{V} & \text{for } x' \in V \\ 0 & \text{otherwise} \end{cases}$$

the filtered variable becomes

$$\bar{\phi}(x, t) = \frac{1}{V} \int \phi(x', t) dx, \quad x' \in V.$$

Filtering the original Navier-Stokes equations gives filtered Navier-Stokes equations that are the governing equations in LES as presented in Figure 2.4.

$$\begin{array}{l}
 \text{N-S} \\
 \text{equation}
 \end{array}
 \quad
 \frac{\partial u_i}{\partial t} + \frac{\partial u_i u_j}{\partial x_j} = -\frac{1}{\rho} \frac{\partial p}{\partial x_i} + \frac{\partial}{\partial x_j} \left(\nu \frac{\partial u_i}{\partial x_j} \right)$$


$$\begin{array}{l}
 \text{Filtered N-S} \\
 \text{equation}
 \end{array}
 \quad
 \frac{\partial \bar{u}_i}{\partial t} + \frac{\partial \bar{u}_i \bar{u}_j}{\partial x_j} = -\frac{1}{\rho} \frac{\partial \bar{p}}{\partial x_i} + \frac{\partial}{\partial x_j} \left(\nu \frac{\partial \bar{u}_i}{\partial x_j} \right) - \frac{\partial \tau_{ij}}{\partial x_j}$$

$$\tau_{ij} \equiv \overline{u_i u_j} - \bar{u}_i \bar{u}_j \quad \leftarrow \text{Needs modeling}$$

Sub-grid scale (SGS) stress

Figure 2.4 Spatial-filtering in Large Eddy Simulation (LES)

The filtered momentum equations look very similar to RANS momentum equations. Additional terms, the sub-grid scale (SGS) stresses τ_{ij} are introduced due to the filtering operation, just like Reynolds stresses in RANS momentum equations that arise as a consequence of time-averaging. A substantial portion of τ_{ij} are attributable to convective momentum transport due to interactions between unresolved or SGS eddies, which similarly require the need for modelling them to mathematically close the problem.

FLUENT offers several eddy viscosity sub-grid scale models which include: Smagorinsky-Lilly model, Wall-Adapting Local Eddy-Viscosity (WALE) model, Dynamic Smagorinsky-Lilly Model and Dynamic Kinetic Energy Transport model (FLUENT, 2005a).

The main advantage of LES over RANS is that deterministic unsteadiness of large eddy motions can be resolved. As a consequence of LES resolving the eddies of the turbulence itself, it typically requires higher spatial and temporal resolution and, thus, is more costly. In addition, LES requires a very long integration time to build an ensemble averaged solution and is only appropriate for flow problems where there is a need to explicitly account for unsteady fields as in airflow development and pollution dispersion in urban and industrial complexes.

2.2 Numerical Methods

The numerical approaches used for the present investigations are described in this sub-section.

2.2.1 Reynolds-averaged Navier-Stokes

2.2.1.1 *Steady Reynolds-averaged Navier-Stokes*

In steady-state Reynolds-averaged Navier-Stokes (RANS) modelling, the flow properties are disintegrated into their mean and fluctuating components by Reynolds decomposition and substituted into the Navier-Stokes equations, which on time-averaging yields the RANS equations for incompressible Newtonian fluids,

$$\frac{\partial \bar{u}_i}{\partial x_i} = 0,$$

and

$$\bar{u}_j \frac{\partial \bar{u}_i}{\partial x_j} + \overline{u_j' \frac{\partial u_i'}{\partial x_j}} = \bar{f}_i - \frac{1}{\rho} \frac{\partial \bar{p}}{\partial x_i} + \nu \frac{\partial^2 \bar{u}_i}{\partial x_j^2} + S_i.$$

\bar{u}_i and u_i' are the mean and fluctuating parts of the velocity component u_i in the x_i -direction, respectively, p is the mean pressure, ρ is the density, ν is the kinematic viscosity, and S_i is the momentum sink defined for the fluid zone demarcated as porous media in order to model the tree crowns. Appearance of the fluctuations associated with turbulence have consequences on the time-averaged Navier-Stokes equations where the velocity fluctuations give rise to additional stresses in the fluid, the so called Reynolds stresses, $\overline{\rho u_i' u_j'}$, which need to be modelled in order to mathematically close the problem.

In the present study, only the standard $k-\varepsilon$ and RSM models are employed for the investigation. The major difference between the two chosen turbulence closure schemes is that the standard $k-\varepsilon$ model assumes the Reynolds stresses to be isotropic (i.e. employs the Boussinesq hypothesis (Hinze, 1975)) and

solves for only two additional equations, one for the kinetic energy, k and another for the dissipation rate, ε . On the other hand, RSM solves for seven extra equations to account for the six individual components of the Reynolds stresses and one for dissipation rate, ε (Versteeg and Malalasekera, 2007).

The transport equations for k and ε are

$$\frac{\partial}{\partial x_i}(\rho k u_i) = \frac{\partial}{\partial x_j} \left[\left(\mu + \frac{\rho C_\mu k^2}{\sigma_k \varepsilon} \right) \frac{\partial k}{\partial x_j} \right] - \rho \overline{u_i' u_j'} \frac{\partial U_j}{\partial x_i} - \rho \varepsilon,$$

and

$$\begin{aligned} \frac{\partial}{\partial x_i}(\rho \varepsilon u_i) &= \frac{\partial}{\partial x_j} \left[\left(\mu + \frac{\rho C_\mu k^2}{\sigma_\varepsilon \varepsilon} \right) \frac{\partial \varepsilon}{\partial x_j} \right] + C_{1\varepsilon} \frac{\varepsilon}{k} \left(-\rho \overline{u_i' u_j'} \frac{\partial U_j}{\partial x_i} \right) \\ &\quad - C_{2\varepsilon} \rho \frac{\varepsilon^2}{k}. \end{aligned}$$

$C_\mu = 0.09$; $\sigma_k = 1.00$; $\sigma_\varepsilon = 1.30$; $C_{1\varepsilon} = 1.44$; $C_{2\varepsilon} = 1.92$ are the default closure constants obtained from a comprehensive data fitting over a wide range of canonical turbulent flows (FLUENT, 2005a).

The transport equations for each component of the Reynolds stress are

$$\begin{aligned} \frac{\partial}{\partial x_k}(\rho u_k \overline{u_i' u_j'}) &= -\frac{\partial}{\partial x_k} \left[\rho \overline{u_i' u_j' u_k'} + p(\delta_{kj} u_i' + \delta_{ik} u_j') \right] \\ &\quad + \frac{\partial}{\partial x_k} \left[\mu \frac{\partial}{\partial x_k} (\overline{u_i' u_j'}) \right] + \Phi_{ij} - \varepsilon_{ij}, \end{aligned}$$

where Φ_{ij} is the pressure strain term and ε_{ij} the dissipation term. Further details on the models can be found from the reference texts (FLUENT, 2005a, Pope, 2005, Wilcox, 2006).

2.2.1.2 Unsteady Reynolds-averaged Navier-Stokes

In addition to steady-state RANS, unsteady RANS (URANS) is available which essentially solves similar transport equations but with addition of an unsteady term

$$\frac{\partial \bar{u}_i}{\partial t}$$

in the Reynolds-averaged momentum equation

$$\frac{\partial \bar{u}_i}{\partial t} + \bar{u}_j \frac{\partial \bar{u}_i}{\partial x_j} = -\frac{1}{\rho} \frac{\partial \bar{p}}{\partial x_i} + \nu \frac{\partial^2 \bar{u}_i}{\partial x_j^2} - \overline{u_j' \frac{\partial u_i'}{\partial x_j}} + S_i.$$

It should be noted that although URANS solves for unsteadiness, they are only applicable to non-stationary flows such as periodic or quasi-periodic flows involving deterministic structures (for example, they can occasionally predict vortex shedding i.e. largest unsteady scales) and falls most often short of capturing the remaining large scales (FLUENT, 2005a). This is because they still solve the mean flow equations but in addition perform ensemble averaging (i.e. realizations of the mean flow over many instances) and thus, are not a suitable replacement for LES (FLUENT, 2005b).

2.2.2 Large Eddy Simulation

In RANS discussed in the previous section, the entire spectrum of turbulent scales is modelled. However in LES, the large scale eddies are solved directly and only the influences of the small scale eddies on the large scale eddies are modelled. A spatial filtering operation is used to separate the large scale and small scale eddies of the flow, resulting in the filtered continuity and momentum equations of the incompressible Navier-Stokes

$$\frac{\partial \bar{u}_i}{\partial x_i} = 0,$$

and

$$\frac{\partial \bar{u}_i}{\partial t} + \bar{u}_j \frac{\partial \bar{u}_i}{\partial x_j} = -\frac{1}{\rho} \frac{\partial \bar{p}}{\partial x_i} + \nu \frac{\partial^2 \bar{u}_i}{\partial x_j^2} - \frac{\partial \tau_{ij}}{\partial x_j} + S_i.$$

Here, the overbar indicates spatial filtering, and not time-averaging as in RANS. Therefore, \bar{u}_i and \bar{p} are the filtered velocity and pressure, respectively. It is worth noting that the filtered momentum equations look similar to the RANS momentum equations. The spatial filtering operation is an integration, just like time-averaging in the derivation of the RANS equations, the difference being that in LES the integration is carried out in space unlike time-averaging in RANS (Versteeg and Malalasekera, 2007).

Additional tensor terms, $\tau_{ij} = \overline{u_i u_j} - \bar{u}_i \bar{u}_j$ are introduced due to the filtering operation analogous to the Reynolds stresses resulting from Reynolds-averaging, requiring the need for them to be modelled in order to mathematically close the problem. Substantial portions of τ_{ij} are attributable to convective momentum transport due to interactions between the unresolved eddies and, thus, are commonly termed the sub-grid scale (SGS) stresses. FLUENT employs the Boussinesq hypothesis (Hinze, 1975) as in the RANS modelling, computing SGS turbulent stresses from

$$\tau_{ij} - \frac{1}{3} \tau_{kk} \delta_{ij} = -2\mu_t \bar{S}_{ij},$$

where μ_t is the sub-grid scale turbulent viscosity, and \bar{S}_{ij} is the rate-of-strain tensor for the resolved scale defined by

$$\bar{S}_{ij} \equiv \frac{1}{2} \left(\frac{\partial \bar{u}_i}{\partial x_j} + \frac{\partial \bar{u}_j}{\partial x_i} \right).$$

The eddy-viscosity is modelled by

$$\mu_t = \rho L_s^2 |\bar{S}|,$$

where L_s is the mixing length for the sub-grid scales and $|\bar{S}| \equiv \sqrt{2\bar{S}_{ij}\bar{S}_{ij}}$. In FLUENT, L_s is computed using

$$L_s = \min(\kappa d, C_s V^{1/3}),$$

where κ is the von Kármán constant (0.4), d is the distance to the closest wall, C_s is the Smagorinsky constant, and V is the volume of the computational cell. The porous media momentum sink term S_i also contributes to the eddy viscosity.

The original Smagorinsky-Lilly model as first proposed by Smagorinsky (1963) remains widely used due to its algorithmic simplicity and numerical stability, in order to account for the SGS stresses. However C_s is not a universal constant as assumed in the original model, but is flow-dependent and ad hoc modifications are required particularly near solid surfaces (e.g. by introducing a van Driest damping function) as discussed by Cebeci and Smith (1974).

The dynamic Smagorinsky-Lilly model, initially conceived by Germano et al. (1991) and subsequently by Lilly (1992) eliminates some of these shortcomings by dynamically computing the Smagorinsky constant, C_s , based on the information provided by the resolved scales of motion and obviates the need for users to specify the model constant in advance. Further details on the dynamic model as implemented in FLUENT can be found in the paper by Kim (2004). In the present study, the dynamic Smagorinsky-Lilly SGS model is chosen since no homogeneous direction exists in the flow.

Momentum, mass, energy, and other passive scalars are transported mostly by large scale eddies and they tend to be more problem dependent, whereas small scale eddies are less dependent on the geometry, are more isotropic, and are consequently more universal. By employing LES in a complex flow simulation such as the case of airflow and pollutant transport within urban street canyons, less approximation but more direct resolving is achieved as opposed to RANS. The trade-off though, is that LES requires substantially finer meshes and needs to be run for sufficiently longer flow-through times in order to obtain stable statistics of the flow being modelled. As a result, the computational cost associated with LES is normally orders of magnitudes higher than that of steady RANS calculations in terms of memory (RAM) and CPU time.

2.3 Summary

This section summarises the three approaches to dealing with turbulence in CFD, name Direct Numerical Simulation (DNS), Reynolds-averaged Navier-Stokes (RANS) model and Large Eddy Simulation (LES). Figure 2.5 visually illustrates the three approaches together with the energy cascade (Richardson, 1922).

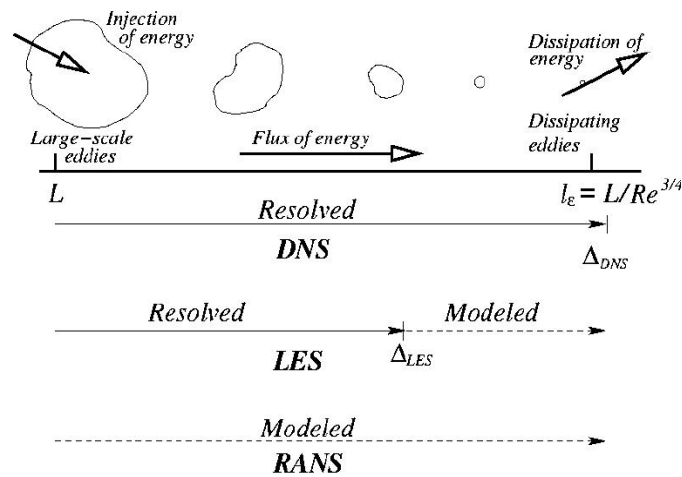


Figure 2.5 Prediction methods in CFD (FLUENT, 2005b)

3 WALL y^+ APPROACH

The flow field developments within urban street canyons are complex owing to flow separation, reattachment and recirculation resulting from buildings obstructing wind. To obtain meaningful and accurate numerical results it is important to properly account for the large gradients in the flow field variables.

Obstacles such as trees intensify the fluctuations by modifying the turbulence structures due to increased shear strain within tree-lined canyons. In order to accurately capture the aerodynamic effects of trees, it is paramount that appropriate mesh configurations are selected that would allow for compromise between numerical accuracy and computational cost.

The wall y^+ approach provides guidance in selecting a suitable grid configuration and corresponding turbulence model in CFD investigations of wall-bounded turbulent flows. The behaviours of different RANS models together with their accompanying near-wall treatments are described for different wall y^+ resolving the viscous sublayer, buffer layer and log-law region.

The approach is used in the present project to assist in the selection of the optimal grid resolution. This also demonstrates its general applicability for airflow and pollutant dispersion simulations in urban street canyons, thus increasing confidence in the research and industrial community in applying it to studies related to wall-bounded turbulent flows.

3.1 Motivation for the Wall y^+ Approach

The majority of time spent on CFD projects in industry is usually devoted to successfully generating a mesh for the domain that allows for a compromise between desired accuracy and solution cost. The preferred method for determining the most accurate mesh is to carry out test runs on different cell sizes and mesh configurations, with further alterations and re-runs, so as to match the converged numerical solution as closely as possible to available

experimental or benchmark data. This is termed the grid independence test, which is considered a time-consuming procedure (Tu et al., 2008) .

Initially, based on a simple 2D model, numerical investigations were carried out for both undisturbed and disturbed turbulent flows over a solid ridge bounded by a flat smooth wall at $Re_H = 17,000$ with the bulk velocity and ridge height as characteristic dimensions by Salim and Cheah (2009). The recommendations included the behaviour and suggested usage of the inbuilt RANS turbulence models and near-wall treatments using FLUENT. This study was carried out as an undergraduate final year project.

Turbulence is inherently 3D in nature, and in order to capture the intricate flow structures, simulation of a wall mounted cube in a turbulent channel flow at two different Reynolds numbers , $Re_H = 1,870$ and $Re_H = 40,000$, were performed to build on the initial study. It also presents a general configuration that is relevant to many engineering applications ranging from prediction of wind loading on structures and air pollution in urban areas to cooling of turbines and electronic components in circuit boards.

The investigations were carried out for two turbulent cases, dealing with low Reynolds number, $Re_H = 1,870$ and high Reynolds number, $Re_H = 40,000$ flows, respectively. The cases are chosen due to the simple geometry but complex vortical structures. The considerable variation in the Reynolds number also warrants a different set of recommendations based on the computed wall y^+ and turbulence models for each case.

The standard $k-\varepsilon$, standard $k-\omega$, Reynolds Stress Model (RSM), Spalart-Allmaras (SA) and renormalization group (RNG) $k-\varepsilon$ models were employed to solve the closure problem in both cases. Their behaviour together with the accompanying near-wall treatment is investigated.

A brief overview of near-wall treatment and the wall y^+ is introduced in the next section.

3.2 Near-wall Treatment

Near-wall regions (Figure 3.1), where momentum and other scalar transports occur most vigorously, have large gradients in the solution variables (FLUENT, 2005a).

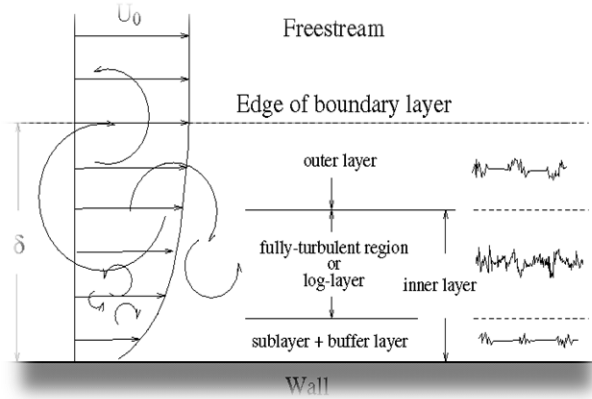


Figure 3.1 Near-wall region (FLUENT, 2005a)

The wall y^+ is a non-dimensional distance similar to local Reynolds number. In the context of CFD, it is used to describe how coarse or fine a mesh is for a particular flow. It determines whether the influences in the wall-adjacent cells are laminar, transitional or turbulent, hence indicating the part of the turbulent boundary layer that is resolved (FLUENT, 2005a). It is described as

$$y^+ = \frac{u_* y}{\nu},$$

where y is the height from the wall to the mid-point of the wall-adjacent cells, ν is the kinematic viscosity and u_* is the friction velocity defined as

$$u_* = \sqrt{\frac{\tau_w}{\rho}},$$

with τ_w as the wall shear stress and ρ as the fluid density at the wall.

From Figure 3.2 it can be observed that the viscosity-affected region is made up of roughly three zones (with their corresponding wall y^+):

- Viscous sublayer: $y^+ < 5$ (velocity profile is assumed to be linear and viscous stress dominates the wall shear).
- Buffer layer: $5 < y^+ < 30$ (both viscous and turbulent shear dominates).
- Log-law region: $y^+ > 30$ (corresponds to the region where turbulent shear dominates).

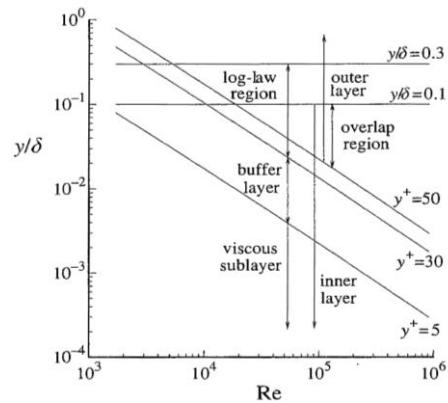


Figure 3.2 The sub-divisions of the near-wall region (FLUENT, 2005a)

Very close to the wall, viscous damping reduces the tangential velocity fluctuations, while kinematic blocking reduces the normal fluctuations. However, towards the outer part of the near-wall region the turbulence is rapidly augmented by the production of turbulent kinetic energy due to the large gradients in mean velocity (FLUENT, 2005a).

In CFD, accurate resolution of the flow in the near-wall region determines successful prediction of wall bounded turbulent flows. Values of y^+ close to the lower bound ($y^+ \approx 30$) are most desirable for wall-functions whereas values of $y^+ \approx 1$ are better for near-wall modelling.

FLUENT offers two approaches to modelling the near-wall regions. In the first approach, the viscosity-affected inner region (viscous sublayer and buffer layer) is not resolved. Instead, semi-empirical formulas called wall-functions are used to bridge the viscosity-affected region between the wall and the log-law region. In the second approach, the turbulence models are modified to enable the viscosity-affected region to be resolved with a mesh all the way to the wall, including the viscous sublayer, and are termed near-wall modelling. These two approaches are depicted schematically in Figure 3.3.

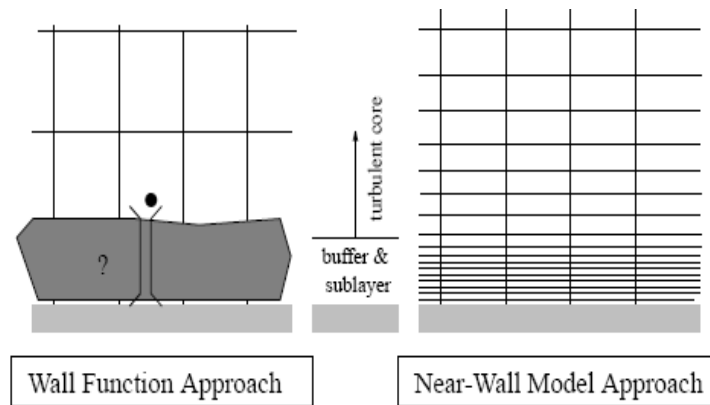


Figure 3.3 Near-wall treatments in FLUENT (FLUENT, 2005a)

The $k-\varepsilon$ and RSM models are primarily valid for turbulent core flows (somewhat far from the walls) and hence are coupled with wall-functions to bridge them with the solution variables in the viscosity-affected region. SA and $k-\omega$ are applicable throughout the boundary layer, provided the near-wall mesh resolution is fine enough (FLUENT, 2005a, Versteeg and Malalasekera, 2007, Pope, 2005, Wilcox, 2006).

3.3 The Wall y^+ Approach

The main results and conclusions based on the wall y^+ approach in determining the most suitable mesh configuration and corresponding turbulence model are discussed and presented in this section. This includes discussion on near wall-treatment for any generic study dealing with wall-bounded turbulent flows over smooth surfaces without pressure gradients.

The wall y^+ is not known *a priori* and requires that a few meshes are first constructed followed by simulations using simple turbulence models (in most cases the standard $k-\varepsilon$ is deemed sufficient). Once the solution has converged, the wall y^+ is calculated and the mesh resolution is accessed to see whether it is appropriate depending on the Reynolds number of the main flow. The choice of turbulence model and near-wall treatment to apply is then decided.

3.3.1 Low Reynolds Number

For a low Reynolds number flow, only a wall y^+ resolving either the viscous sublayer or buffer layer is physically viable as resolving into the log-law region would require an unrealistically large wall-adjacent cell height.

A wall y^+ resolving the viscous sublayer (i.e. $y^+ < 5$) in this case is deemed a better choice, since the wall y^+ resolving into the buffer layer is discarded because neither wall functions nor near-wall modelling accounts for it accurately.

The SA turbulence model is sufficiently accurate, considering a compromise between computational cost and numerical accuracy. SA is a two-zonal model that requires no wall functions to bridge it to the solution variables at the wall, unlike $k-\varepsilon$ and RSM (FLUENT, 2005a).

The wall functions are not expected to perform well in the viscous sublayer since they are formulated predominantly for the log-law region.

3.3.2 High Reynolds Number

For a high Reynolds number flow, a mesh configuration with a wall $y^+ > 30$ resolving the log-law region is sufficiently accurate incurring a lower computational cost as opposed to working all the way into the viscous sublayer.

It is observed that for fluid problems with complex turbulent flow structures, e.g. separations and recirculation bubbles, most steady-flow RANS turbulence models are able to predict the flow broadly to an agreeable extent. However, different flow regions have different ‘best’ models for their flow prediction.

RSM predicts best the region with large gradients, such as separation and recirculation, followed by $k-\varepsilon$.

3.4 Example on Reynolds number $Re_H = 40,000$

The wall y^+ approach is demonstrated by an example for a high Reynolds number flow problem, as the present research on the aerodynamic effects of trees in urban street canyons is based on a similar Reynolds number flow.

3.4.1 Model Description

The computational domain shown in Figure 3.4 is identical to that used by Lakehal and Rodi (1997) in their numerical analysis that replicates the experimental setup of Martinuzzi and Tropea (1993). A fully developed turbulent flow is set at the inlet with $Re_H = 40,000$. No-slip conditions are applied on the channel floor, top wall and all the cube's faces, whereas the side walls are defined as symmetry to reduce computational cost, since they are sufficiently far from the cube to influence the main flow.

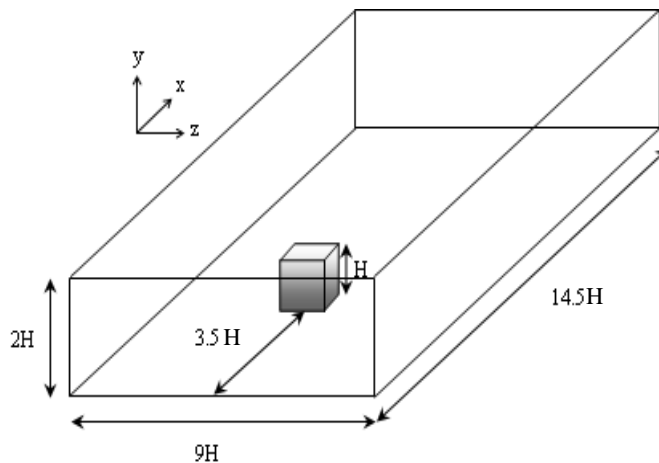


Figure 3.4 Computational geometry of studied case replicating experimental investigation of Martinuzzi and Tropea (1993)

Steady-flow RANS equations are implemented to solve the problem and the turbulence models tested are standard $k-\epsilon$, standard $k-\omega$, RSM, SA and RNG $k-\epsilon$. Figure 3.5, Figure 3.6 and Figure 3.7 show the computational grids with different mesh configurations used for the investigation. The height of the

wall-adjacent cells for Mesh 1, Mesh 2 and Mesh 3 are $0.004 H$, $0.025 H$ and $0.038 H$ resulting in 479,200 cells, 324,960 cells and 181,835 cells, respectively. The successive ratios (growth rate of consecutive cells) employed for all mesh configurations are 1.10 in the x -direction, 1.05 in the y -direction and 1.10 in the z -direction.

This allows an analysis of how different turbulence models and accompanying near-wall treatments behave for different regions of resolution as defined by the wall y^+ .

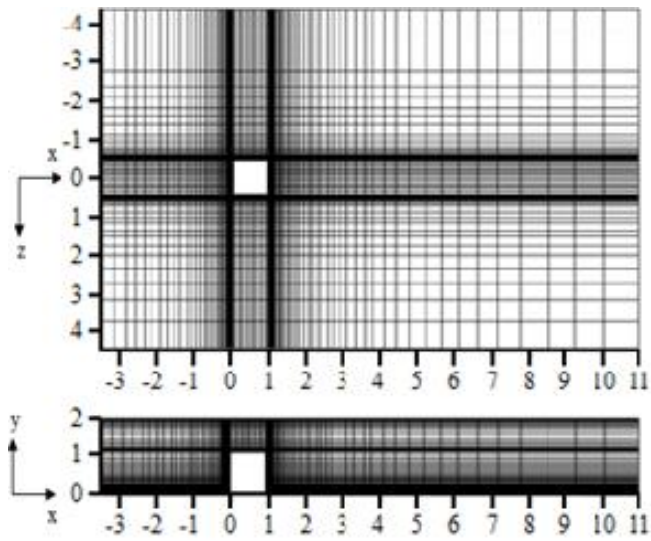


Figure 3.5 Computational grid (Mesh 1)

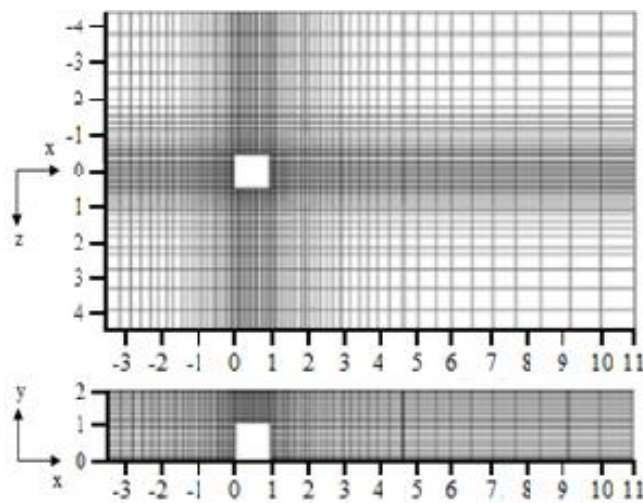


Figure 3.6 Computational grid (Mesh 2)

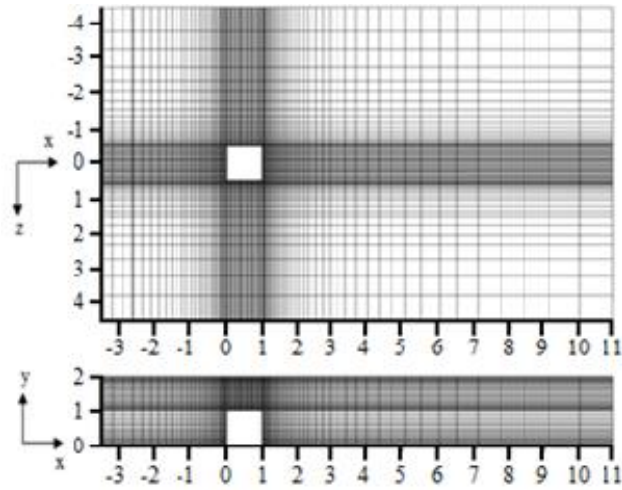


Figure 3.7 Computational grid (Mesh 3)

3.4.2 Results

3.4.2.1 Mesh Configuration

The y^+ values obtained by standard $k-\varepsilon$ for the three considered meshes are approximately 5, 22, and 33 corresponding to resolution in the viscous sublayer, buffer layer and log-law region, respectively. These are graphically presented in Figure 3.8, which illustrate the variation of the y^+ values along the x -direction of the domain. The region around $0.5 x/H$ is where the cube is located and the fluctuations behind and in front of the cube are as a result of flow separation and recirculation

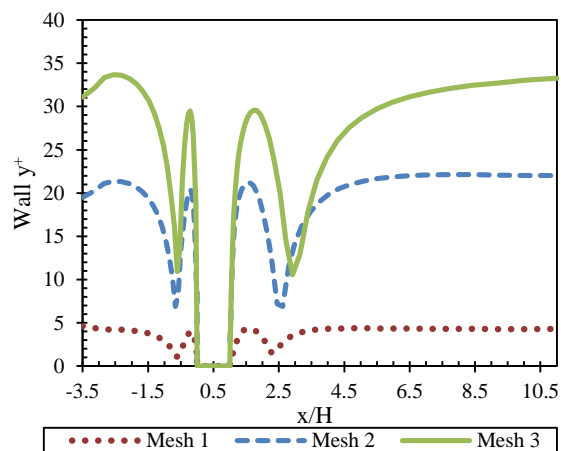


Figure 3.8 Wall y^+ of the considered meshes

The proceeding results of mean streamwise velocity are presented for different dimensionalised x -distances with $x = 0$ set at the front face of the cube.

Figure 3.9 and Figure 3.10 show the comparison of mean streamwise velocity profiles in the symmetry line at $x/H = 0.5$, simulated by standard $k-\varepsilon$ and RSM. Standard $k-\varepsilon$ predicted the velocity profiles similarly for all three meshes. By comparison, the prediction of velocity profiles by RSM is better, noting that the reverse flow is captured on top of the cube.

No data for Mesh 1 could be included in Figure 3.10 as RSM was unable to converge for Mesh 1 with a very fine grid near the wall ($y^+ \approx 5$). It requires wall functions to bridge the solution variables to the wall and as previously indicated wall functions do not generally work well in the viscous sublayer as they are formulated using law of the wall which is accurate in the log-law region only.

For Mesh 2 with wall y^+ value 22 and Mesh 3 with y^+ value 33, RSM predicted the velocity profiles much more accurately as opposed to standard $k-\varepsilon$ when compared against experimental data. Mesh 2, which resolved a wall y^+ in the buffer layer was discarded, because neither wall functions nor near-wall modelling resolves them correctly (FLUENT, 2005a, Salim and Cheah, 2009).

3.4.2.2 Turbulence Model

It can be seen that the choice of turbulence model is insignificant in the mean velocity profiles calculation for undisturbed approach flows, as illustrated in Figure 3.11(a). In Figure 3.11(b), RNG $k-\varepsilon$ and RSM agree better with experimental results in predicting reverse flow on top of the cube at $x/H = 0.5$. RSM is recommended because it accounts for all components of turbulent stresses, unlike the other RANS models that assume isotropic Reynolds stresses.

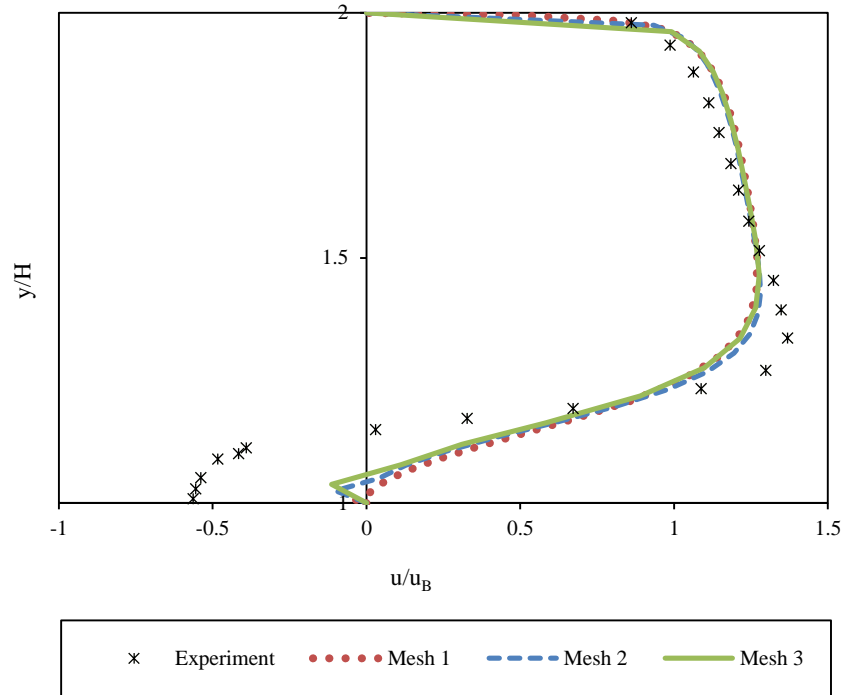


Figure 3.9 Comparison of mean streamwise velocity profiles in the symmetry line $x/H = 0.5$ using Standard $k-\epsilon$

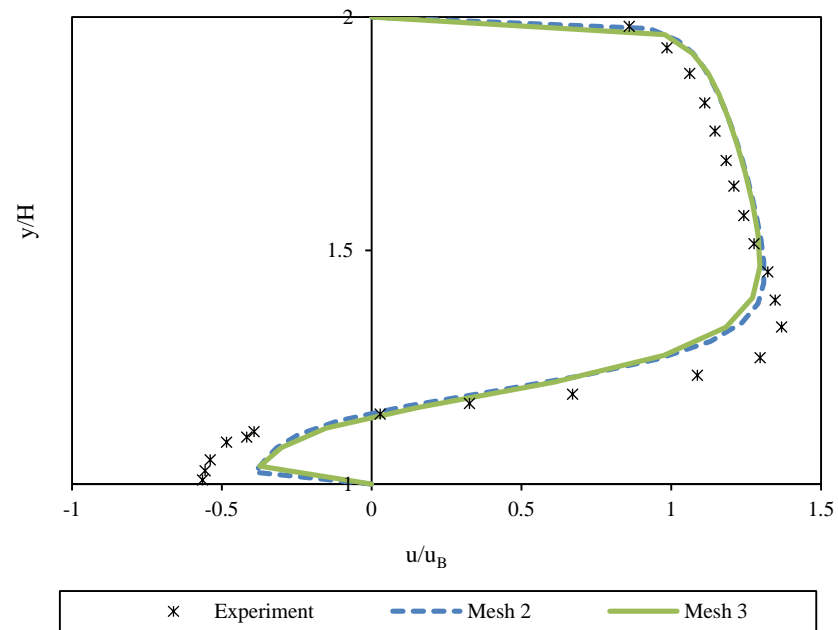


Figure 3.10 Comparison of mean streamwise velocity profiles in the symmetry line $x/H = 0.5$ using RSM

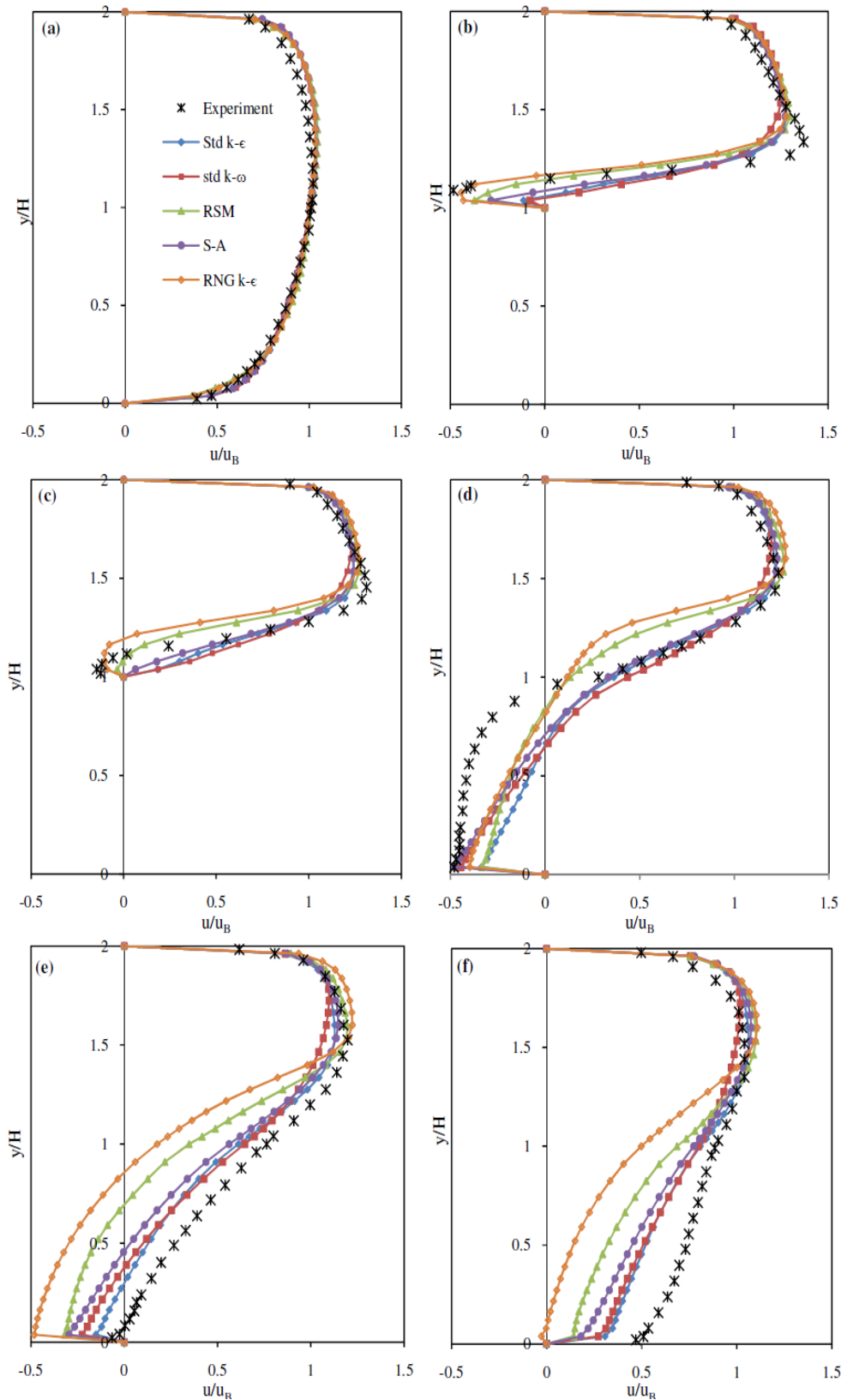


Figure 3.11 Comparison of the mean streamwise velocity profiles of Mesh 3 in the symmetry line (a) $x/H = -1.0$, (b) $x/H = 0.5$ (c) $x/H = 1.0$, (d) $x/H = 1.5$, (e) $x/H = 2.5$ and (f) $x/H = 4.0$. Legends are the same in all plots

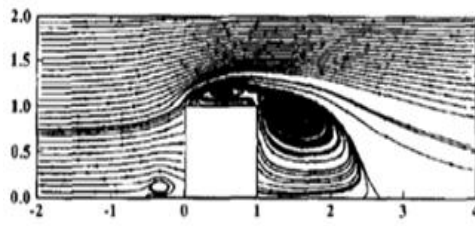
Figure 3.11(d) - 18(f) show the mean streamwise velocity profiles downwind of the cube starting with recirculation and leading to reattachment, as the flow recovers from separation at the front face and on top of the cube due to an adverse pressure gradient introduced by the cube in the flow path. All RANS turbulence models, particularly RSM and RNK $k-\varepsilon$, underpredict the flow recovery.

The simulated flow predicts a larger recirculation region and recovers later than what is observed in the experiment of Martinuzzi and Tropea (1993). Standard $k-\varepsilon$ together with standard $k-\omega$ model performed comparatively better. A similar underprediction of flow recovery is obtained by Lakehal and Rodi (1997) using various versions of the $k-\varepsilon$ model with an improvement observed by Shah and Ferziger (1997) employing the more computationally expensive LES.

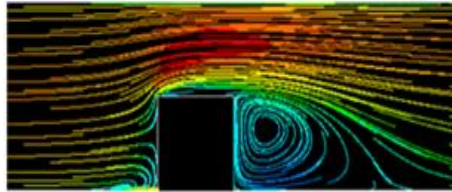
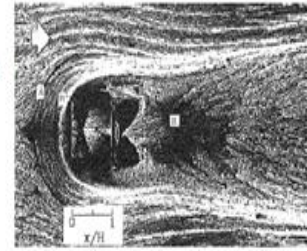
The vortex structures of the flow are investigated by comparing streamlines generated using different RANS turbulence models in FLUENT, with that of the experimental oil-film visualisation (Martinuzzi and Tropea, 1993) as illustrated in Figure 3.12. The separation and recovery regions of the flow can be compared qualitatively and the most accurate turbulence models can be identified.

For the front and upper separation regions, RSM and RNG $k-\varepsilon$ give better agreement by reproducing a larger vortex on top of the cube and a front separation length, X_F closer to the experimental observation. This is supported by the discussion of the velocity profiles as mentioned earlier [See Figure 3.11(b)].

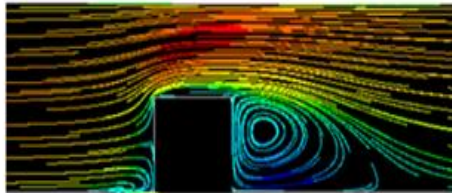
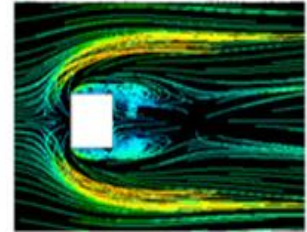
The flow recirculation behind the cube is overpredicted in all cases resulting in a larger reattachment length which consequently underpredicts flow recovery. Standard $k-\varepsilon$ performs better than the other models in capturing this region, with a reattachment length, X_R nearest to the experimental results, as can be seen in Figure 3.12 and Table 3.1.



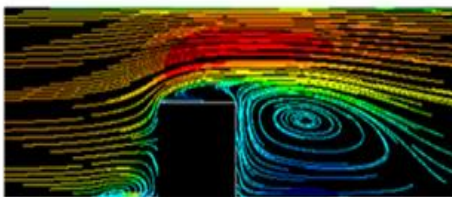
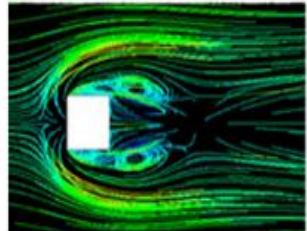
Experiment by Martinuzzi et al. (1993) reproduced with kind permission of ASME.



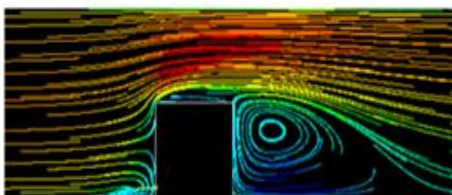
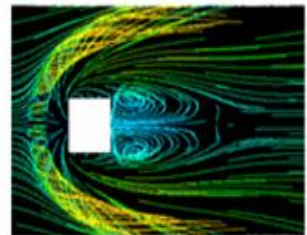
Standard k-ε



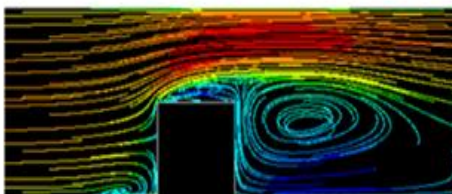
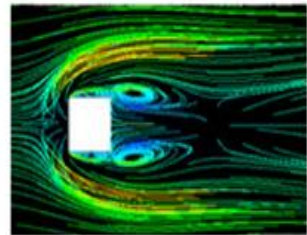
Standard k-ω



Reynolds Stress Model (RSM)



Spalart Allmaras (SA)



RNG k-ε

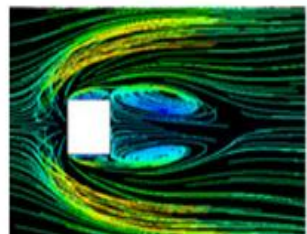


Figure 3.12 Comparison of streamlines in symmetry plane $z/H = 0$ (left) and first cell from bottom wall (right)

Table 3.1 Summary of frontal separation (X_F) and reattachment lengths (X_R) for a wall-mounted cube by different turbulence models

Turbulence Models	$X_F(H)$	$X_R(H)$
Experiment (Martinuzzi et al., 1993)	1.040	1.612
Std $k-\varepsilon$	0.69	1.98
Std $k-\omega$	0.68	2.05
RSM	0.70	2.40
SA	0.68	2.12
RNG $k-\varepsilon$	0.72	2.54

3.5 Conclusion

The present chapter outlines guidance on selecting the appropriate mesh configuration and corresponding turbulence model based on the computed wall y^+ and demonstrates its applicability for use in any generic problem related to wall-bounded turbulent flows, including flow in urban and industrial complexes. This is achieved by comparing the numerical simulation of flow over a cube against experimental data by Martinuzzi and Tropea (1993).

Contrary to what one might assume, having a higher mesh resolution (i.e. finer mesh) does not necessarily mean that the numerical accuracy would improve, albeit increasing the computational expenditure. Take for example the case for high Reynolds number flow. It has been demonstrated that when using RSM or standard $k-\varepsilon$, resolving into the log-law region ($y^+ > 30$) produces better results as opposed to having a very fine mesh resolving all the way into the viscous sublayer ($y^+ < 5$).

The wall y^+ approach is implemented in the selection of the appropriate mesh configuration in the study of airflow and pollutant dispersion within urban street canyons both in the absence and presence of trees.

4 WIND TUNNEL EXPERIMENT

This chapter describes the experimental wind tunnel (WT) set up, boundary conditions and tree crown modelling, on which the numerical investigations builds on and numerical (i.e. CFD) results are compared against.

4.1 Experimental Setup

An extensive wind tunnel (WT) experimental database has been established at the Laboratory of Building and Environmental Aerodynamics, Karlsruhe Institute of Technology (KIT). The database is known by the acronym CODASC which stands for Concentration Data of Street Canyon. Wind tunnel concentration data are accessible to the scientific community with interest in validating numerical analyses and other experimental investigations and can be found online at www.codasc.de (CODASC, 2008). The experimental setup and results have also been presented and discussed in the works of Gromke and Ruck (2007, 2009). **Appendix A** shows a screenshot of the online database.

The test section (Figure 4.1) is 2 m wide, 1 m high, 2 m long and covered by an adjustable ceiling allowing for compensation of pressure losses in the streamwise direction. By means of vertical Irwin-type vortex generators, a horizontally ground-mounted tripping device and a fetch of 6 m length covered with roughness elements, an atmospheric boundary layer flow, typical for urban environment, was generated.

Flow field and concentration level measurements were performed for a scale street canyon in the atmospheric boundary layer WT. A boundary layer flow with mean velocity, $u(z)$ profile exponent, $\alpha = 0.30$ and turbulence intensity, I_u profile exponent, $\alpha_I = 0.36$, according to the power law formula were reproduced in the test section

$$\frac{u(z)}{u(z_{ref})} = \left(\frac{z}{z_{ref}} \right)^\alpha,$$

and

$$\frac{I_u(z)}{I_u(z_{ref})} = \left(\frac{z}{z_{ref}} \right)^{-\alpha_I}.$$

A flow velocity of $u(z_{ref}=H) = 4.70 \text{ ms}^{-1}$ (H being building height) was obtained. In the test section, a 1:150 scaled model of an isolated street canyon of length $L = 180 \text{ m}$ and street width $W = 18 \text{ m}$ with two flanking buildings of height $H = 18 \text{ m}$ and width $B = 18 \text{ m}$ was mounted perpendicular to the approach flow. The Reynolds number of the main flow was $Re_H = 50,000$ calculated using the main stream velocity and building height ensuring a Reynolds number independent flow. For more comprehensive information on the simulated atmospheric boundary layer flow, including data on the integral length scale profile, $L_{ux}(z)$ and spectral distributions of turbulent kinetic energy, $S_{uu}(z,f)$ see Gromke and Ruck (2005).

Integrated in the model street, line sources, designed according to the method described by Meroney et al. (1996), were used for simulating the release of traffic exhausts. In this approach, tracer gas streamed in a line-like chamber mounted below the model setup with openings facing the street side. The homogeneity of the line sources were assured by small, equidistantly spaced openings with a high pressure drop, making the tracer gas release independent of local and instantaneous pressure fluctuation at street level. In order to account for the traffic exhausts released on the sidewise street intersections, the line sources exceeded the street canyon by approximately 10% on each side. The line sources strength was monitored and controlled by a flow meter, ensuring a constant tracer gas supply during the measurements. Tree plantings were placed inside the street canyon arrangement and their influence on the dispersion of traffic exhaust and local flow field were investigated.

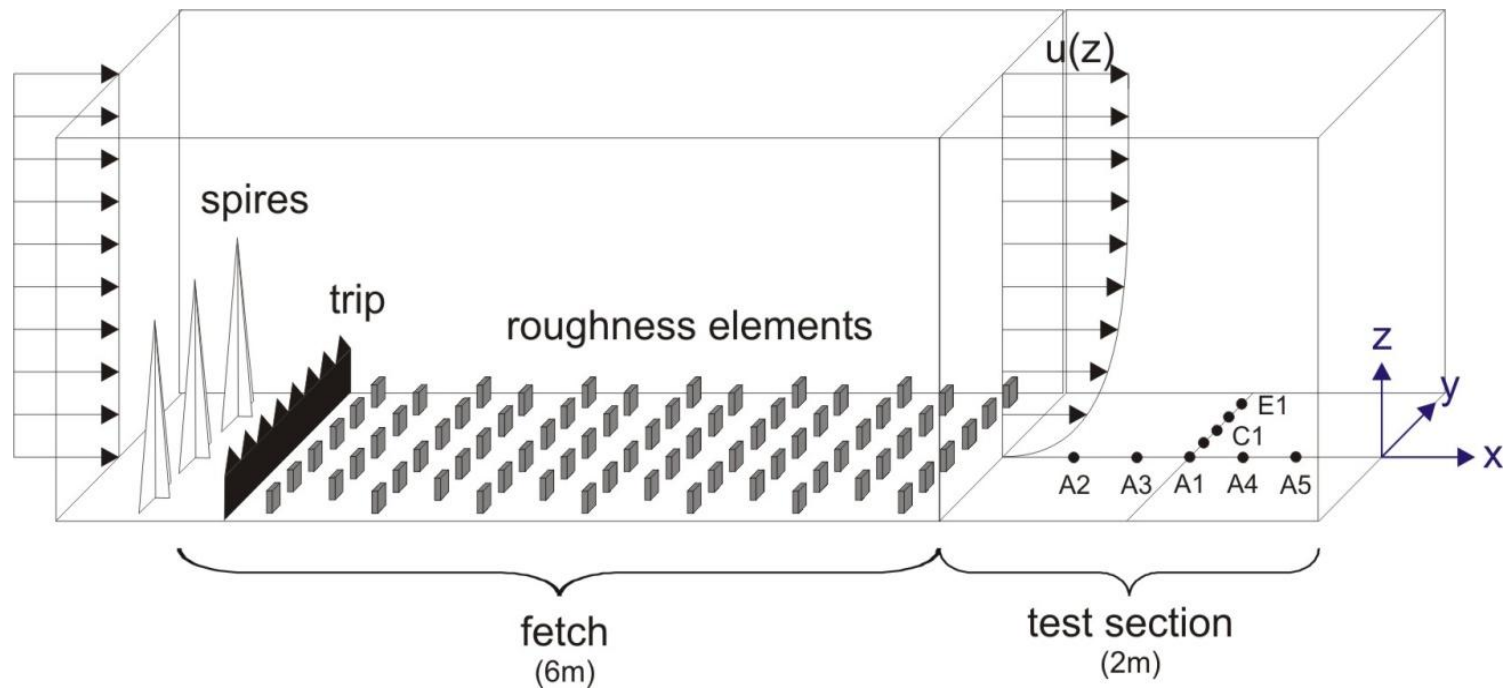


Figure 4.1 Schematic of wind tunnel experimental setup showing the fetch and test sections (CODASC, 2008)

Sulphur hexafluoride (SF_6) was used as tracer gas to simulate the release of traffic exhausts. The emission rate Q was maintained at 10 gs^{-1} . Mean concentrations, C^+ of the gas were measured at the canyon walls and normalised according to

$$C^+ = \frac{Cu_H H}{Q/l},$$

with C measured concentration, u_H flow velocity at height H in the undisturbed approach flow and Q/l tracer gas source strength per unit length. Samples were analyzed by an electron capture detection device.

Figure 4.2 show examples of two real-life street canyon configurations, which are the focus of the present study. Figure 4.3 summarizes the WT setup cases that are used for comparison with the numerical investigations.



Figure 4.2 Real-life street canyons with single row of trees (left) and double row of trees (right)

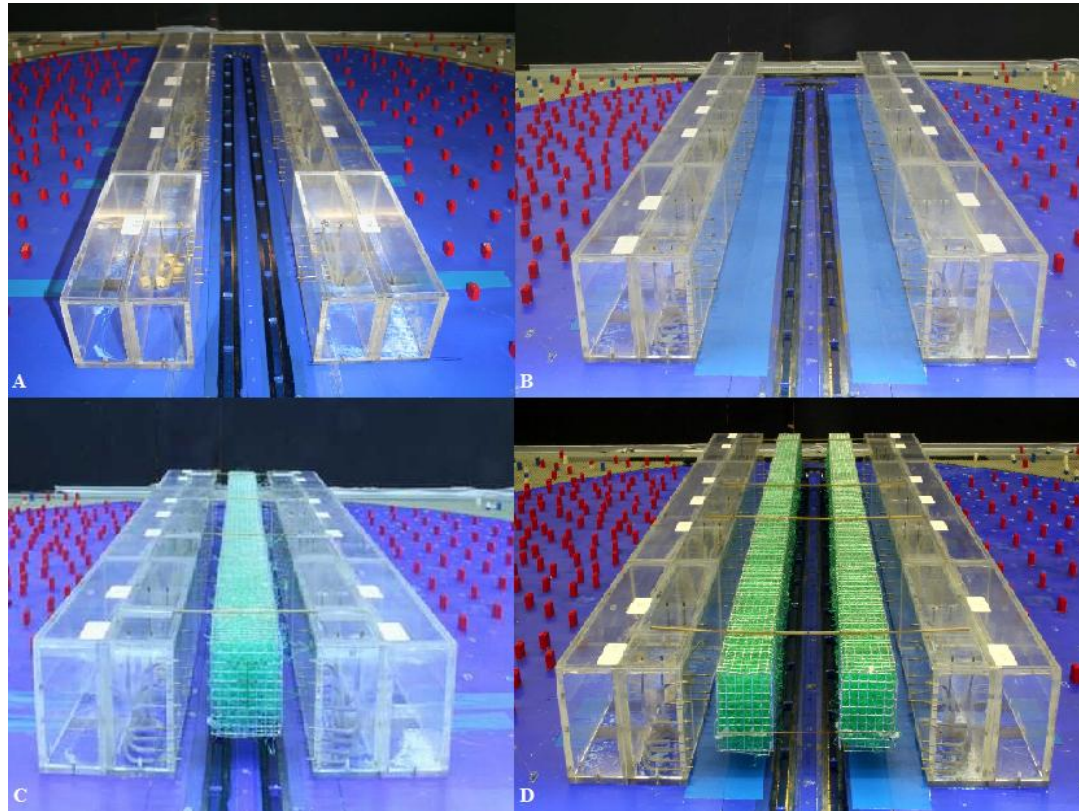


Figure 4.3 The wind tunnel experimental setup with a) $W/H = 1$ for tree-free street canyon, b) $W/H = 2$ for tree-free street canyon, c) $W/H = 1$ with single row of trees and d) $W/H = 2$ with two rows of trees (CODASC, 2008)

4.2 Experimental Tree Crown Modelling

Real trees crowns consist of branches and leaves, which form a porous body that are permeable to airflow. The porosity of real tree crowns, expressed in pore volume fraction [m^3m^{-3}], roughly varies from 93% to 99%, with deciduous trees showing generally larger pore volume fractions than conifers according to research done by Gross (1987), Ruck and Schmitt (1986) and Zhou et al. (2002).

In the WT investigations of Gromke and Ruck (2007, 2009), porous tree crowns were modelled using custom-made lattice cages forming cubes with cross-sections of $0.42 H$ width and $0.67 H$ height. The lattice cages were homogeneously filled with filament/fibre-like synthetic wadding materials to facilitate uniform distribution of the wadding materials (see Figure 4.4).

Pore volume fractions of $P_{vol} = 96\%$ (densely filled) and $P_{vol} = 97.5\%$ (loosely filled), typical of deciduous trees were modelled. The height of the branch free trunk was $1/3 H$ in all cases.



Figure 4.4 Close-up of wind tunnel tree crown model (for $W/H = 1$)
(CODASC, 2008)

In the WT experiment, the aerodynamic characteristics of the tree crowns were described by a pressure loss coefficient, λ [m^{-1}] evaluated in forced convection conditions according to

$$\lambda = \frac{\Delta p_{stat}}{p_{dyn}d} = \frac{p_{windward} - p_{leeward}}{(1/2)\rho u^2 d},$$

with Δp_{stat} the difference in static pressure of the windward and leeward sides of the porous obstacle, p_{dyn} the dynamic pressure, u the mean streamwise velocity and d the porous obstacle thickness in the streamwise direction. Measurements resulted in pressure loss coefficients of $\lambda = 200 \text{ m}^{-1}$ and $\lambda = 80 \text{ m}^{-1}$ for the cases of $P_{vol} = 96\%$ and $P_{vol} = 97.5\%$, respectively (Gromke et al., 2008).

5 SIMULATION SETUP

The domain discretization, boundary conditions treatment, flow simulation setup, dispersion modelling, and tree crown modelling of the numerical investigations are presented in this chapter. The simulations are performed in the CFD commercial code FLUENT.

The wall y^+ approach described in Chapter 3 is implemented in selecting the appropriate mesh configuration. Treatment of the wall roughness in relation to horizontal homogeneity is also examined.

A User Defined Function (UDF) is programmed in C Language and interpreted in the CFD code for the inlet boundary conditions in the numerical investigations.

5.1 Computational Domain and Boundary Conditions

5.1.1 Geometry and Mesh Setup

Numerical simulations are performed using FLUENT with the aim of reproducing the aforementioned WT experiments focusing on the concentration distribution within street canyons of $W/H = 1$ and $W/H = 2$. This is done to compare the prediction accuracy between RANS (standard $k-\varepsilon$ and RSM) and LES, and to investigate the aerodynamic impacts of trees on the airflow and pollution dispersion.

The research also includes examining the mesh (i.e. spatial) and temporal resolution sensitivity on the prediction accuracy.

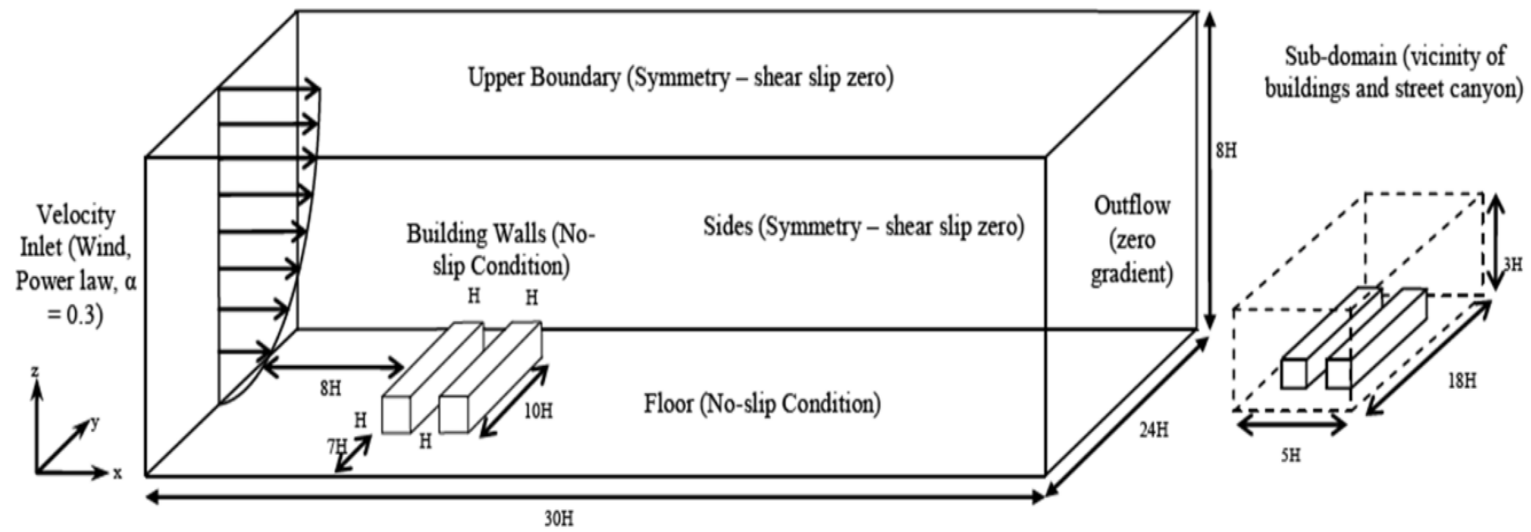


Figure 5.1 Computational domain and boundary conditions for the CFD simulation setup

An inlet boundary condition is defined at the entrance. Non-slip conditions are applied for the building walls and floor. Symmetry conditions are specified for the top and lateral sides of the computational domain to enforce a parallel flow and to reduce the computational cost as the faces are sufficiently far from the street canyon to affect the main flow.

At the face downwind of the obstacles, where the flow leaves the computational domain, an outflow boundary condition is imposed to force all the derivatives of the flow variables to vanish, resulting in a fully developed flow. These are based on recommendations from the COST Action (Britter and Schatzmann, 2007), and are verified in the proceeding section.

The computational domain and boundary conditions are summarized in Figure 5.1.

The domain is discretized using hexahedral elements incorporating recommendations based on the wall y^+ approach presented in Chapter 3. The Reynolds number of the main flow is $Re_H = 50,000$. A $y^+ > 30$ is selected for the meshes in order to resolve the log-law region because wall functions work best for the selected RSM and standard $k-\varepsilon$ turbulence models.

The computed wall y^+ for the selected mesh configuration (i.e. Mesh B) is demonstrated in Figure 5.2. (The region between 7.5 and $11 H$ is where the street canyon is positioned).

Three meshes are generated to assess the grid dependence and are summarized in Table 5.1. Approximately half of the total cells are placed in the sub-domain defining the vicinity of the buildings and street canyon (see Figure 5.1 – with a volume of $250 H^3$). This imposes a finer mesh resolution in the region of interest, where large gradients in the flow variables exists i.e. separation, reattachment and recirculation.

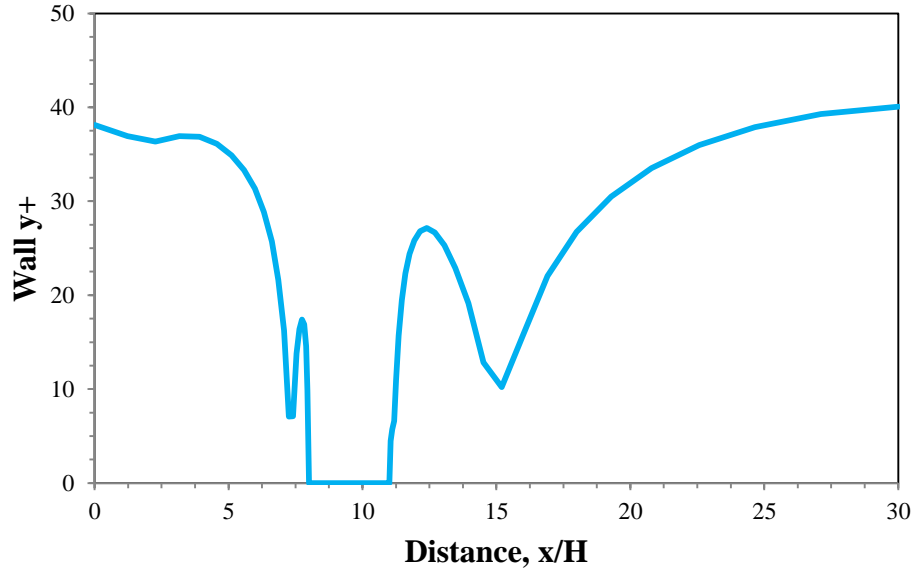


Figure 5.2 Wall y^+ for the generated meshes (shown for Mesh B)

Cell stretching (i.e. use of successive ratio) particularly within the sub-domain is avoided since no homogeneous direction exists in the flow, and therefore, equal spatial resolution is imposed in all directions. **Appendix B** shows a sample of the mesh generation procedure performed using GAMBIT, which is the pre-processor to FLUENT.

Table 5.1 Mesh Resolution for the computational domain

Mesh identity	Minimum grid spacing	Cell count in canyon	Total cell count
Mesh A (Coarse)	$\Delta x = \Delta y = \Delta z = 0.1 H$	250,000	538,000
Mesh B (Fine)	$\Delta x = \Delta y = \Delta z = 0.077 H$	598,246	1,111,246
Mesh C (Finest)	$\Delta x = \Delta y = \Delta z = 0.067 H$	728,568	1,569,242

Investigation with both RANS and LES indicate that Mesh B provides more accurate computational results as opposed to Mesh A, albeit having twice the computational cost. The improvement obtained from simulations with a finer spatial resolution (i.e. more cells) in Mesh C does not warrant the additional cost because results do not improve significantly. **Appendix C** provides a snapshot of the grid independence study performed.

5.1.2 Inlet Boundary Condition

In order to replicate the WT experiment, the inlet wind velocity is represented in the power law profile form

$$u(z) = 4.7 \left(\frac{z}{0.12} \right)^{0.3} \text{ ms}^{-1},$$

while turbulent kinetic energy and dissipation rate profiles are specified as

$$k = \frac{u_*^2}{\sqrt{C_\mu}} \left(1 - \frac{z}{\delta} \right),$$

and

$$\varepsilon = \frac{u_*^3}{\kappa z} \left(1 - \frac{z}{\delta} \right),$$

where δ is the boundary layer depth (≈ 0.5 m), $u_* = 0.54 \text{ ms}^{-1}$ is the friction velocity (known from log-law curve fitting of WT mean velocity profile), κ the von Kàrmàn constant ($= 0.4$) and $C_\mu = 0.09$.

A User Defined Function (UDF) is compiled using C language and interpreted in FLUENT to implement these boundary conditions into the simulation. The concatenated source code is presented in **Appendix D** defining the velocity, turbulent kinetic energy and dissipation rate profiles.

The resulting vertical distributions of quantities, specifically the velocity profile and turbulent kinetic energy (TKE), at the inlet are presented in Figure 5.3. The simulated (i.e. UDF) profiles match closely to the actual WT conditions.

The velocity, turbulent kinetic energy and turbulent dissipation rate profiles are also shown in Figure 5.4, Figure 5.5 and Figure 5.6, respectively for a flow development in an ‘empty’ computational domain, which demonstrate the implemented boundary conditions resulted in a fully developed turbulent flow at the exit boundary

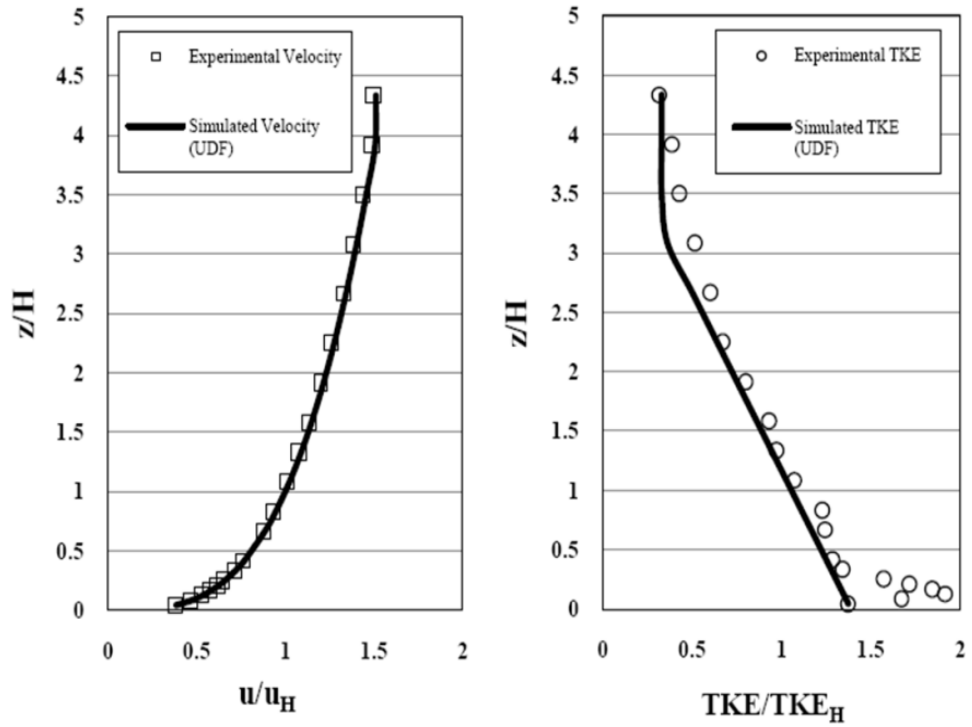


Figure 5.3 Velocity and turbulent kinetic energy (TKE) profiles for the inlet boundary condition comparing UDF and experimental profiles

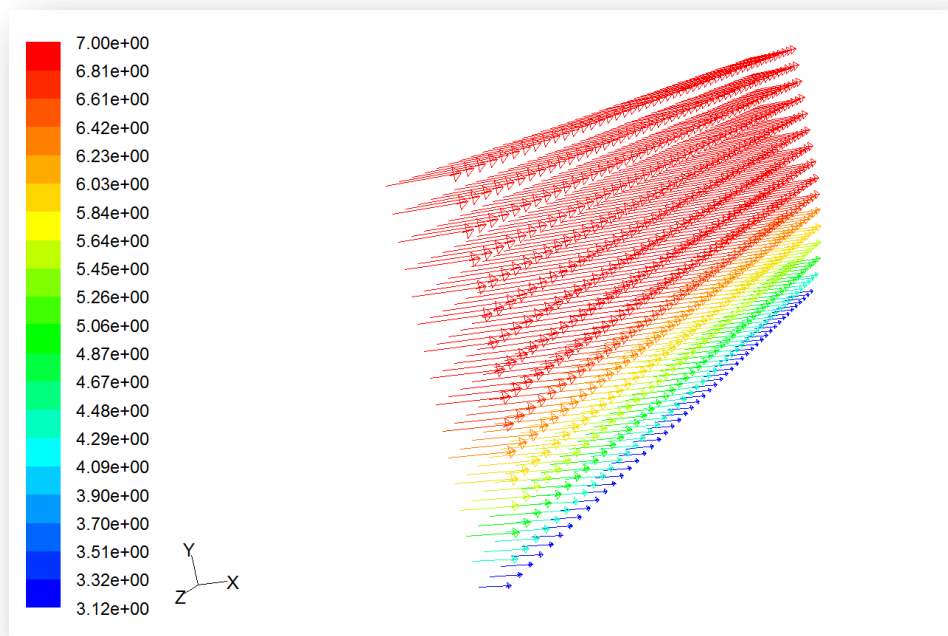


Figure 5.4 Velocity vectors coloured by magnitude

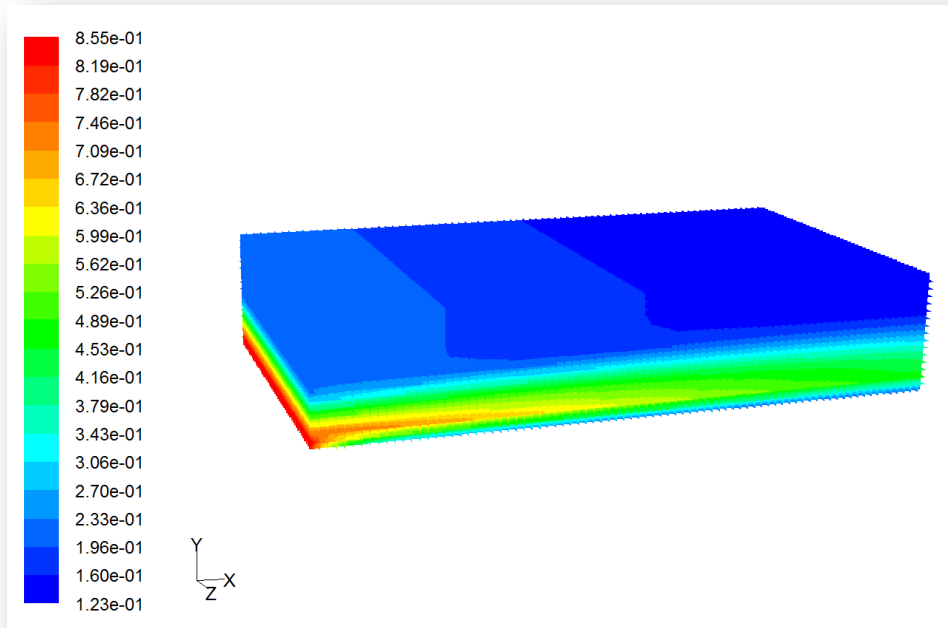


Figure 5.5 Contours of turbulent kinetic energy, k

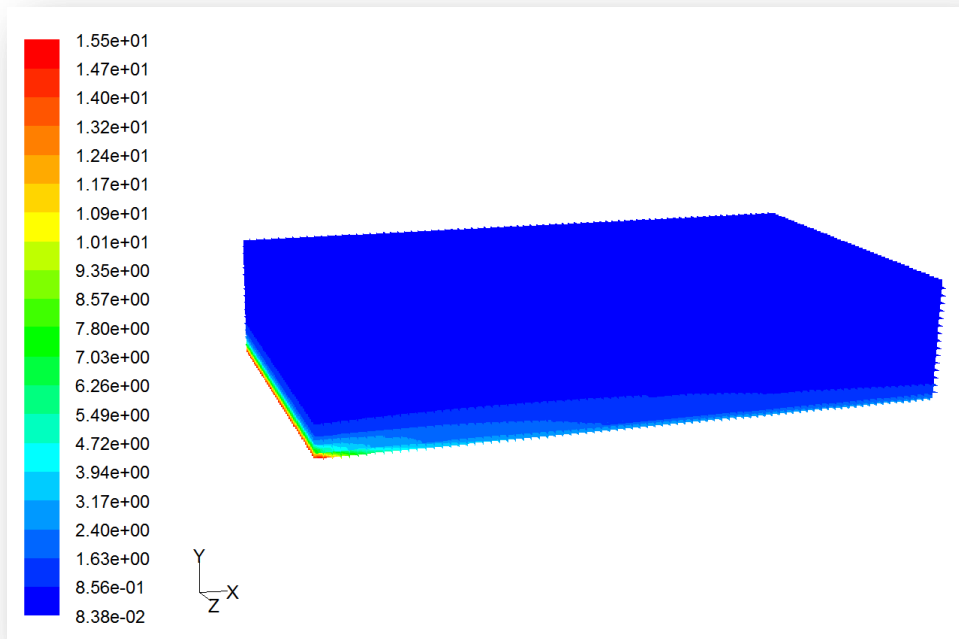


Figure 5.6 Contours of turbulent dissipation rate, ϵ

FLUENT inbuilt spectral synthesiser is used to convert the converged mean flow solution obtained from RANS computation for use in LES. The spectral synthesiser (Smirnov et al., 2001) creates an unsteady flow field by superimposing turbulence on top of the mean flow field in order to translate the initial and boundary conditions defined for the RANS simulation for use in LES, thus reducing the computational cost and time.

5.1.3 Wall Roughness

Horizontal homogeneity of the turbulent boundary layer is achieved with the present conditions on examination in an ‘empty’ computational domain. The term “horizontal homogeneity” refers to the absence of streamwise gradients in the vertical profiles of the mean wind velocity and turbulence quantities, i.e. inlet profiles are maintained with downstream distance as discussed by Blocken et al. (2007a, 2007b).

In FLUENT, the surface roughness is expressed in terms of a sand grain roughness, K_s , instead of the aerodynamic roughness, z_0 as is the case in most meteorological codes.

In order to circumvent problems with a coarse grid resolution near the ground due to a large sand grain roughness value, Gromke et al. (2008) set K_s equal to aerodynamic roughness length, z_0 which was found to be $z_0 = 0.0033$ m in the WT experiment. They agreed that setting $K_s = z_0$ was not correct in a strong sense but justified the choice from the results obtained.

Only minor reduction (about 10% of the inlet values) in the velocity profiles up to the location of the streamwise building occurred for both standard $k-\varepsilon$ and RSM. The predicted turbulence intensity tended to become smaller near the ground ($z/H < 1$), where less than 10% change were found, within range of those recommended by Blocken et al. (2007a, 2007b)

Figure 5.7 shows the velocity profile at different downstream locations ($x/H = 0, 2, 4, 6, 8, 10$ and 12) for simulations between a smooth and rough wall for the present study. It can be observed that for a smooth wall, the velocity profile

is not maintained downstream, as opposed to flow over a rough wall, which is free of streamwise gradients.

Similar wall roughness parameters as Gromke et al. (2008) are specified for the present RANS simulations, but the ground is treated as smooth in LES by default in FLUENT.

To identify to what extent this would affect the prediction accuracy in LES since wall roughness could not be specified in FLUENT, an investigation is carried out comparing concentration data between a smooth and rough wall for the ‘built-up’ domain (i.e. including the street canyon), validated against WT measurements.

In order to compare against the WT measurements, the numerically obtained pollutant concentrations were normalized according to

$$C^+ = \frac{Cu_H H}{Q/l}.$$

with C measured concentration, u_H flow velocity at height H in the undisturbed approach flow and Q/l tracer gas source strength per unit length.

It is demonstrated in Figure 5.8 that for both standard $k-\varepsilon$ and RSM, the concentrations at Wall A (leeward) and Wall B (windward) did not vary much between assumptions of a smooth and rough wall, with only slight improvements in prediction obtained when accounting for roughness. This verifies that although the roughness influences the horizontal homogeneity of the approach flow in an ‘empty’ domain, its effects are negligible within the ‘built up’ domain.

The observation could be explained by the fact that the impact of the buildings (macro-scale roughness) overwhelmed the minor effects of the ground roughness (micro-scale), due to the large Reynolds number of the main flow and the domination of the large-scale eddies – i.e. separation, recirculation and reattachment within the canyon.

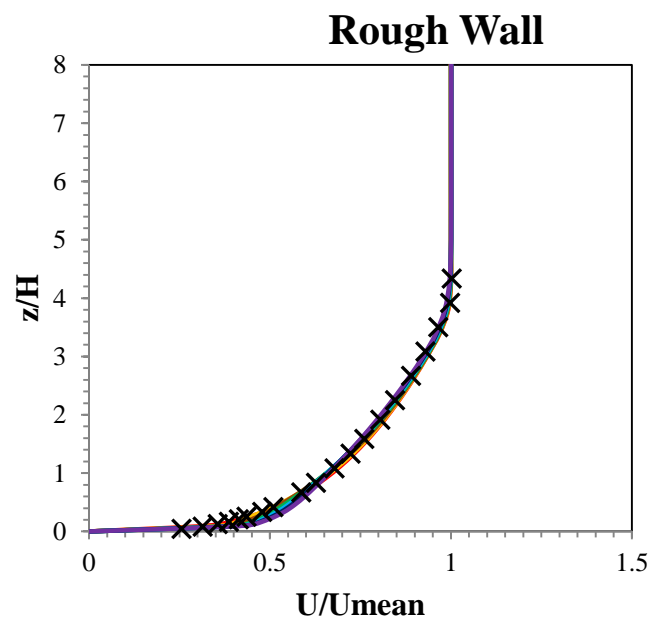
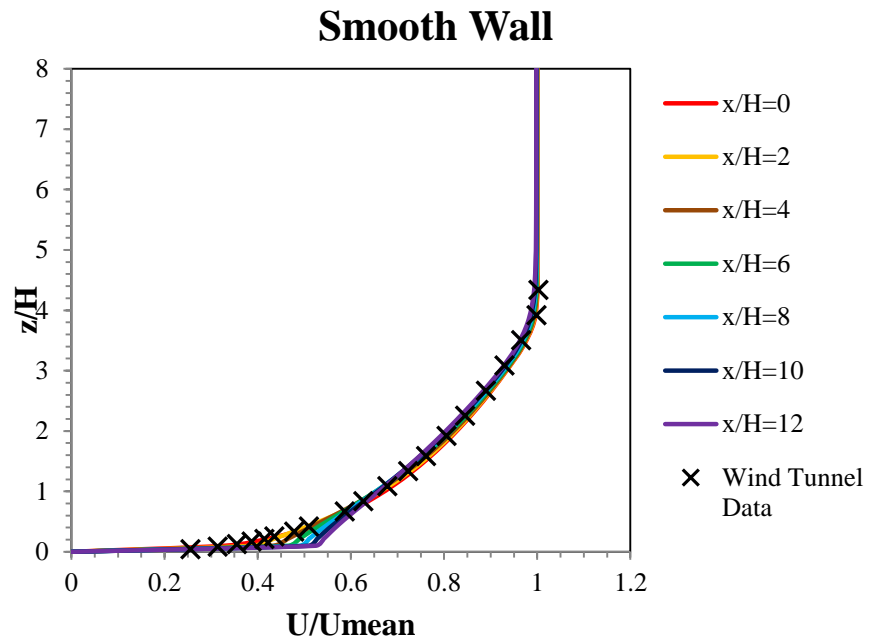


Figure 5.7 Horizontal homogeneity between a smooth and rough wall performed using RSM. Legends are same in both graphs

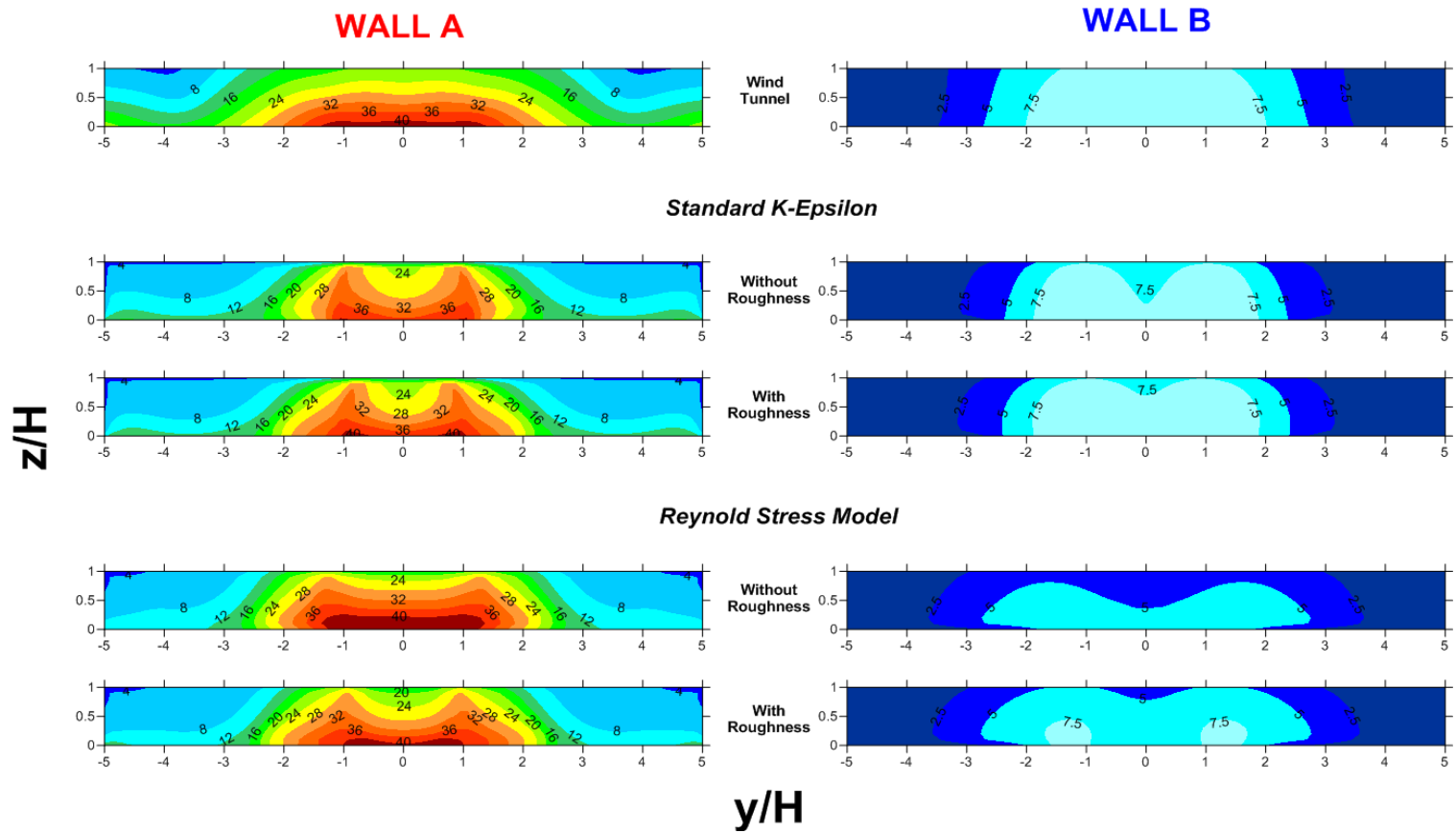


Figure 5.8 Comparison of pollutant prediction at Wall A (leeward) and Wall B (windward) between a smooth and rough wall for the RANS simulations against WT data

5.2 Flow Simulation

The steady-state RANS mean solutions are obtained using standard $k-\varepsilon$ and RSM turbulence models. A second order upwind numerical scheme is employed for all transport equations to reduce numerical diffusion except for pressure, where *Standard* interpolation is used instead. The scaled residual criteria for all flow properties are set at 1×10^{-5} and pressure-velocity coupling is achieved using *SIMPLE*.

In LES, the dynamic Smagorinsky-Lily SGS model together with the bounded central differencing scheme for momentum, second order time-advancement and second order upwind for species and energy transport equations are selected. *PRESTO* and *SIMPLEC* are selected for pressure and pressure-velocity coupling, respectively. Convergences for the scaled residuals are set at 1×10^{-3} .

Following the work of Cai et al. (2008), the turnover time of the primary circulation, t_c , in the canyon is of the order of

$$t_c = \frac{W + H}{U_c},$$

where U_c is the velocity scale of the mean wind in the canyon which is found to be $\sim 0.14 \text{ ms}^{-1}$ resulting in a value of $t_c = 2 \text{ s}$. Initially, the simulation is performed for 33 flow-through time ($T_f = L/U_b$ with L being the streamwise length of the domain and U_b the bulk velocity) corresponding to $10 t_c$. Statistically steady-state is achieved at this point. The flow statistics are then reset, and the simulation is performed for a further 33 flow-through time ($= 10 t_c$) to ensure that the final time-averaged results are independent of the initial conditions.

A check is done comparing the mean solutions obtained from an average of 50 flow-through time ($= 15 t_c$) to 33 flow-through time ($= 10 t_c$), and it is observed that both symmetry and mean flow property magnitudes do not vary between the two sampling sizes, further supporting the fact that the solution has

achieved statistically stationary state. Therefore, neither further iterations nor reduction in time-step size are necessary.

In addition, a time resolution, $\Delta t/T_b$ (with Δt the time-step size and $T_b = H/U_b$) sensitivity is performed for LES i.e. different time-step sizes, Δt are investigated, maintaining the same number of flow-through time, T_f and turnover time, t_c . This is summarized in Table 5.2.

Table 5.2 Temporal resolution for LES

Temporal resolution $\Delta t/T_b$	Study performed on corresponding mesh	Total number of dimensionless time- steps
1/4	Mesh A	8,000
1/8	Mesh A & Mesh B	16,000
1/16	Mesh B & Mesh C	32,000

On investigating various resolutions with different meshes, a temporal resolution of 1/8 was chosen, as its prediction accuracy was much better than 1/4, whereas 1/16 did not result in any significant improvement albeit requiring twice the number of dimensional time-steps, translating to nearly twice the computational effort.

The cell Courant number was less than 0.5 within the street canyon and in the upstream and downstream vicinity of the buildings. All simulations were performed in parallel on an Intel® Xeon® workstation (4 CPUs).

A typical simulation with standard $k-\varepsilon$ took approximately 2 hours, RSM about 48 hours, and LES four weeks to obtain stable flow statistics.

Numerically predicted vertical flow velocities, $u(z)$ were normalised by the velocity of the undisturbed flow u_H according to

$$w = \frac{u(z)}{u_H}.$$

5.3 Dispersion Modelling

In turbulent flows, FLUENT models the dispersion of airborne material by computing the mass diffusion, J based on the advection-diffusion (AD) method as

$$J = -\left(\rho D + \frac{\mu_t}{Sc_t}\right)\nabla Y,$$

where D is the molecular diffusion coefficient for the pollutant in the mixture, μ_t is the turbulent eddy viscosity, Y is the mass fraction of the pollutant, ρ is the mixture density. In RANS the turbulent viscosity is computed as

$$\mu_t = \rho \left(\frac{C_\mu k^2}{\varepsilon}\right),$$

whereas in LES the subgrid-scale turbulent viscosity is used instead, defined as

$$Sc_t = \frac{\mu_t}{\rho D_t}$$

where Sc_t is turbulent Schmidt number and D_t is the turbulent diffusivity. Default values of $Sc_t = 0.7$ are used and fine tuning is avoided as recommended by Rossi and Iaccarino (2009), where they examined the literature and explained that altering the turbulent Schmidt number is problem dependent and thus not encouraged. Previous numerical studies by Gromke et al. (2008) and Tominaga and Stathopoulos (2009), amongst others, artificially varied Sc_t to improve the diffusivity and obtain closer match to experimental measurements.

The line sources are simulated by ear-marking sections of the volume in the geometry and defining them as separate fluid zones at the required discharge positions. SF₆ source terms with emission rate $Q = 10 \text{ gs}^{-1}$ are then set for these zones to replicate the WT experiment.

5.4 Tree Crown Modelling

Similar to the line sources, the tree crowns are modelled by demarcating sections of the volume in the geometry and defining them as separate porous zones at the desired positions, then assigning pressure loss coefficients, λ to these regions.

In FLUENT, the porous media model adds a momentum sink to the standard fluid flow equations, incorporating an empirically determined flow resistance in the region of the computational domain (i.e. fluid zone defined as porous), which are determined to be $\lambda = 80$ and 200 m^{-1} from the WT measurements.

The source term (acting as momentum sink in this case) is composed of two parts: a viscous loss term (Darcy, the first term on the right-hand side) and an inertial loss term (the second term on the right-hand side),

$$S_i = - \left(\sum_{j=1}^3 D_{ij} \mu v_j + \sum_{j=1}^3 C_{ij} \frac{1}{2} \rho |v| v_j \right),$$

where S_i is the source term for the i th (x , y , or z) momentum equation, $|v|$ is the magnitude of the velocity and D and C are prescribed matrices. The momentum sink contributes to creates a pressure drop that is proportional to the fluid velocity (or velocity squared) in the porous cell. FLUENT solves the standard conservation equations for turbulence quantities in the porous medium and turbulence is treated as though the solid medium has no effect on the turbulence generation or dissipation rates. S_i contributes to the turbulent eddy viscosity μ_t as a result of additional strain resulting from the inertial resistance thus further altering the flow field and consequently the pollutant dispersion.

Recalling the WT investigations, the aerodynamic characteristics of the tree crowns are described by pressure loss coefficients $\lambda [\text{m}^{-1}]$ evaluated in forced convection conditions according to

$$\lambda = \frac{\Delta p_{stat}}{p_{dyn}d} = \frac{p_{windward} - p_{leeward}}{(\frac{1}{2})\rho u^2 d},$$

with Δp_{stat} the difference in static pressure of the windward and leeward sides of the porous obstacle, p_{dyn} the dynamic pressure, u the mean streamwise velocity and d the porous obstacle thickness in the streamwise direction. Measurements resulted in pressure loss coefficients of $\lambda = 200 \text{ m}^{-1}$ and $\lambda = 80 \text{ m}^{-1}$ for the case of $P_{vol} = 96\%$ and $P_{vol} = 97.5\%$, respectively (Gromke et al., 2008).

These porosities are selected as they represent majority of real-life tree crown permeability of deciduous trees (Gross, 1987, Ruck and Schmitt, 1986, Zhou et al., 2002).

The position of the trees and line sources in the WT setup and computational domain are illustrated in Figure 5.9 and Figure 5.10 for the configuration of $W/H = 1$ and $W/H = 2$, respectively.

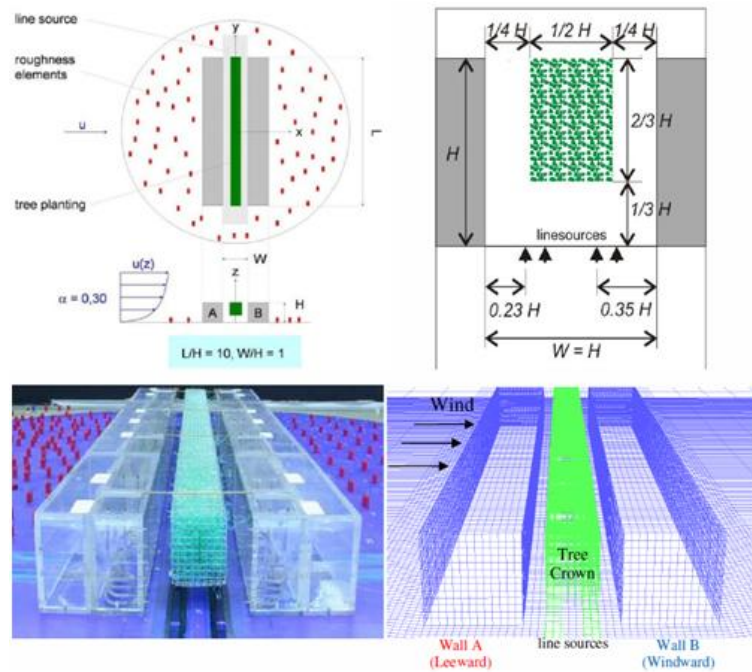


Figure 5.9 Positions of line source and tree planting shown for the WT experiment (CODASC, 2008) and present computational domain for $W/H = 1$

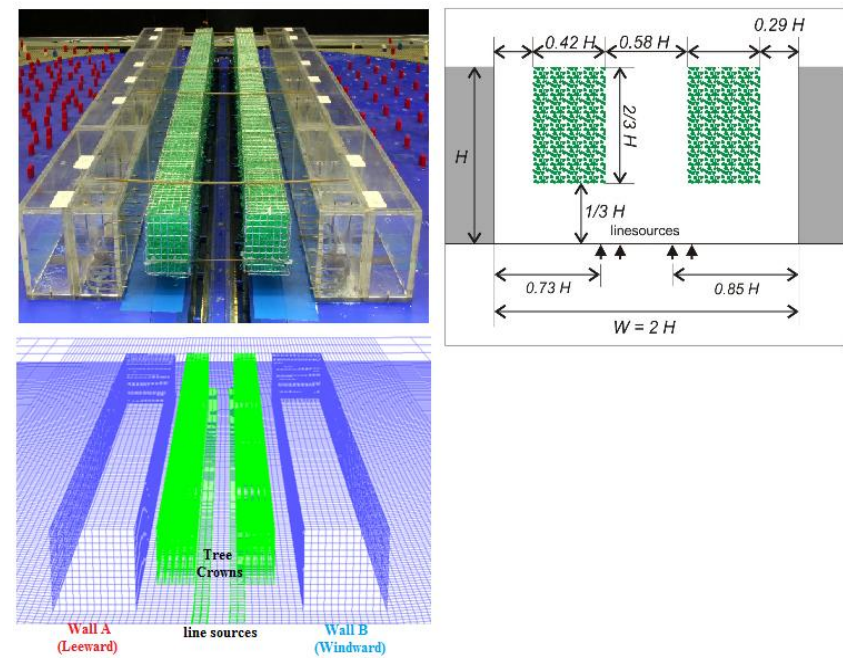


Figure 5.10 Positions of line source and tree planting shown for the WT experiment (CODASC, 2008) and present computational domain for $W/H = 2$

6 TREE-FREE STREET CANYONS

Numerical investigations for tree-free street canyons of $W/H = 1$ and $W/H = 2$ are presented comparing RANS (standard $k-\varepsilon$ and RSM) and LES against WT experimental measurements.

The ability of LES to resolve the instantaneous flow field is demonstrated. In addition, URANS is shown not to be a suitable replacement for LES.

6.1 Comparison between LES and RANS

Mean normalised concentration contours at the canyons leeward (Wall A) and windward (Wall B) walls are presented for tree-free street canyons of $W/H = 1$ and $W/H = 2$ in Figure 6.1 and Figure 6.2, respectively.

Numerical results obtained from RANS ($k-\varepsilon$ and RSM) and LES simulations are compared against WT data. LES results are time-averaged over 8000 non-dimensional time-steps (after initially running for 8000 non-dimensional time-steps and resetting statistics on achieving statistical steady-state), WT concentration data were acquired over a sampling period of 105 seconds and RANS simulations are performed in steady-state.

From a qualitative overview of Figure 6.1 and Figure 6.2, it can be observed that LES performs better than RANS in capturing the spatial distribution of the pollutant for both $W/H = 1$ and $W/H = 2$. This is particularly pronounced in the vicinity of the centreline ($y/H = 0$) at the walls, where the maximum concentration levels occur and is therefore deemed to be the most critical region.

For $W/H = 1$, the standard $k-\varepsilon$ overpredicts the concentration levels at the leeward wall and underpredicts the concentration levels on the windward wall, while RSM underpredicts the concentration levels at the centreline of both walls.

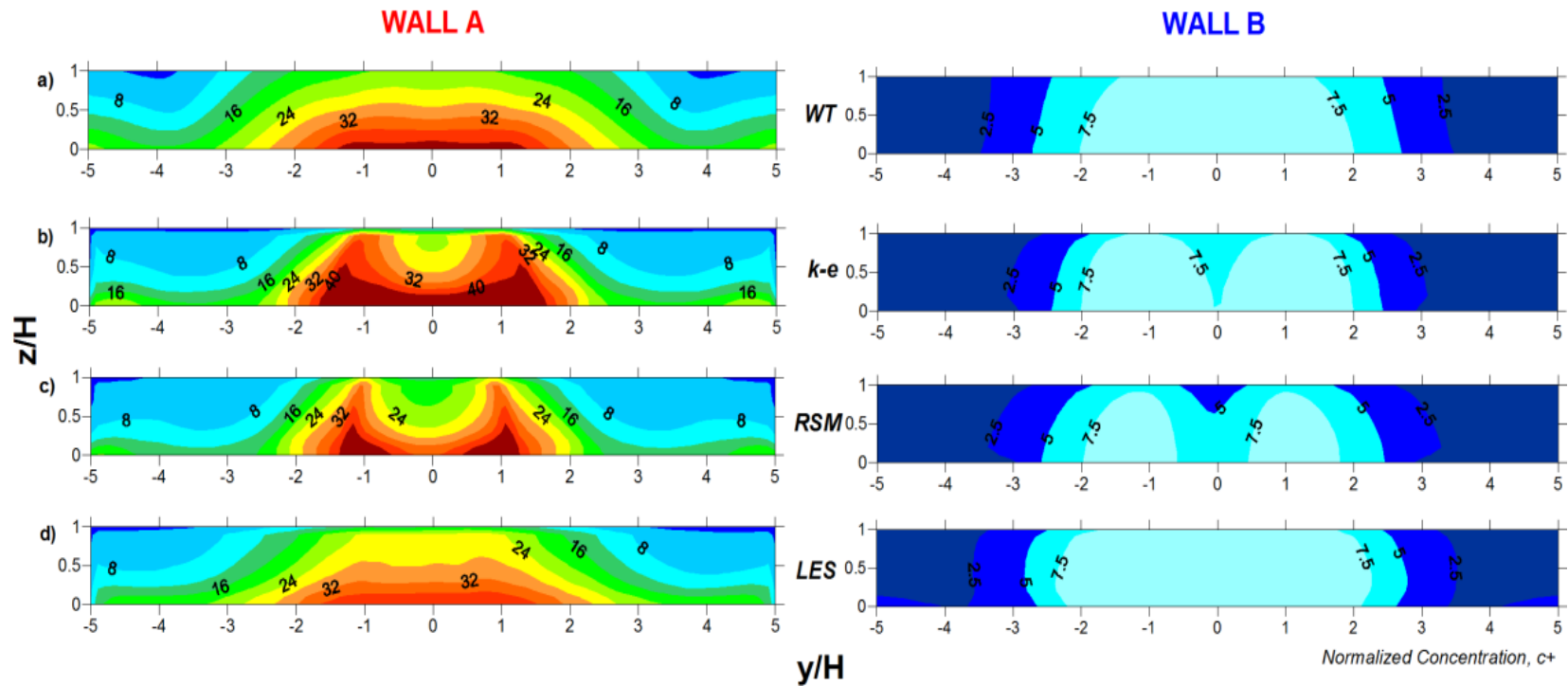


Figure 6.1 Mean normalised concentration data on Wall A (leeward) and Wall B (windward) showing comparison between a) WT data (CODASC, 2008) and numerical results performed with b) standard $k-\epsilon$, c) RSM and d) LES ($W/H = 1$)

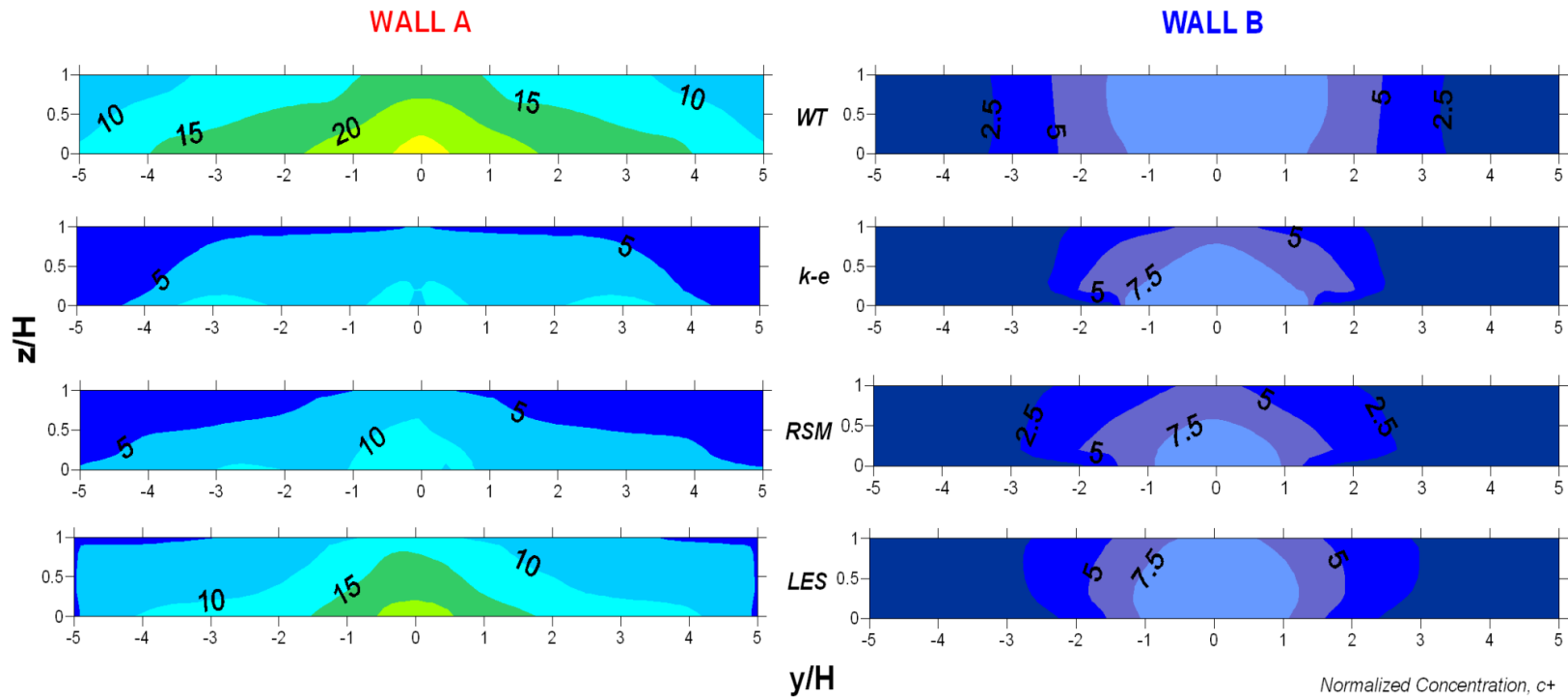


Figure 6.2 Mean normalised concentration data on Wall A (leeward) and Wall B (windward) showing comparison between WT data (CODASC, 2008) and numerical results performed with standard $k-\epsilon$, RSM and LES ($W/H = 2$)

For $W/H = 2$, the standard $k-\varepsilon$ grossly underpredicts the pollutant concentration especially at the leeward wall qualitatively, with RSM showing an improvement in comparison to predictions in $W/H = 1$.

Figure 6.3 and Figure 6.4 graphically presents the quantitative analysis of the concentration profiles at six different vertical locations along both walls (three at each wall: $y/H = 0, 1.26$ and 3.79) for $W/H = 1$ and $W/H = 2$, respectively.

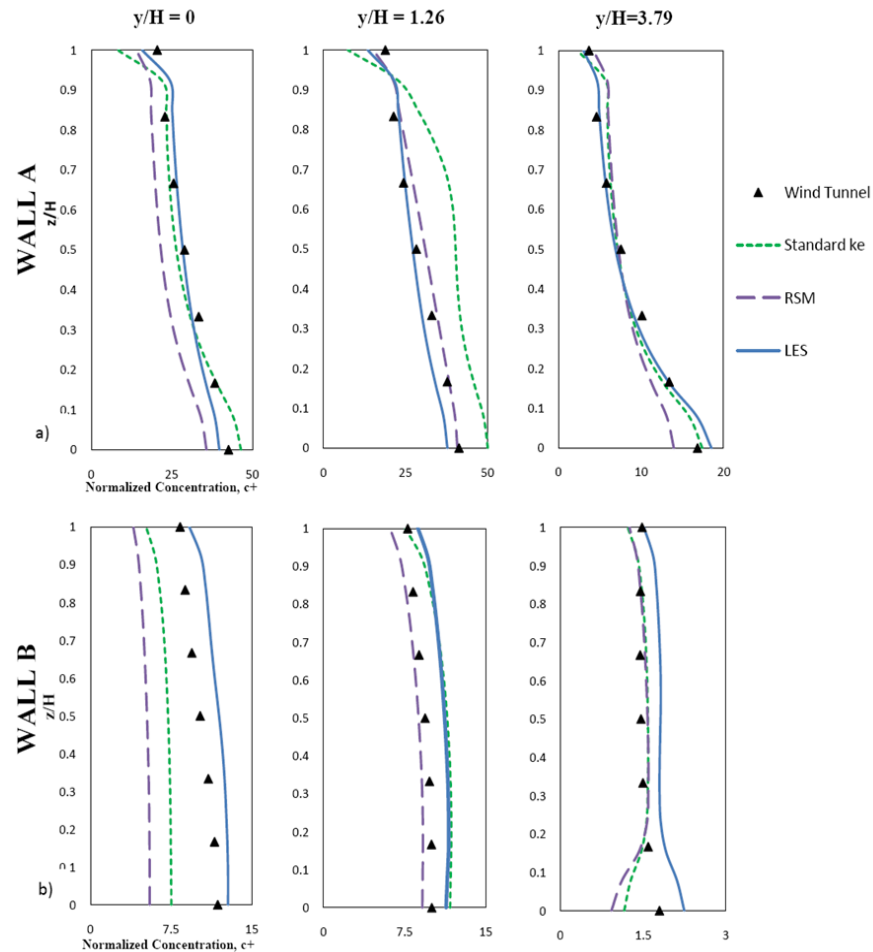


Figure 6.3 Mean concentration profiles at three different locations on a) Wall A (leeward) and b) Wall B (windward) to compare the different numerical results to experimental data ($W/H = 1$). Legends and axis title are the same for all graphs

Starting with analysis of Figure 6.3, not only is LES better at predicting the concentration levels in comparison to RANS, but also provides more consistent results. LES predicts well at all locations along Wall A and only slightly overpredicts at Wall B.

In contrast, RSM underpredicts then overpredicts the concentration levels at some locations along Wall A, and significantly underpredicts at the centreline of Wall B. Standard $k-\varepsilon$ significantly overpredicts along $y/H = 1.26$ at Wall A and considerably underpredicts the concentration level at the centreline of Wall B.

Moving to Figure 6.4, it is observed that similar to $W/H = 1$, LES performs better than RANS in simulating the concentration levels at both walls, albeit slightly underpredicting. In addition LES demonstrates better consistency in the predictions.

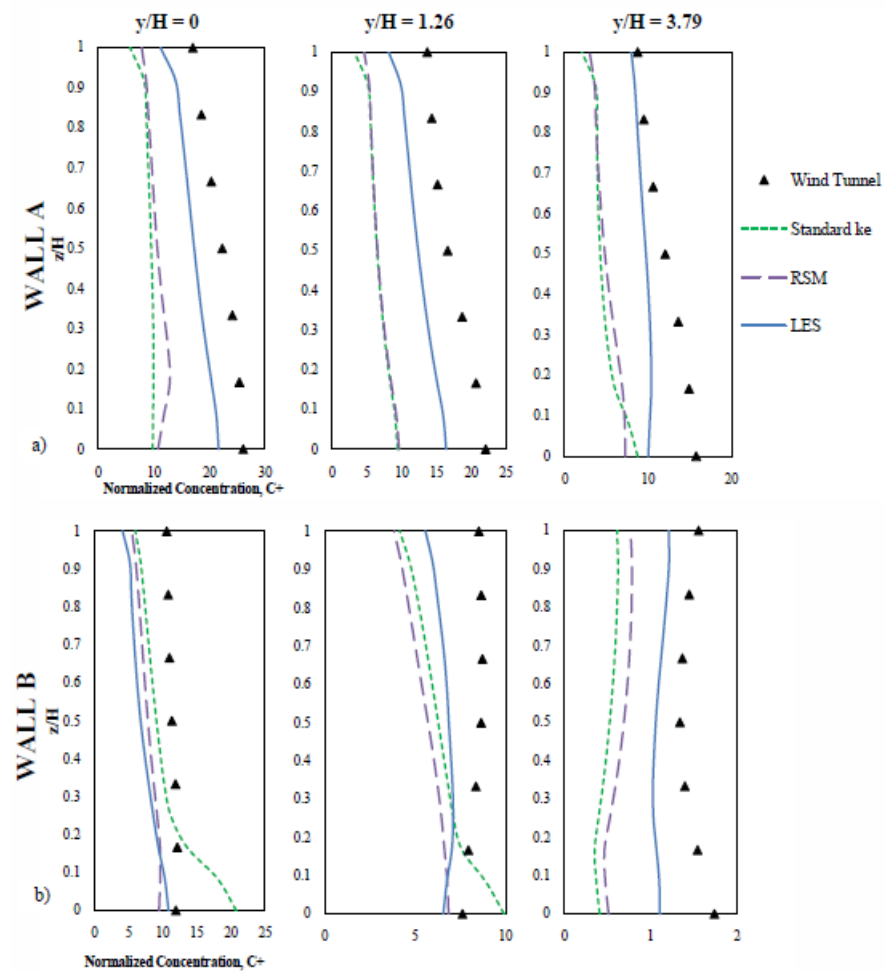


Figure 6.4 Mean concentration profiles at three different locations on a) Wall A (leeward) and b) Wall B (windward) to compare the different numerical results to experimental data ($W/H = 2$)

The predictions obtained by the different numerical approaches are compared based on the mean normalised velocities and concentration contours along the mid-plane $y/H = 0$ within the street canyons. This is demonstrated in Figure 6.5 and Figure 6.6.

The transport and hence distribution of pollutants is dependent on the flow field development. No flow field data were available from the WT database, but since it has been established that the numerical prediction of the pollutant concentration levels by LES is most accurate and a number of studies have also indicated LES to be more superior than RANS when validating flow fields and turbulence structures against experiments (Tominaga and Stathopoulos, 2010, Rodi, 1997), using LES as benchmark for the purpose of comparison to RANS is justified.

Starting with $W/H = 1$ illustrated in Figure 6.3, it can be observed that both the standard $k-\varepsilon$ and RSM underpredicts the concentration levels at the centreline of the in-canyon walls (i.e. $y/H = 0$). This underprediction is more pronounced for RSM. Referring to Figure 6.5, the dip in concentration levels could be explained by the fact that RANS models, particularly RSM, underpredict the in-canyon circulation strength. In other words, lower maximum magnitudes of negative and positive velocities are predicted by RANS when compared to LES.

Furthermore, it is noted that RANS models predict an accumulation of pollutant towards the leeward walls as opposed to LES, which reproduces a greater spread within the canyons. This is explained by the fact that LES captures the transient mixing, dispersion and diffusion of the pollutants, thus, performing better than RANS.

A similar pattern is evident in $W/H = 2$, shown in Figure 6.6. It is observed that the in-canyon circulation is grossly underpredicted by RANS models and as a consequence the pollutant concentration levels at the walls are underpredicted too.

On the other hand, LES demonstrates a stronger in-canyon circulation strength and greater spread of pollutants within the street canyons, resulting in better predictions as seen in the graphical plot of Figure 6.4.

In terms of resource demand and computational cost, standard $k-\varepsilon$ took around two hours; RSM took a day and LES two weeks on a similar high performance workstation. But with the richness in detail and increased accuracy, the computational cost of LES is justified when taking into account the associated cost and time of an equivalent experimental investigation.

6.2 $W/H = 1$ vs. $W/H = 2$

Comparison of different aspect ratios of urban street canyons have been extensively covered in the literature and is not the focus of the present study, but is briefly revisited in respect to pollutant concentration levels.

For a wide street canyon, $W/H = 2$, pollutant concentration levels are lower than in a narrow street canyon, $W/H = 1$, due to the fact that improved air circulation and ventilation is promoted in the former reducing the amount of pollutants trapped at street level.

Comparing mean vertical velocities in Figure 6.5a and Figure 6.6a it is observed that the in-canyon circulation strength is stronger in $W/H = 2$ and as a result more pollutant is transported out of the canyon due to improved air exchange with the above-roof flow.

Maximum concentration levels are in the range of $C^+ = 25$ for $W/H = 2$ as opposed to $C^+ = 40$ for $W/H = 1$. Analogous observations can be deduced from Figure 6.1 and Figure 6.2, illustrating the wall concentration levels at the windward and leeward walls.

Images of velocity vectors are not illustrated, as velocity contours better demonstrate the flow field development, particularly for transient simulations by LES and URANS. The velocity vectors and contours essentially convey the same information as can be seen in **Appendix E**.

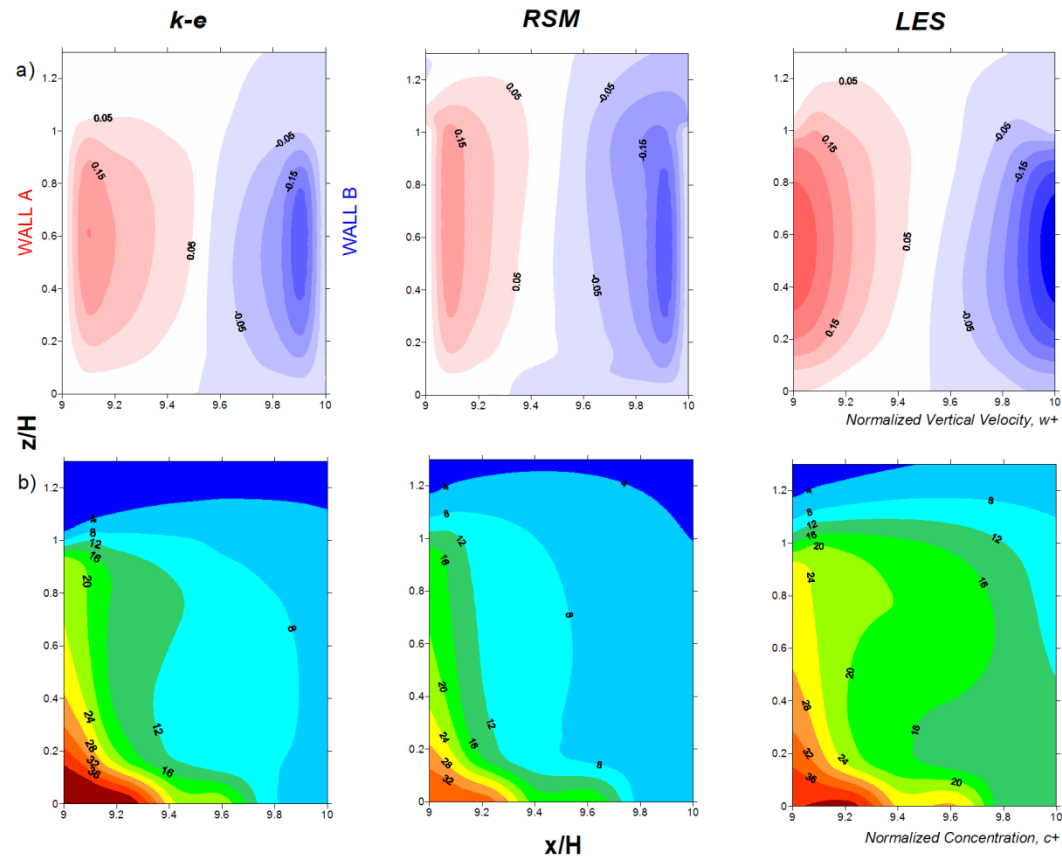


Figure 6.5 a) Mean normalised vertical velocity contours, w^+ and b) corresponding mean normalised concentration contours, C^+ at the mid plane of the street canyon (that is $y/H = 0$ for $x/H = 9$ to 10) comparing standard $k-\epsilon$, RSM and LES ($W/H = 1$)

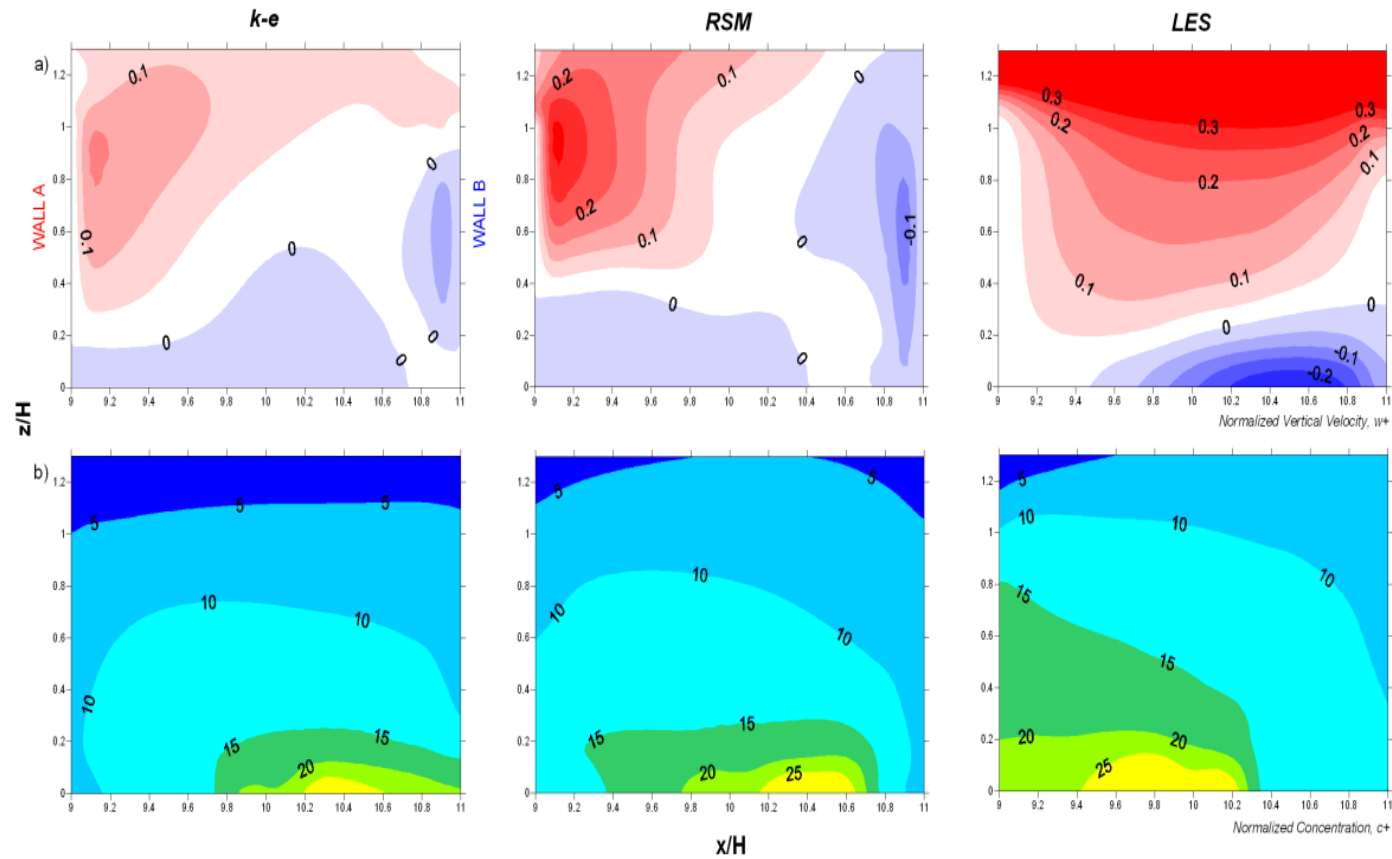


Figure 6.6 a) Mean normalised vertical velocity contours, w^+ and b) corresponding mean normalised concentration contours, C^+ at the mid plane of the street canyon (that is $y/H = 0$ for $x/H = 9$ to 11) comparing standard $k-\epsilon$, RSM and LES ($W/H = 2$)

6.3 Instantaneous Solution

The WT experiment only provided the mean concentration data averaged over a sampling period hence is not a true indicator of airflow and pollutant dispersion in real situations, which may vary significantly both in time and space as illustrated by the instantaneous solution

The LES results in Figure 6.7 support the statement by Louka et al. (2000), who strongly recommend resolving the unsteady and intermittent fluctuations of a flow field in order to achieve agreeable results to experimental observations. The time-evolution of the concentration field indeed shows significant variations in peak concentration levels. This is only shown for $W/H = 1$ as similar trends were observed for $W/H = 2$.

This is further supported by the time-evolution of the in-canyon flow and concentration field presented in Figure 6.8. While the time-averaged results show a neat bubble of positive and negative velocities at the leeward and windward walls, respectively, it can be seen that this is not the case with time, because the flow field varies significantly.

Furthermore, LES captures pockets of opposing velocities intertwining that promote turbulent mixing, and is one of the underlying factors of why it performs better than RANS.

The transport of pollutants is dependent on the flow field development in addition to dispersion as a result of diffusivity of the airborne material; hence accurate resolutions of turbulent flow fields are paramount to good predictions of pollutant dispersion. This is successfully achieved by LES.

The relationship between pollutant dispersion and flow field development can be deduced from Figure 6.8. At $t = 20$ sec, the magnitude of the velocity leaving the canyon is relatively small and as a result, more pollutant accumulates near the bottom corner of Wall A. On the other hand, the pollutant spreads vertically along Wall A due to the strong positive velocity field leaving the canyon at $t = 40$ sec.

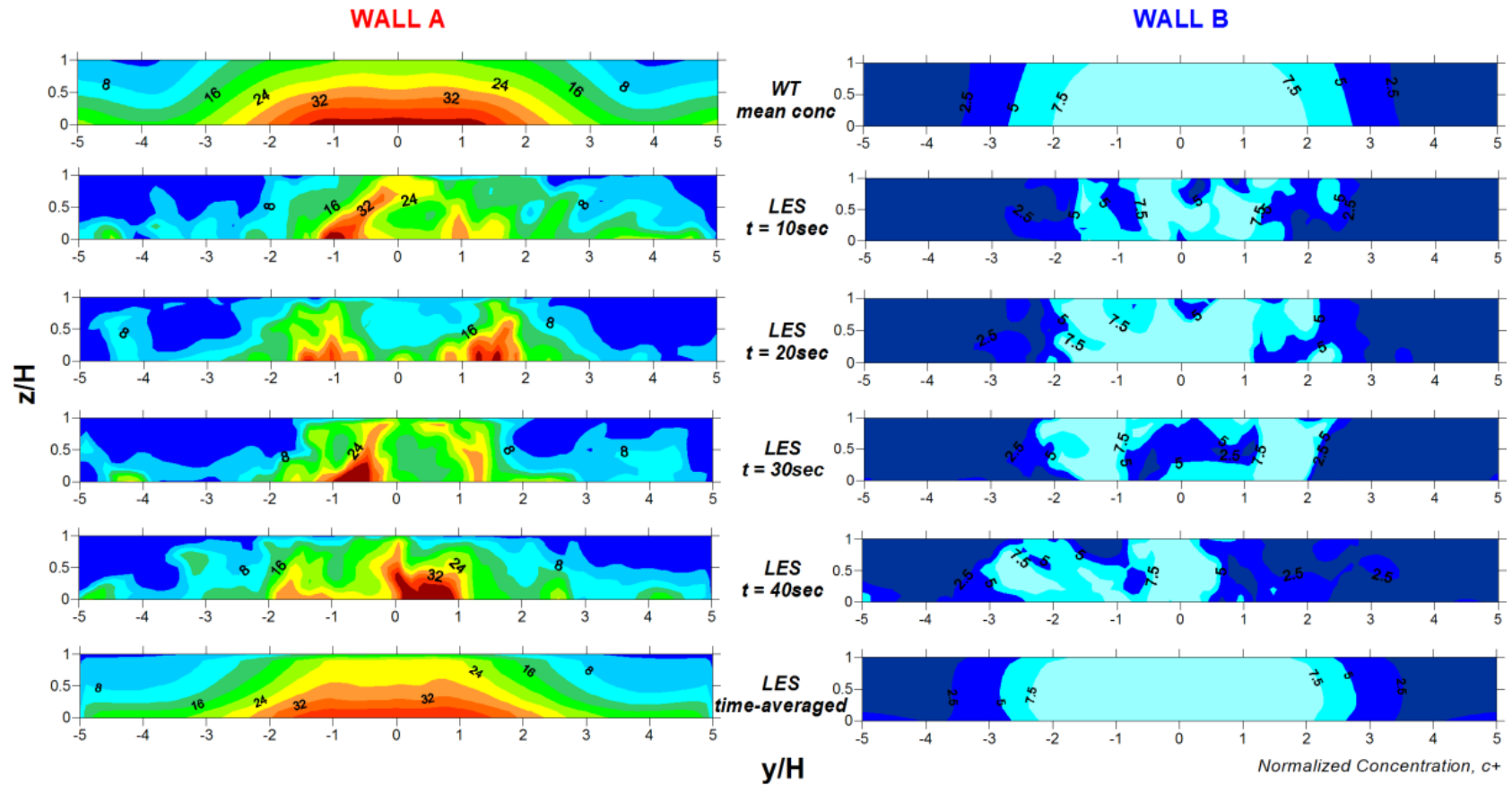


Figure 6.7 Instantaneous normalised concentration data on Wall A (leeward) and Wall B (windward) for different time instances obtained by LES compared to mean data from WT and LES ($W/H = 1$)

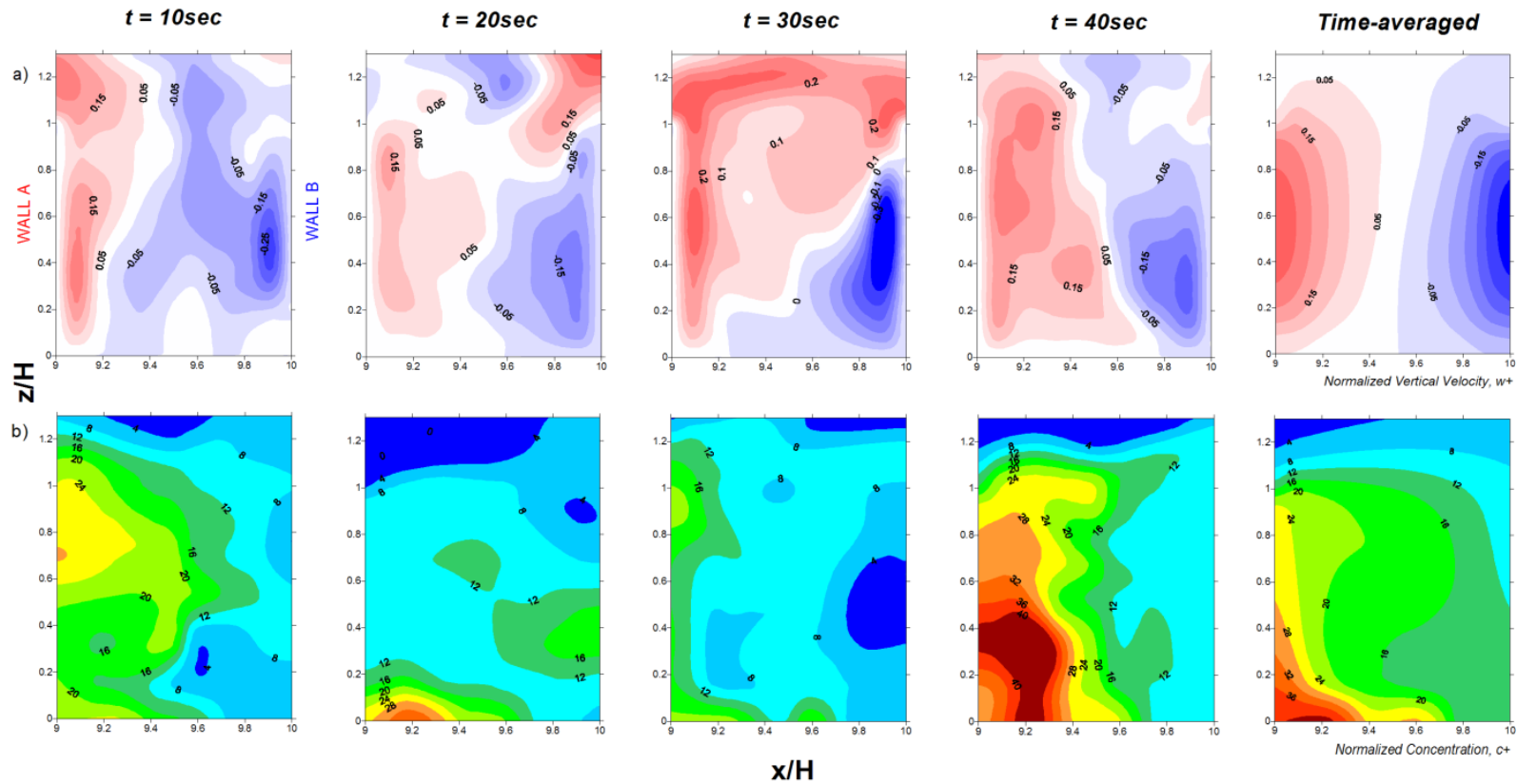


Figure 6.8 a) Instantaneous normalised vertical velocity contours, w^+ and b) corresponding instantaneous normalised concentration contours, C^+ at mid plane of the canyon (that is $y/H=0$ from $x/H=9$ to 10) obtained using LES showing the time-evolution ($t = 10, 20, 30$ and 40 s) and mean results ($W/H = 1$)

At $t = 30$ sec, the relatively large circulation of air within the canyon (i.e. both strong positive and negative velocity bubbles) about the mid-plane disperses the pollutant out of the canyon and away from the centrelines at both walls (this explains why the mid-plane concentration levels at $t = 30$ sec is relatively small at both walls in Figure 6.7).

Although the mean results indicate that the maximum pollutant concentration levels occur at the centrelines, it is only true on time-averaging, as the peak concentration levels are shown to vary significantly over time and space, analogous to what is observed for the wall concentration levels.

6.4 LES vs. URANS

In the introductory notes, it was asserted that URANS is incapable of capturing internally induced fluctuations of flow fields and, hence, is not a direct replacement for LES when needing to account for transient mixing and pollutant dispersion processes within urban street canyons.

This is demonstrated in Figure 6.9 and Figure 6.10, which compares numerical results between URANS, specifically unsteady RSM, and LES at the mid-plane of the canyon (i.e. $y/H = 0$), and at the leeward (Wall A) and windward (Wall B) walls, respectively.

It is shown that for URANS, the solution did not vary with time when compared against LES.

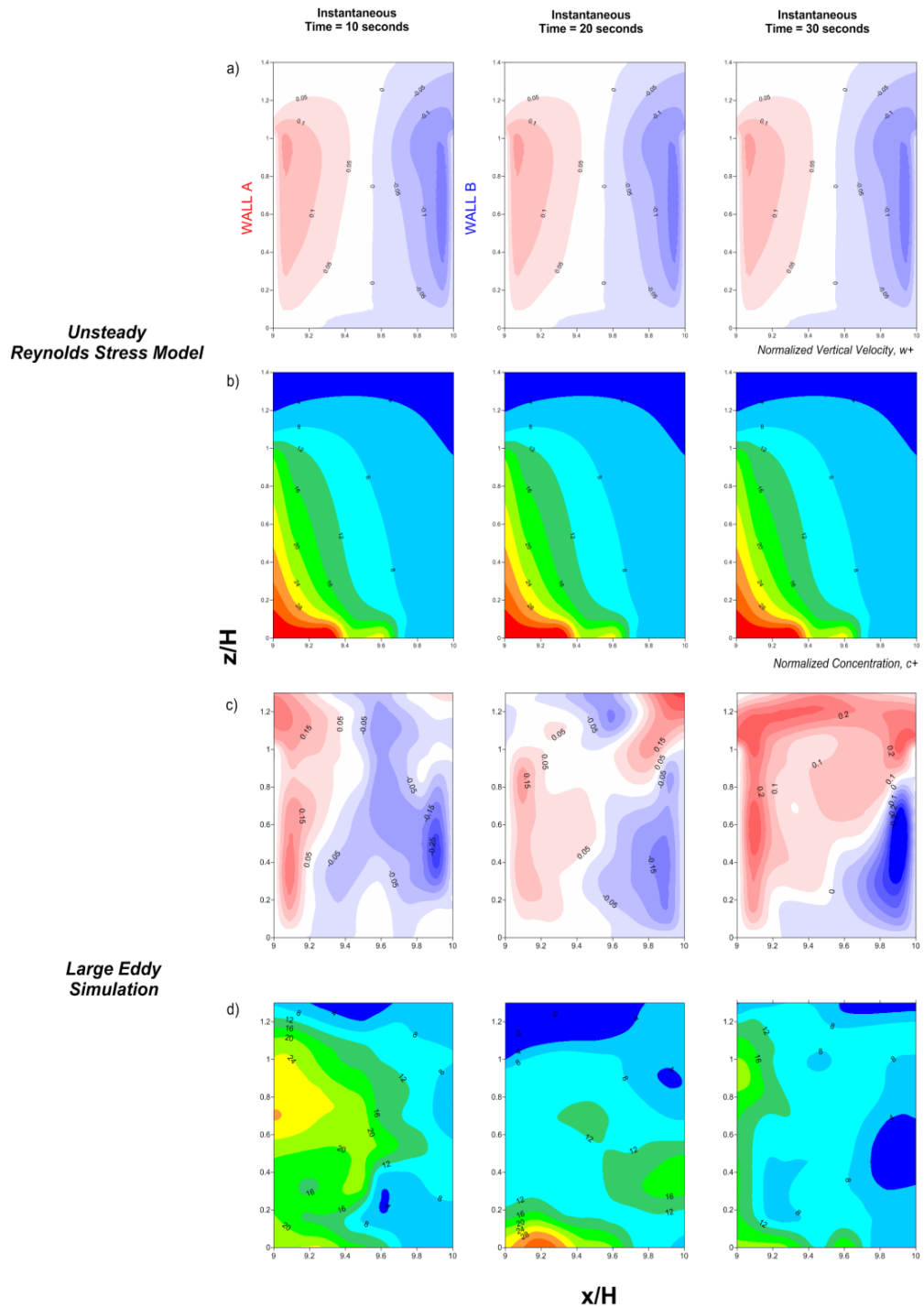


Figure 6.9 URANS against LES for unsteady simulations at $t = 10, 20$ and 30 s showing the mid-plane normalised vertical velocities, w^+ (a and c) and corresponding normalised concentrations, C^+ (b and d) ($W/H = 1$)

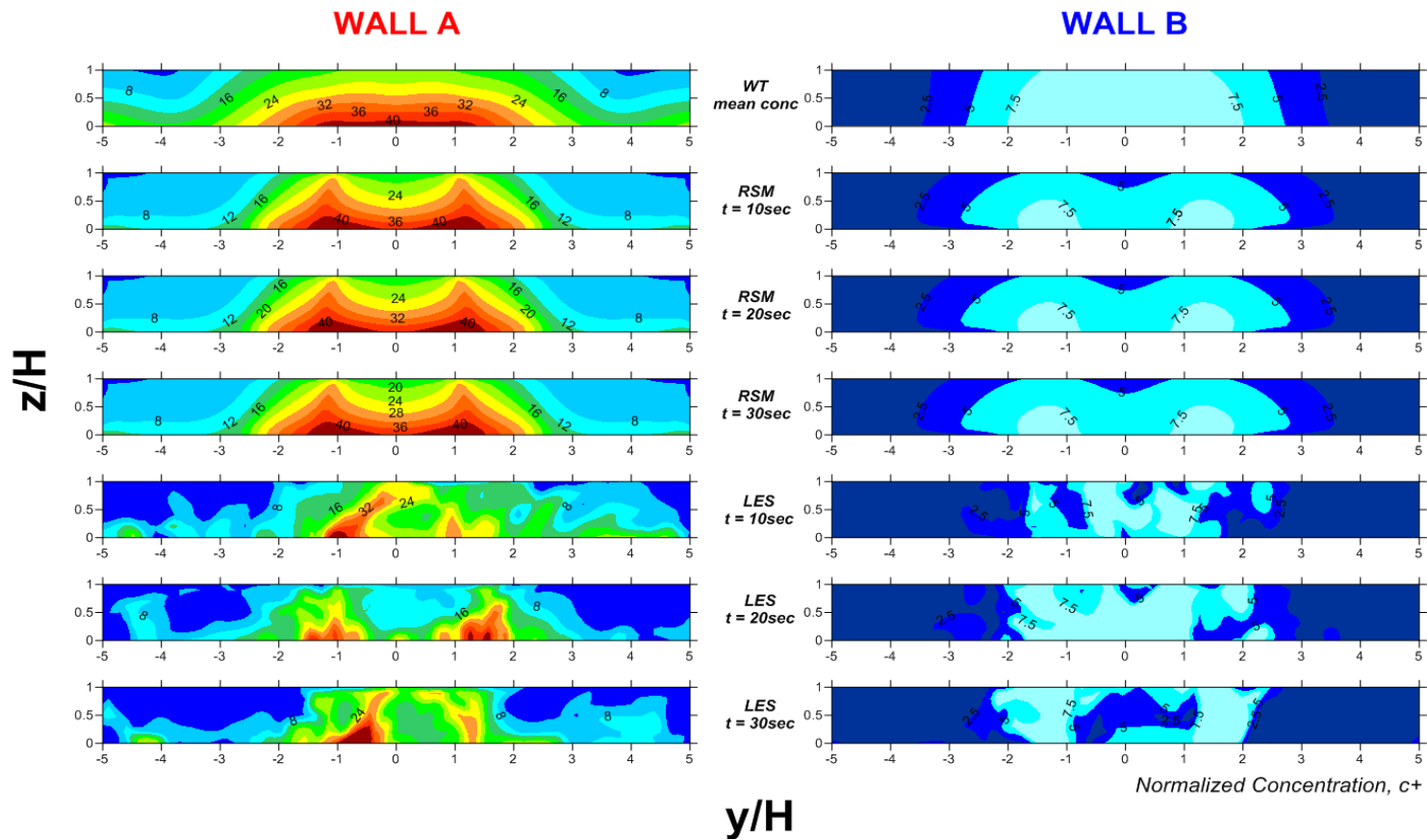


Figure 6.10 URANS against LES for unsteady simulation at $t = 10, 20$ and 30 s showing the wall concentration levels at Wall A (leeward) and Wall B (windward) against WT data (CODASC, 2008) ($W/H = 1$)

6.5 Conclusion

The widely employed RANS turbulence models provide numerical predictions of qualitative agreement to experimental observations, although they are not capable of reciprocating quantitatively the solutions of complex flow structures with which the dispersion of airborne materials depend on. RANS simulations are therefore only recommended for implementation in initial design stages or where quantitative agreement is not of utmost importance.

Not only does LES significantly improve flow and pollutant dispersion predictions resulting in better and more consistent solutions, but they also provide time-evolution and statistical distribution of flow variables.

In other words, LES provides important information on the instantaneous fluctuations and thus is more suitable than either RANS or URANS when detailed and accurate predictions are required, such as in the case of simulating the deliberate or accidental release of hazardous airborne materials.

It should be noted that the enhancement by LES comes with a price, with a computational demand order of magnitudes higher than that of steady-state RANS calculations.

Amongst the RANS models, RSM performs better since it resolves for all the Reynolds Stresses unlike standard $k-\varepsilon$ which assumes isotropic stresses.

LES is capable of capturing both externally and internally induced periodicity and thus, intermittent and unsteady fluctuations of the flow field. This in turn allows transient mixing within the street canyons to be properly accounted for resulting in accurate predictions of the horizontal diffusion of concentration levels.

Finally, a wider street canyon promotes better air circulation, ventilation and exchange with the above-roof flow, resulting in lower pollutant being trapped at street level.

7 TREE-LINED STREET CANYONS

Numerical investigations for tree-lined street canyons of $W/H = 1$ (with single row of trees) and $W/H = 2$ (with two rows of trees) are presented comparing RANS (standard $k-\varepsilon$ and RSM) against LES, using WT experimental measurements as benchmark data.

The aerodynamic impacts of trees are investigated by comparing results of the present tree-lined to previously studied tree-free street canyons. Two tree crown porosities, $\lambda = 80 \text{ m}^{-1}$ and $\lambda = 200 \text{ m}^{-1}$, are examined to determine their significance on the airflow and pollutant dispersion within urban street canyons.

7.1 Comparison between LES and RANS

Numerical results obtained from RANS (standard $k-\varepsilon$ and RSM) and LES are compared against WT measurements. Mean normalised concentration contours at the tree-lined street canyons leeward (Wall A) and windward (Wall B) walls are presented in Figure 7.1 ($W/H = 1$) and Figure 7.2 ($W/H = 2$) for two crown porosities with pressure loss coefficients, $\lambda = 80 \text{ m}^{-1}$ and 200 m^{-1} , respectively.

Similar to tree-free street canyons, LES results are time-averaged over 8000 non-dimensional time-steps, WT concentration data were acquired over a sampling period of 105 seconds and RANS simulations are performed in steady-state. URANS was discarded as discussed in the previous chapter, because it fails to capture the unsteadiness of the flow field.

Figure 7.1 shows the street canyon of $W/H = 1$ with single row of trees. It can be seen that LES performs qualitatively better than RANS in reproducing the spatial distribution of the pollutants when compared to WT data. This is particularly pronounced at the leeward walls for both porosities, where maximum concentration levels occur and is deemed to be the most critical region. On the other hand, standard $k-\varepsilon$ slightly underpredicts for $\lambda = 80 \text{ m}^{-1}$ and overpredicts for $\lambda = 200 \text{ m}^{-1}$. RSM underpredicts the concentration levels for both porosities.

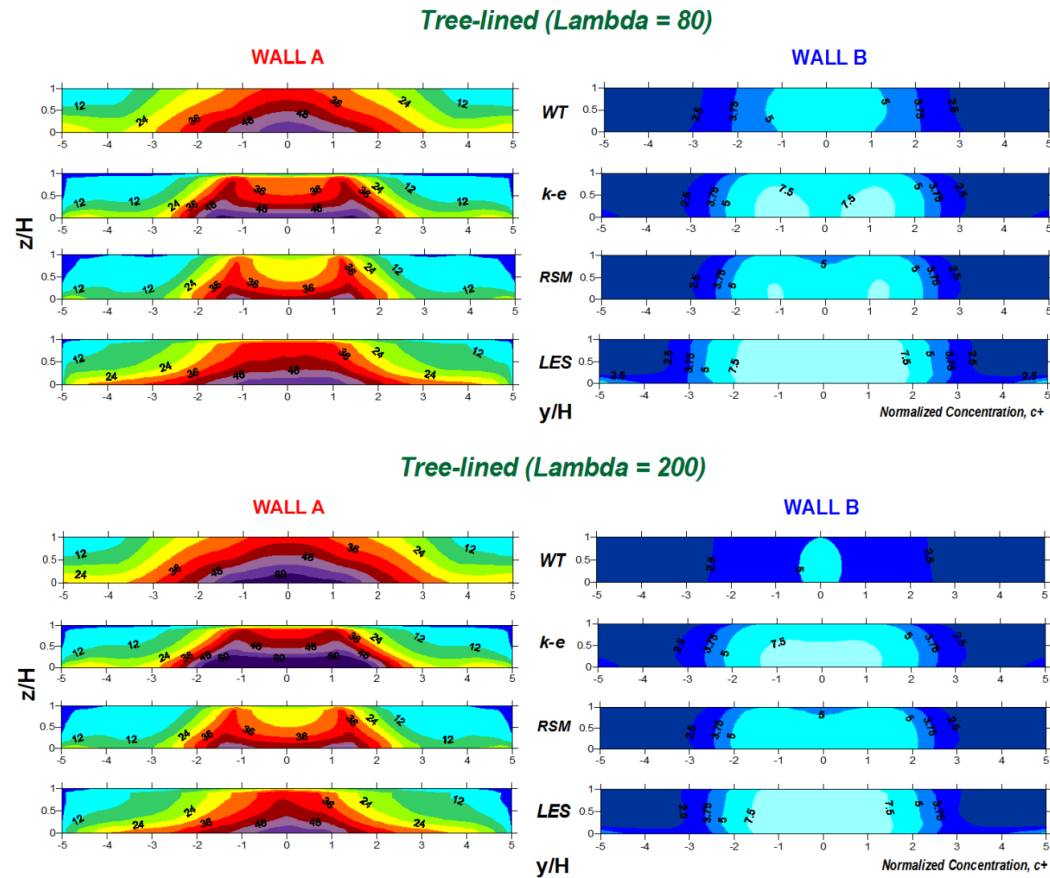


Figure 7.1 Mean concentration data on Wall A (leeward) and Wall B (windward) comparing between WT (CODASC, 2008) and numerical results performed with standard $k-\epsilon$, RSM and LES for tree crowns with porosity $\lambda = 80 \text{ m}^{-1}$ and $\lambda = 200 \text{ m}^{-1}$ ($W/H = 1$)

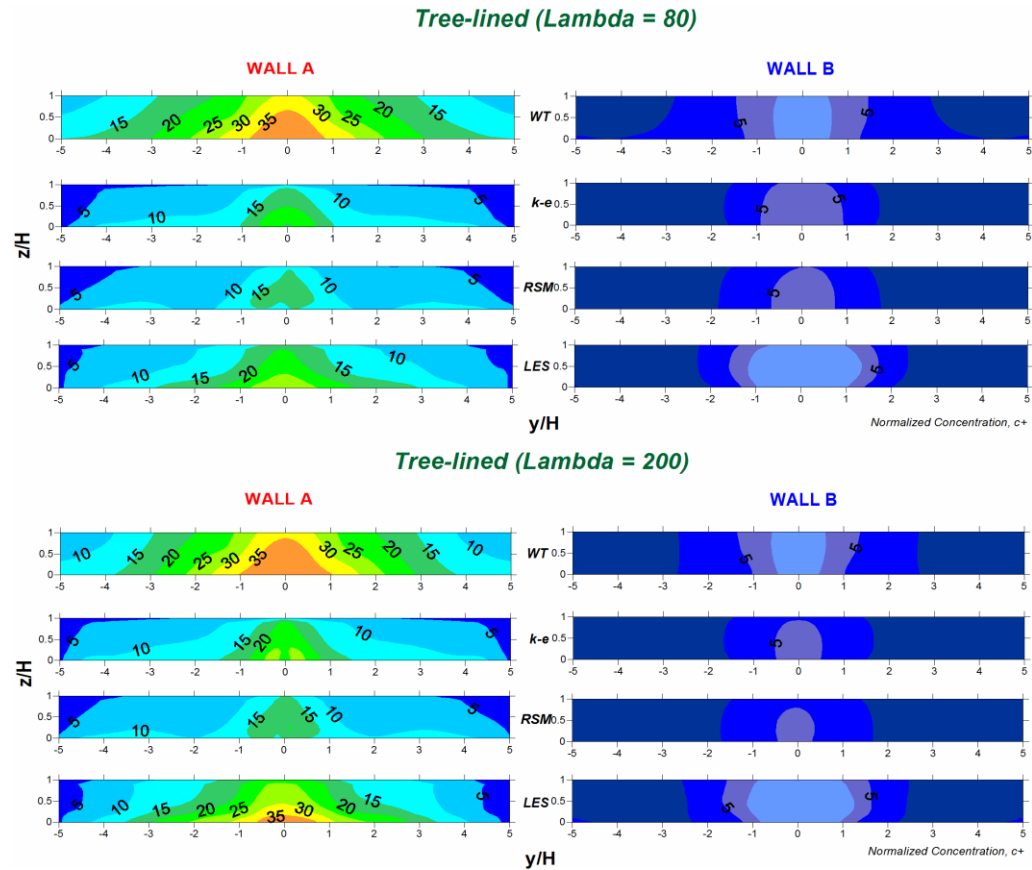


Figure 7.2 Mean concentration data on Wall A (leeward) and Wall B (windward) comparing between WT (CODASC, 2008) and numerical results performed with standard $k-\epsilon$, RSM and LES for tree crowns with porosity $\lambda = 80 \text{ m}^{-1}$ and $\lambda = 200 \text{ m}^{-1}$ ($W/H = 2$)

For the windward walls, all the employed viscous models generally overpredict the concentration levels when compared to WT measurements, with LES presenting much larger overpredictions.

In Figure 7.2 for $W/H = 2$ with two rows of trees, LES again outperforms the other viscous models, albeit slightly underpredicting the pollutant concentration levels at the leeward wall in comparison to WT data. This is more evident for $\lambda = 80 \text{ m}^{-1}$. The two RANS models (i.e. standard $k-\varepsilon$ and RSM) largely underpredict the concentration levels at the leeward walls and overpredict the concentration levels at the windward walls, for both porosities investigated.

Figure 7.3 graphically illustrates the quantitative analysis of the concentration profiles at six different vertical locations along both walls (three at each wall: $y/H = 0, 1.26$ and 3.79) for $W/H = 1$ with single row of trees. Starting with the leeward walls, not only is LES better at predicting the concentration levels, but it also provides more consistent results, doing especially well at all vertical locations along Wall A. In contrast, the standard $k-\varepsilon$ underpredicts and overpredicts at some locations, whereas RSM underpredicts at all locations for both porosities.

Moving to the windward walls, LES overpredicts the concentration levels at all locations, while the two RANS models start off well at the centreline ($y/H = 0$) but then diverges from the WT data towards the street ends.

One thing that is reiterated in the observations is that LES produces much more consistent results as opposed to RANS, which show varying degree of accuracy at various locations and for different porosities.

For $W/H = 2$ with two rows of trees demonstrated in Figure 7.4, similar observations are made, with LES performing better than RANS although slightly underpredicting the concentration levels at some locations along Wall A and overpredicting at some locations along Wall B.

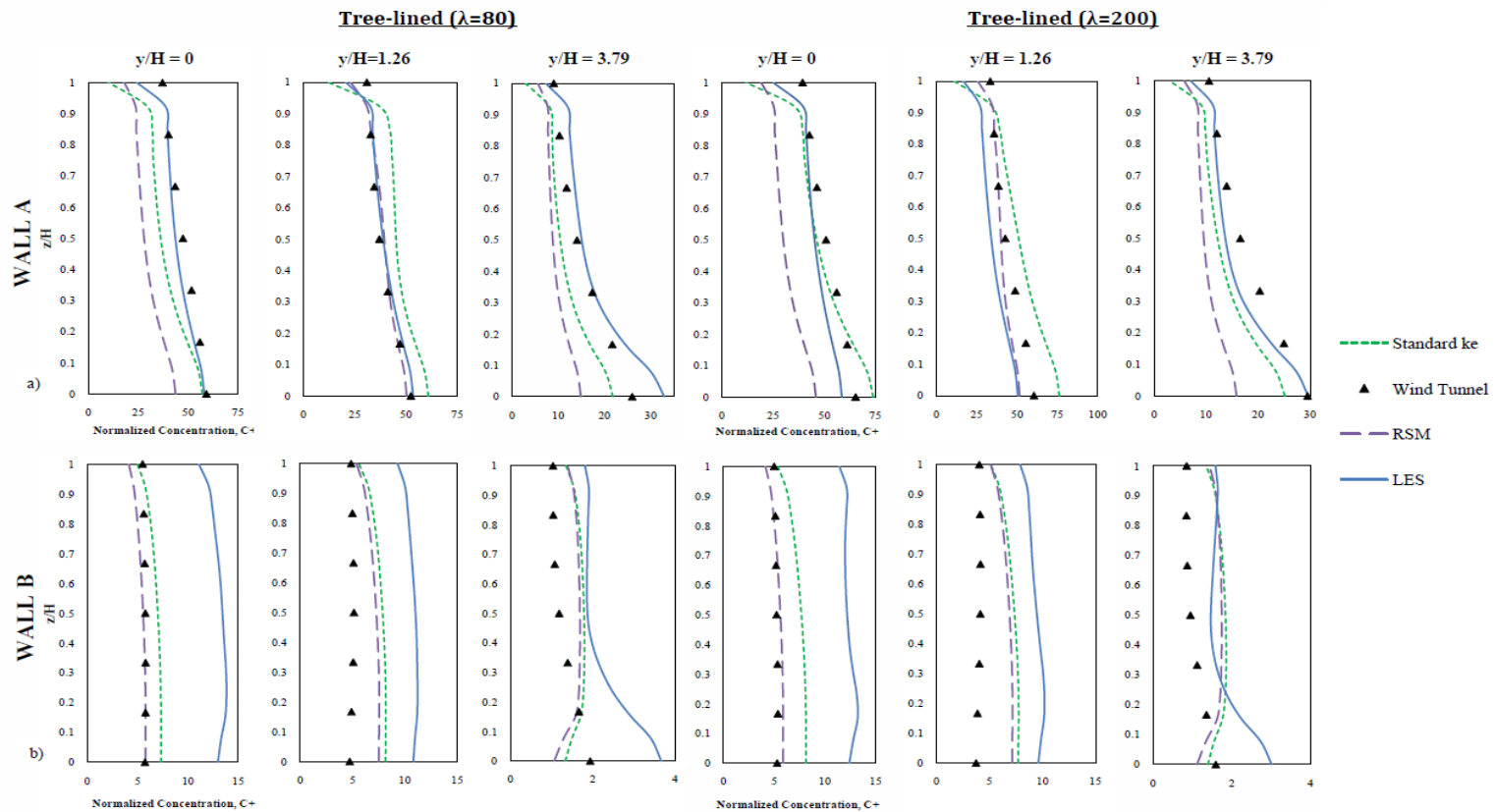


Figure 7.3 Mean concentration profiles at three different locations on a) Wall A (leeward) and b) Wall B (windward) comparing numerical results against WT data for tree crowns with porosity $\lambda = 80 \text{ m}^{-1}$ and $\lambda = 200 \text{ m}^{-1}$ ($W/H = 1$)

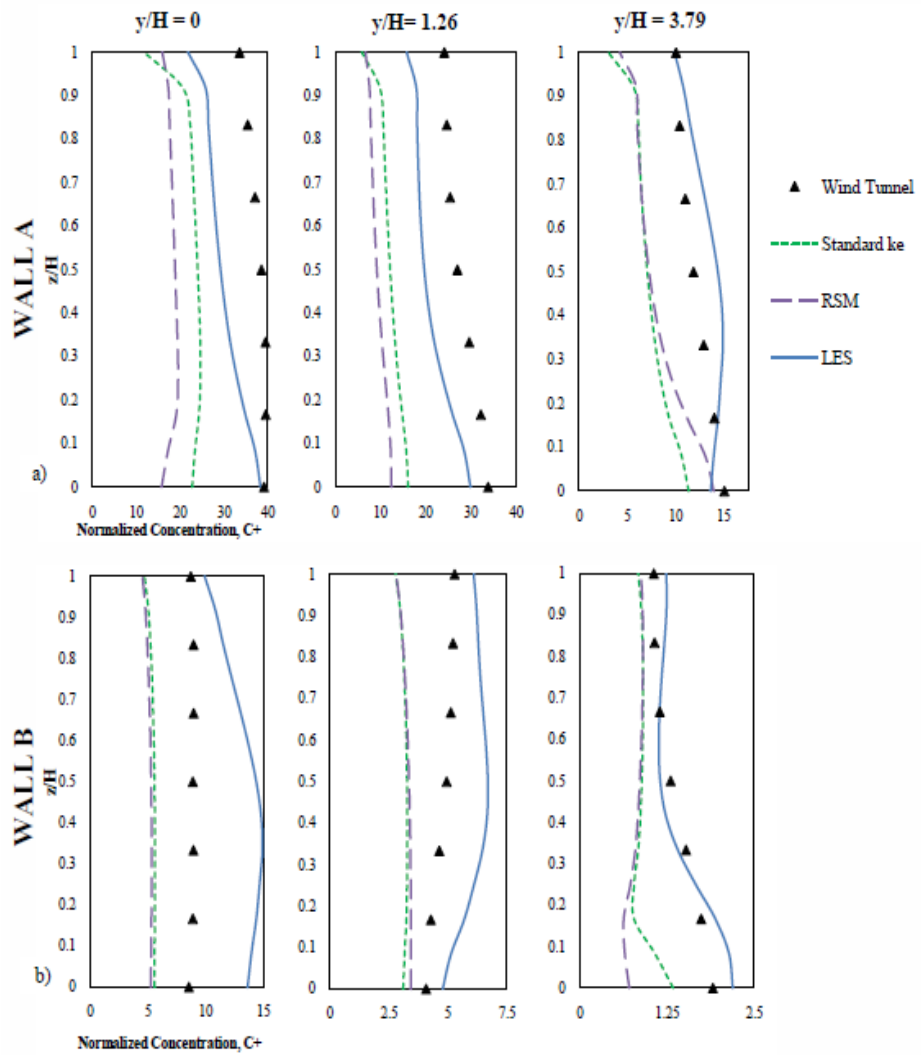


Figure 7.4 Mean concentration profiles at three different locations on a) Wall A (leeward) and b) Wall B (windward) comparing the numerical results against WT data for tree crowns with porosity $\lambda = 200 \text{ m}^{-1}$ ($W/H = 2$)

Turning attention to the differences in tree crown porosity, it will be noted when comparing the concentration levels between the two porosities for $W/H = 1$ (Figure 7.1) and $W/H = 2$ (Figure 7.2) that the choice of λ does not significantly affect the pollutant concentration levels. This is similar to the WT experimental observations by Gromke and Ruck (2007, 2009) and numerical results by Gromke et al. (2008), Buccolieri et al. (2009) and Balczó et al.

(2009). Parallel observations are reiterated in the present study as shown in Figure 7.5.

The predictions obtained by different numerical approaches are compared based on the mean normalised velocities and concentration contours along mid-plane $y/H = 0$ within the street canyons. This is illustrated in Figure 7.5 and Figure 7.6 for $W/H = 1$ with single row of trees and $W/H = 2$ with two rows of trees, respectively.

Referring to Figure 7.5 for $W/H = 1$, the differences in concentration levels between the employed numerical methods could be explained by the fact that the RANS models underpredict the in-canyon flow circulation strength for both porosities studied. In other words, lower maximum magnitudes of negative and positive velocities are reproduced by RANS unlike in LES.

Moving to Figure 7.6 for $W/H = 2$, it is noted that the positive velocity bubble is underpredicted for RANS, resulting in larger underpredictions at the windward wall and overpredictions at the leeward wall, when compared to LES. Furthermore, RANS models predict an accumulation of pollutants towards the leeward walls as opposed to LES which reproduces a wider distribution within the canyons.

7.2 $W/H = 1$ (single row of trees) vs. $W/H = 2$ (two rows of trees)

Similar to tree-free street canyons, wider canyons - $W/H = 2$ lined with 2 rows of trees - promote better air circulation and ventilation compared to narrower canyons - $W/H = 1$ with single row of trees. Wider streets improve air exchange with the above-roof airflow and consequently lesser pollutants get trapped at street level.

It is observed in Figure 7.1, Figure 7.2, Figure 7.5 and Figure 7.6, that the maximum concentration, C^+ obtained for $W/H = 1$ with single row of trees is in the range of 60, whereas it is much lower for $W/H = 2$ at about 35.

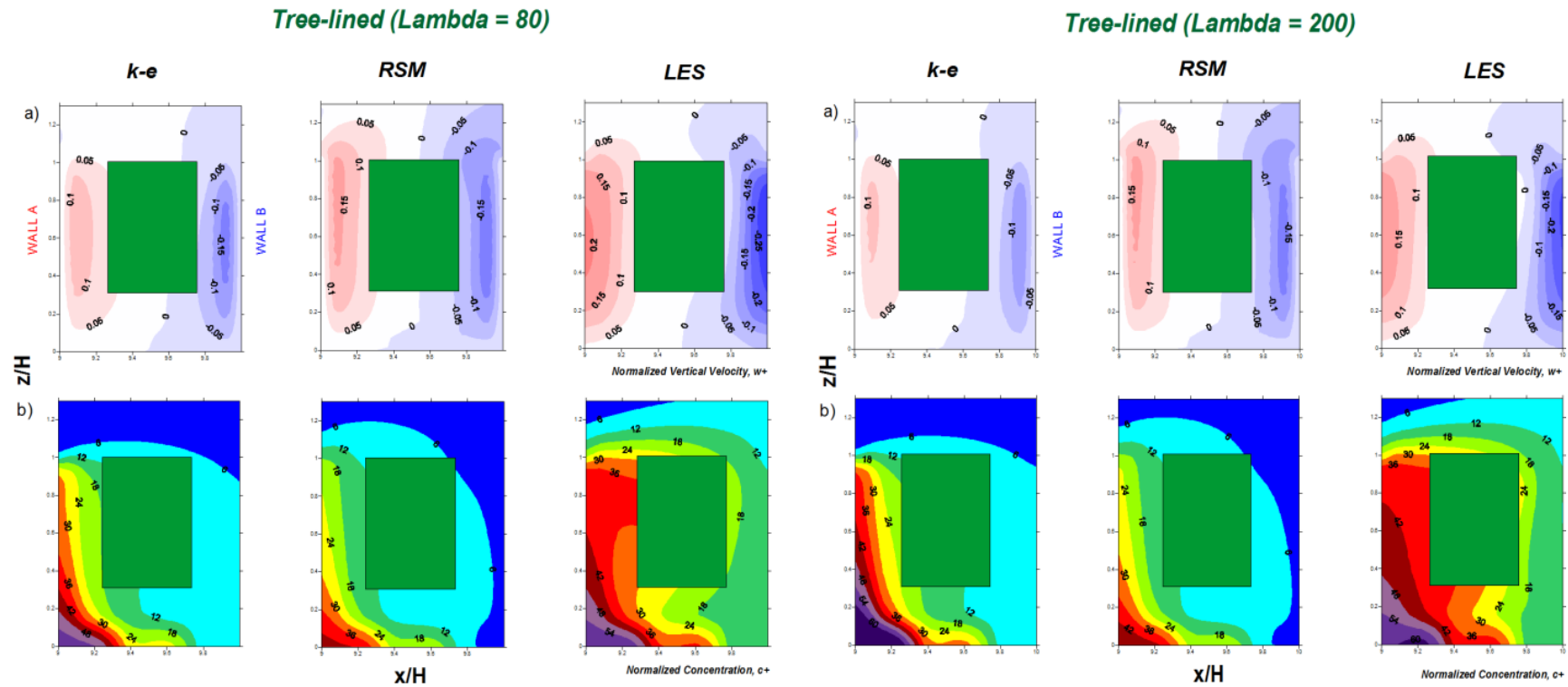


Figure 7.5 a) Mean normalised vertical velocity contours, w^+ and b) corresponding mean normalised concentration contours, C^+ at the mid plane of the street canyon ($y/H = 0$ for $x/H = 9$ to 10) comparing standard *k-ε*, RSM and LES for tree crown with porosity $\lambda = 80 \text{ m}^{-1}$ and $\lambda = 200 \text{ m}^{-1}$ ($W/H = 1$)

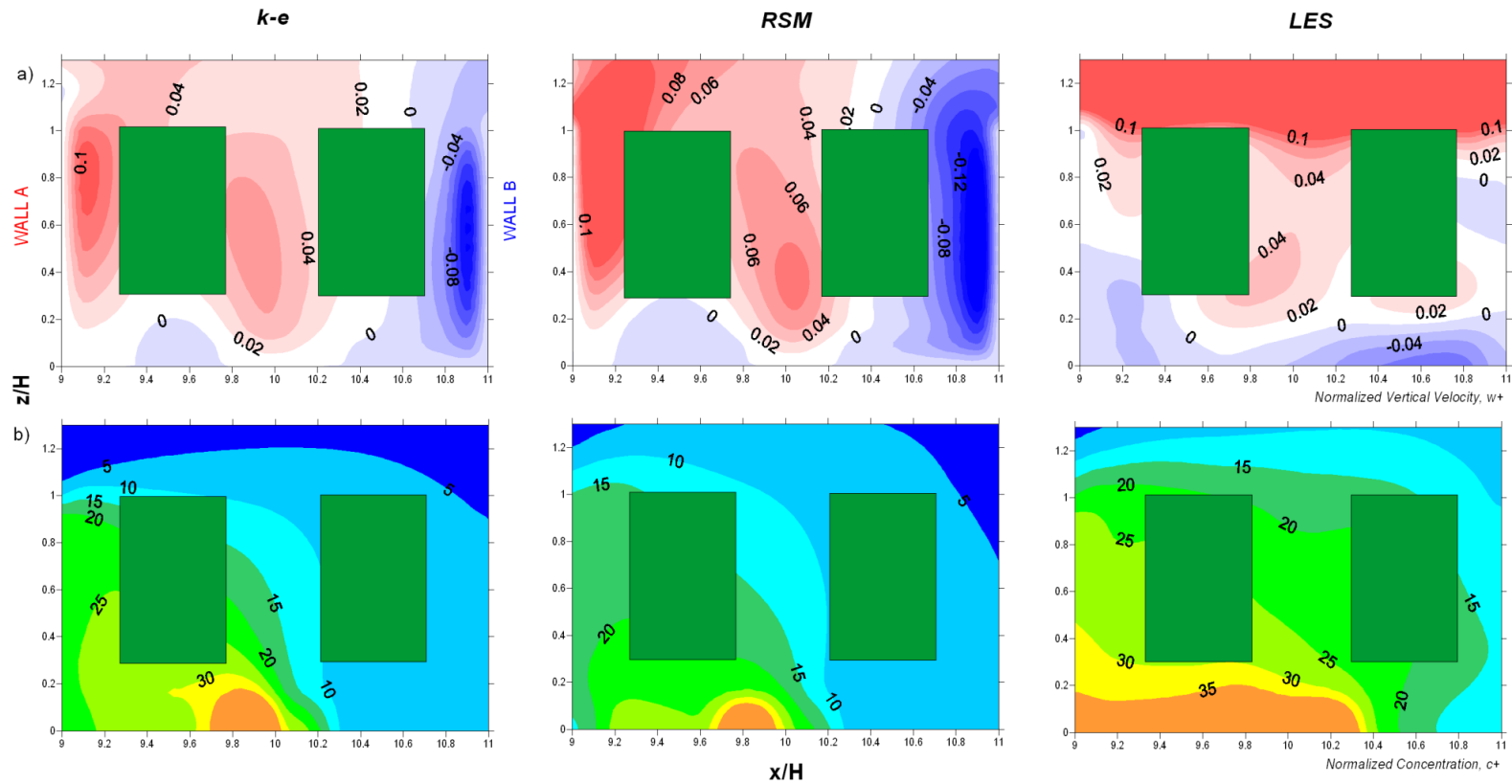


Figure 7.6 a) Mean normalised vertical velocity contours, w^+ and b) corresponding mean normalised concentration contours, C^+ at the mid plane of the street canyon ($y/H = 0$ for $x/H = 9$ to 11), comparing standard $k-\epsilon$, RSM and LES for tree crown with porosity $\lambda = 200 \text{ m}^{-1}$ ($W/H = 2$)

7.3 Instantaneous Solution

The WT experiments only provided the mean concentration data averaged over a sampling period and thus did not reveal a realistic flow field development and corresponding time-evolution of pollutant dispersion. Moreover, majority of previous numerical studies on air quality problems have only presented the mean flow equation results without considering the flow statistics (such as with the case of RANS models used in the present study).

The LES results presented in Figure 7.7 and Figure 7.8 (only illustrated for $\lambda = 200 \text{ m}^{-1}$, $W/H = 1$) support the observations by Louka et al. (2000) who strongly recommend resolving the unsteady and intermittent fluctuations of the flow field. The recommendation is echoed here, where the peak values of the flow and concentration fields are shown to vary significantly with time.

Looking at Figure 7.8a, it can be seen that although the time-averaged results show a neat bubble of positive and negative velocities at the leeward and windward walls, the instantaneous flow field fluctuates. In addition, LES captures pockets of opposing velocities intertwining that promote turbulent mixing resulting in the wider spread witnessed in the in-canyon pollutant distribution. This is one of the foremost reasons why LES performs better than RANS.

7.4 Effect of Trees (Tree-free vs. Tree-lined)

One of the main aims of the present study was to verify that planting of trees in urban street canyons aerodynamically impacts the airflow and dispersion, apart from beautifying and greening cities and adding environmental and socio-economic benefits to the community. It is necessary to account for the presence of trees in CFD studies of urban airflow problems in order to reproduce more 'realistic' representations of typical urban scenarios.

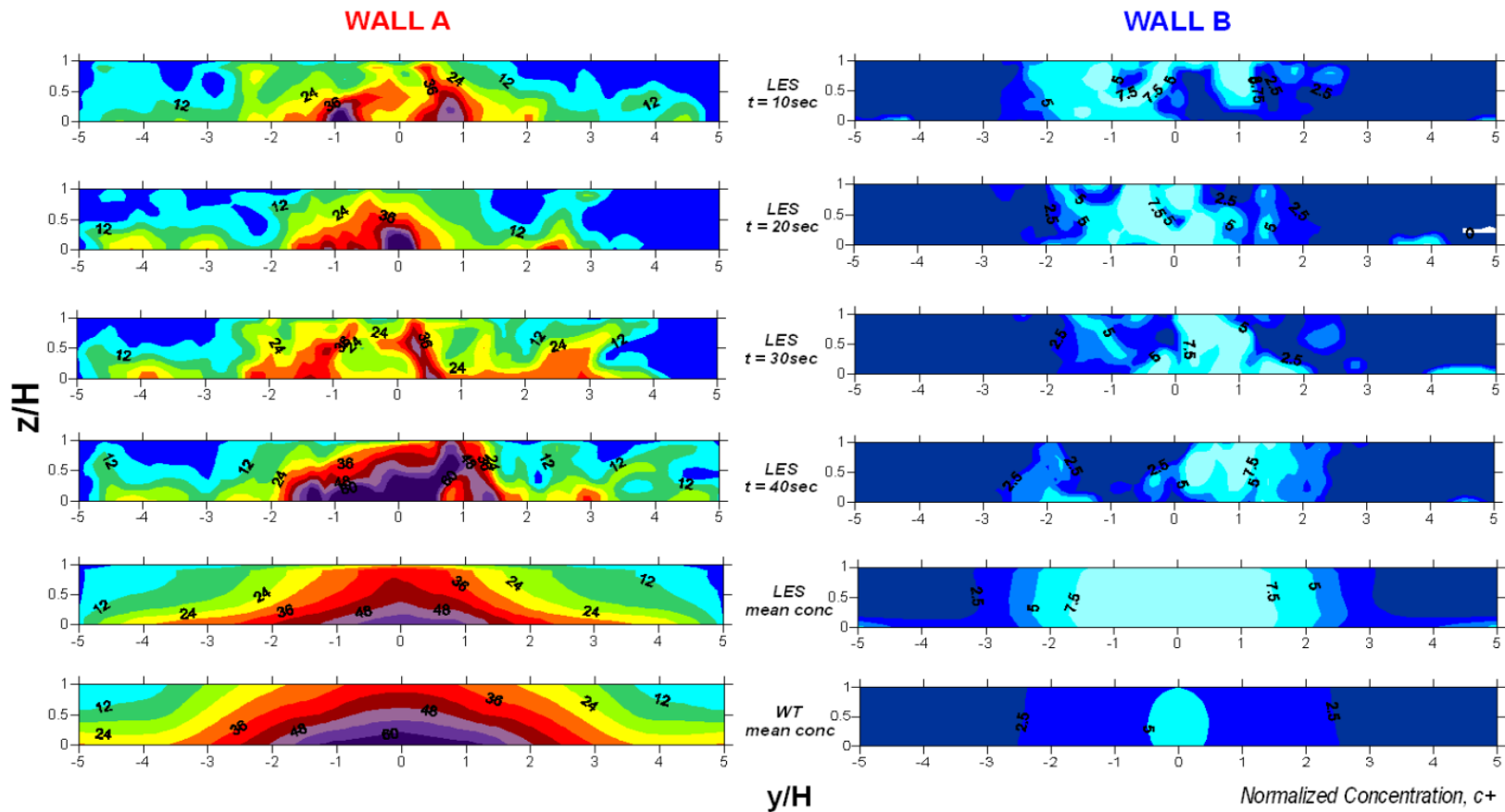


Figure 7.7 Instantaneous normalised concentration data on Wall A (leeward) and Wall B (windward) for different time instances obtained by LES compared against mean data from WT and LES, for tree crown with porosity $\lambda = 200 \text{ m}^{-1}$ ($W/H = 1$)

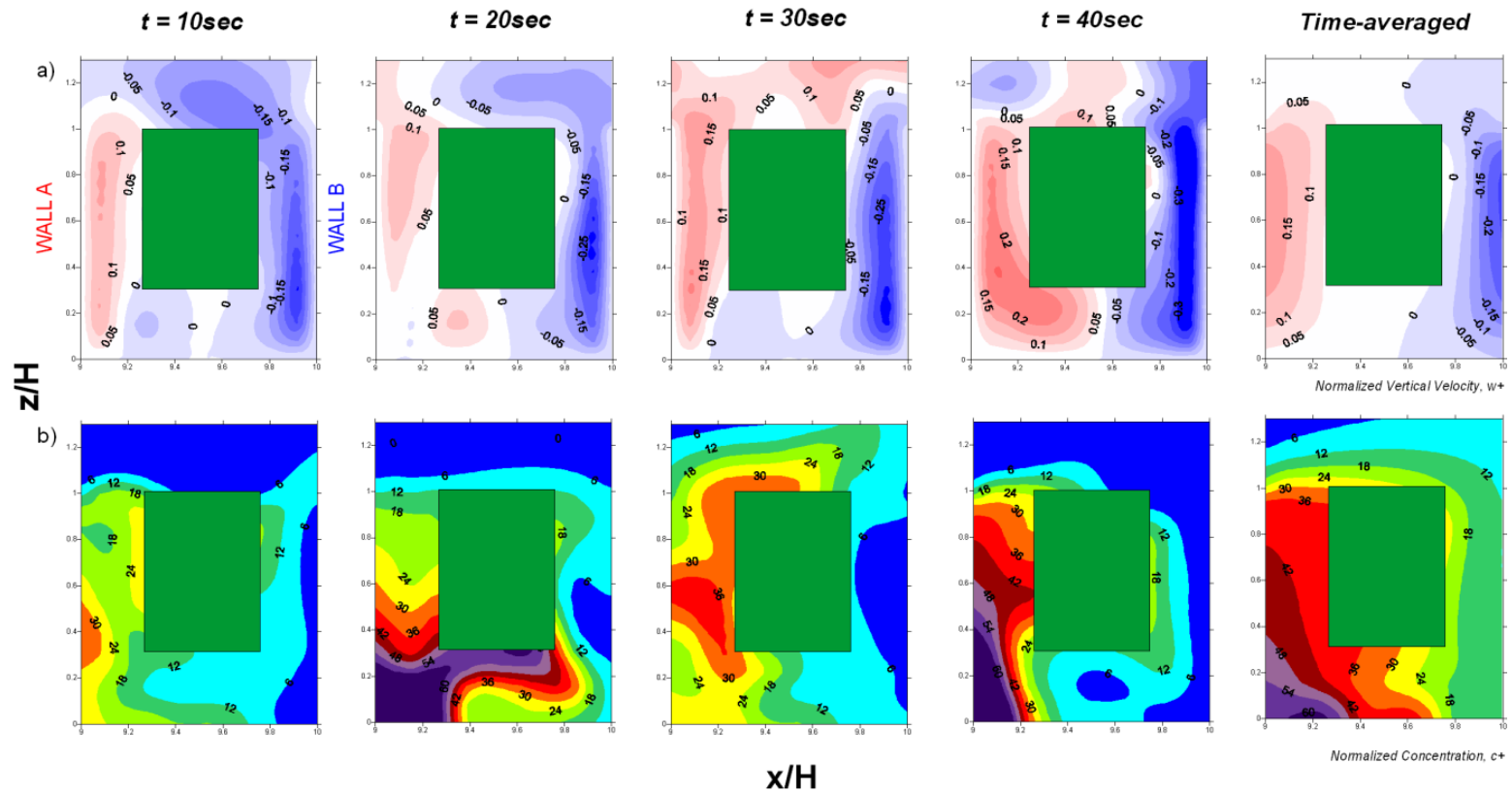


Figure 7.8 a) Instantaneous normalised vertical velocity contours, w^+ and b) corresponding instantaneous normalised concentration contours, C^+ at mid plane of the canyon ($y/H = 0$ from $x/H = 9$ to 10) obtained using LES showing the time-evolution ($t = 10, 20, 30$ and 40 s) and the mean results for tree crown with porosity $\lambda = 200 \text{ m}^{-1}$ ($W/H = 1$)

Figure 7.9 and Figure 7.10 show comparisons between tree-free and tree-lined canyons. (Only presented for $W/H = 1$ as similar patterns are observed in $W/H = 2$). In all cases considered, a common observation is that trees lead to an increase in pollutant concentration levels at pedestrian level when compared to tree-free canyons. In Figure 7.9, it is observed that in the tree-lined canyons the pollutant concentration levels at the leeward walls increases significantly, with slight decreases at the windward walls.

Figure 7.10 helps explain this by relating the flow field development to pollutant concentration levels. In the presence of trees, the in-canyon flow circulation strength is reduced, indicated by reduction in maximum positive and negative velocities. A lower volume of air is exchanged with the above-roof flow and thus lesser pollutants are dispersed out and away from the canyon.

Between the two porosities, the densely packed ($\lambda = 200 \text{ m}^{-1}$) tree crown circulation bubble is slightly weaker than that of the loosely packed model ($\lambda = 80 \text{ m}^{-1}$) resulting in small increases in concentration levels, as opposed to the significant differences found between tree-free and tree-lined canyons.

Referring back to Figure 7.9, which compares WT data to LES results, it can be seen that for all three cases LES reproduces agreeable predictions and resonate a consistency that is absent in RANS.

This study clearly demonstrates that the in-canyon air quality can be considerably altered by the presence of trees, and recommends that trees should not be ignored during the urban planning stage. In addition, LES investigations can provide useful suggestions for the assessment, planning and implementation of air pollution exposure mitigation in street canyons lined with trees.

A wider street canyon with two rows of trees is preferable in comparison to a narrower street canyon with one row of trees. Wider streets, whether lined with trees or empty, encourages improved air circulation and ventilation resulting in less pollutants getting trapped at pedestrian level.

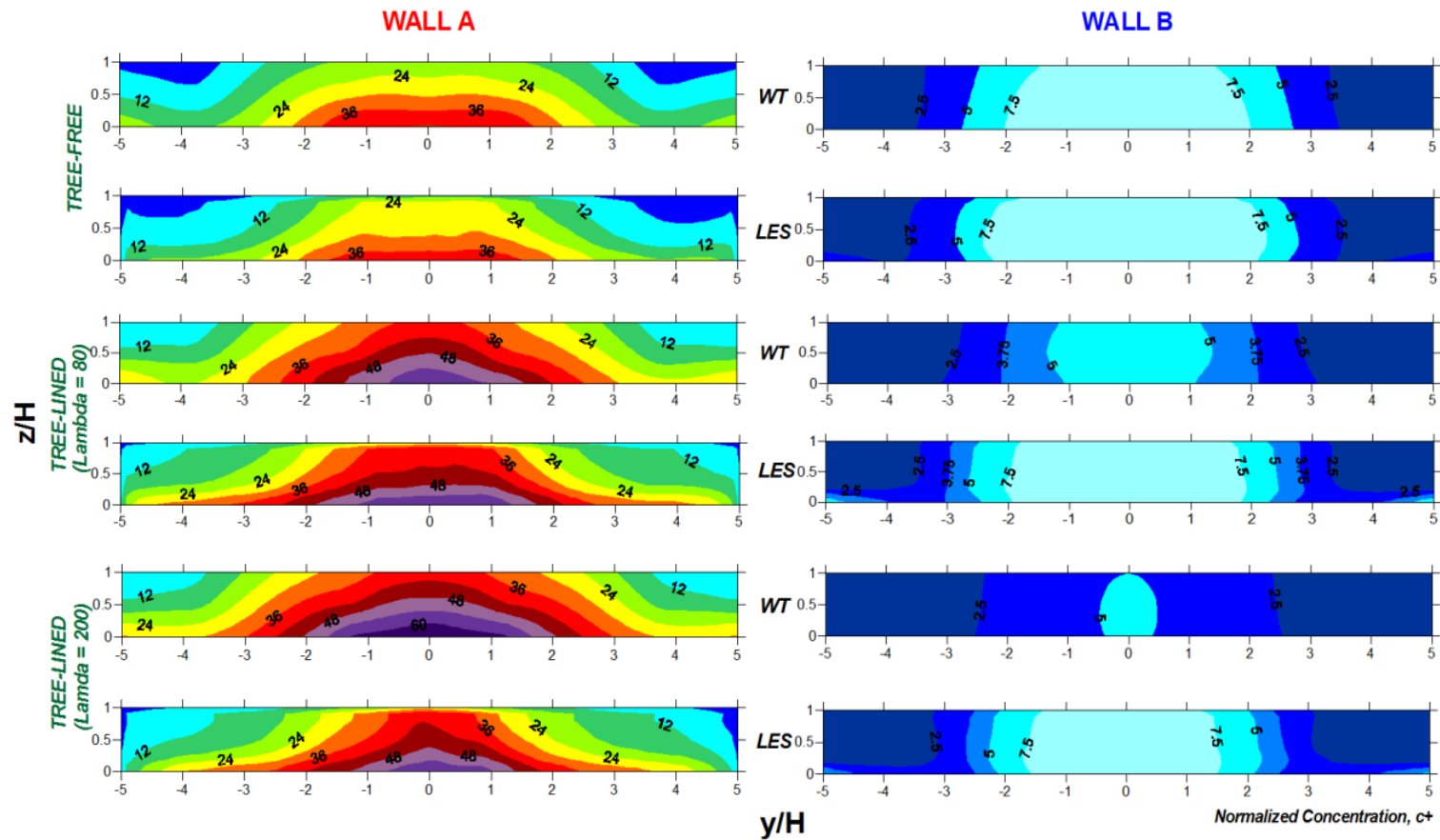


Figure 7.9 Mean normalised concentration data on Wall A (leeward) and Wall B (windward) comparing tree-free to tree-lined canyons, for WT and LES time-averaged results ($W/H = 1$)

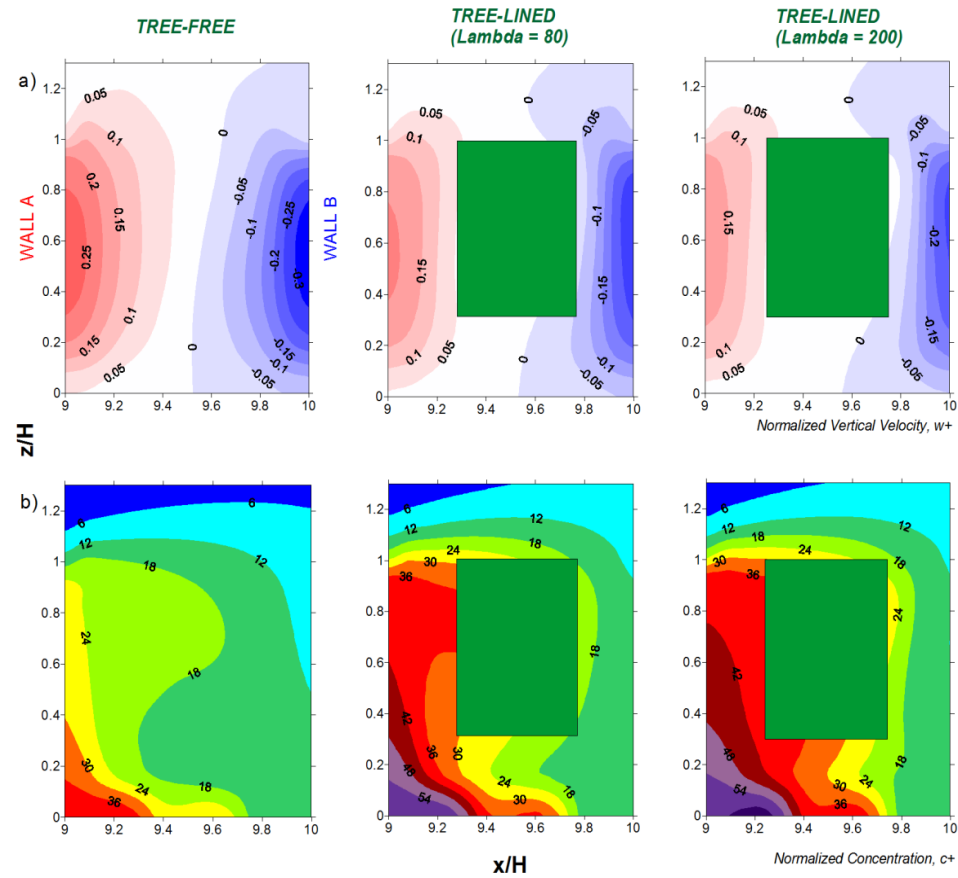


Figure 7.10 Mean normalised vertical velocity contours, w^+ and b) corresponding mean normalised concentration contours, C^+ at mid plane of the canyon ($y/H = 0$ from $x/H = 9$ to 10) obtained using LES comparing tree-free to tree-lined canyons ($W/H = 1$)

7.5 Conclusion

The widely employed RANS turbulence models produce numerical predictions of qualitative agreement to experimental results but at varying degree of accuracy for different measurement locations and tree crown porosities. RANS models are not capable of quantitatively reciprocating the solutions of complex flow structures.

LES significantly improves airflow and pollutant dispersion predictions, reproducing accurate and more reliable results as opposed to RANS. This is because LES resolves the intermittent and unsteady fluctuations of the flow field, allowing the transient mixing to be properly accounted for.

LES also provides important information on the instantaneous fluctuations and thus are more suitable than RANS for situations where detailed predictions are required.

Another important conclusion that can be drawn from this study is that the presences of other large obstacles, such as trees, considerably alter the flow and pollutant concentration field and, therefore, should not be excluded in conventional CFD simulations of urban systems.

Trees obstruct airflow, reducing air exchange with above-roof flows and consequently lesser pollutants are dispersed out of the canyon. It should, however, be noted that only the aerodynamic effects of trees have been taken into consideration, and not biological factors. Other obstacles such as rows of parked cars are expected to alter the flow mechanism and pollutant dispersion processes in urban street canyons, and are left for future investigations.

8 CONCLUSIONS

CFD simulations are performed for the study of airflow and pollutant dispersion within two street canyon configurations of $W/H = 1$ and $W/H = 2$, with a perpendicular approach flow in order to compare numerical results against WT experimental measurements.

LES is shown to improve predictions over previously employed steady-state RANS numerical investigations, which overpredicted pollutant concentration levels.

In addition, the aerodynamic impacts of trees on pollutant concentration levels at pedestrian level are investigated by evaluating between tree-free and tree-lined canyons. Two crown porosities are examined for $P_{vol} = 97.5\%$ and $P_{vol} = 96\%$, corresponding to pressure loss coefficients, $\lambda = 80 \text{ m}^{-1}$ and $\lambda = 200 \text{ m}^{-1}$, respectively, with single row of tree planting for $W/H = 1$ and two rows of tree planting for $W/H = 2$.

The overall conclusions of the work undertaken in the present research project are summarized here. This is followed by an outline of what should be done in future studies.

8.1 Numerical Approach

LES resolves the unsteady fluctuations of flow and pollutant concentration fields, generating accurate and reliable results when compared to RANS models. The in-canyon air circulation is properly accounted for by LES, reproducing the correct pollutant concentration levels similar to wind tunnel experimental measurements.

URANS, albeit solving for unsteadiness was incapable of capturing the internally induced fluctuations of the flow field, and thus failed to reproduce the instantaneous flow field as opposed to LES.

Between the two RANS models investigated, RSM outperforms standard $k-\varepsilon$ due to the ability of the former model to resolve for each and every component

of the Reynolds stresses, unlike standard $k-\varepsilon$ which assumes the stresses to be isotropic.

LES superior performance is due to the fact that it resolves both the internally and externally induced fluctuations, allowing the transient mixing within street canyons to be properly accounted for. This reproduces enhanced numerical predictions of the horizontal diffusion of pollutants.

LES also provides important information on the instantaneous fluctuations and thus are more fitting than RANS for situations where detailed predictions are required, such as in the case of modelling the deliberate or accidental release of hazardous airborne materials

It should however be noted that the improvements obtained by LES comes with a price, costing ten folds the computational effort of RSM and twice more compared to standard $k-\varepsilon$.

It should be appreciated that WT measurement data were used as a benchmark to compare the two different numerical approaches, and are not to be taken as completely accurate. Experimental errors could have affected the accuracy. One noticeable example are the measuring taps which were of significant size thus introducing roughness on the building walls which could have further altered the flow and concentration fields, albeit slightly.

8.2 Wall y^+ Approach

The wall y^+ approach provides suitable guidance for the selection of an appropriate mesh configuration in any generic study dealing with wall-bounded turbulent flows.

The wall y^+ approach is implemented in the present study investigating the effects of trees on pollution dispersion in urban areas, allowing for the best mesh resolution to be picked. A wall $y^+ > 30$ resolving the log-law region is deemed sufficient for the viscous models employed, ensuring a compromise between computational cost and numerical accuracy.

It is reiterated that a finer mesh, resolving all the way into the viscous sublayer ($y^+ < 5$) does not necessarily improve precision, although the computational effort is avoidably increased.

8.3 Wall Roughness

Blocken et al. (2007a, 2007b) suggest that it is important to account for wall roughness effects in order to achieve horizontal homogeneity in simulations of atmospheric turbulent boundary layer flows. The horizontal homogeneity is verified in the present study when appropriately accounting for the wall roughness.

At the same time it is shown that effects of wall roughness are insignificant for built-up computational domains as the macro-roughness (buildings, trees, etc) overwhelm the minor effects of the micro-roughness (wall roughness), due to the large Reynolds number of the main flow and the domination of the large-scale eddies within the canyon.

8.4 Aerodynamic Effects of Trees

In the presence of trees, reduced in-canyon velocities and increased wall pollutant concentration levels are observed when compared to tree-free canyons. The increase of pedestrian level pollutant concentration levels are a result of the added blockage effect introduced by the trees which further alters the flow field, thus reducing the in-canyon circulation strength. This results in lesser pollutants being dispersed out of the canyon and diluted with the above-roof airflow.

In previous numerical studies (Gromke et al., 2008, Buccolieri et al., 2009, Balczó et al., 2009), although similar observations were observed, there was an overprediction of pollutant concentration levels due to underprediction of flow circulation as a consequence of employing the steady-state RANS turbulence models.

In the present study, LES is shown to overcome this overprediction in concentration levels by accurately reproducing the pollutant concentration levels similar to WT experimental data.

Another conclusion that can be drawn from the study is that it is important to account for the presence of other large obstacles such as trees in urban airflow problems, in order to obtain 'realistic' results. This implies that trees should not be ignored in conventional numerical simulations of real urban studies as they significantly alter the airflow and pollutant dispersion.

8.5 Influence of Tree Crown Porosity

Two crown porosities ($\lambda = 80 \text{ m}^{-1}$ and $\lambda = 200 \text{ m}^{-1}$) were compared for both $W/H = 1$ and $W/H = 2$, and the results indicated that the crown porosity did not significantly affect the flow and concentration fields. The concentration levels changes were negligible between the two porosities examined as opposed to the significant differences found between tree-free and tree-lined canyons.

8.6 Street Canyon Aspect Ratio

In both the tree-free and tree-lined street canyons, having a larger street width to height ratio is desirable in order to promote air ventilation and circulation and reduce the amount of pollutants trapped at street-level.

In this study, it is shown that having a wider canyon, $W/H = 2$ is preferable to a narrower street of $W/H = 1$, whether trees are planted or not within the canyons. This is true for a perpendicular wind flow direction investigated in the present work, which literature (Vardoulakis et al., 2003, Ahmad et al., 2005, Li et al., 2006) has identified as resulting in the most critical pollutant accumulation in urban street canyons.

8.7 Direction of Future Research

It has been ascertained that LES resolves the unsteady fluctuations of the flow and concentration fields within urban street canyons, generating accurate results similar to WT experimental data.

The presence of trees in street canyons has been demonstrated to significantly alter these processes and it is recommended that they should be appropriately accounted for in order to achieve reliable numerical results.

This study has significantly contributed to the body of research on airflow and pollution dispersion in urban street canyons, but many questions still remain unanswered. For example, the pollutants were assumed inert and the biological impacts of trees were not taken into account in the investigation. In reality, trees can interact with air and pollutants in many other ways such as particle deposition (and re-suspension), chemical reaction, emission of ozone, altering of micro-climate, to name a few.

In light of these findings, the investigation can be extended to cover other factors in order to establish better understanding of urban airflows and remedy ways to mitigate air pollution problem in built up areas. The local climate and city morphology of a particular region of interest can be incorporated. In addition, biological factors such as ozone emission and its contribution to the total pollutant level should be considered. This would also require further field and WT measurements to complement numerical investigations.

Detailed investigations on realistic tree geometries with various characteristics and planting arrangements should be performed in order to establish a series of benchmark simulations encompassing the influence of trees on airflow, temperature distribution and pollutant dispersion process in urban street canyons.

In addition, fluctuating winds with varying directions should also be studied including their influence on different street configurations, tree planting arrangements and canyon aspect ratios.

The simulations could also investigate moving traffic and buoyancy effects due to thermal stratification as a result of urban heat island formations, amongst others. These factors further alter the turbulent structures within the street canyons, consequently modifying the airflow and pollutant dispersion.

The generated benchmark data can be used to enhance existing or develop new CFD models to be used for operational purposes by policy makers and urban planners.

REFERENCES

- Ahmad, K., Khare, M. & Chaudhry, K. K. (2005) Wind tunnel simulation studies on dispersion at urban street canyons and intersections--a review. *Journal of Wind Engineering and Industrial Aerodynamics*, 93, 697-717.
- Anderson, J. D. & Wendt, J. F. (2009) *Computational Fluid Dynamics*, Von Karman Institute.
- Ariff, M., Salim, S. M. & Cheah, S. C. (2009a) Wall y^+ approach for dealing with turbulent flows over a surface mounted cube: Part 1 - low Reynolds number. *7th International Conference on CFD in the Mineral and Process Industries*. Melbourne, CSIRO.
- Ariff, M., Salim, S. M. & Cheah, S. C. (2009b) Wall y^+ approach for dealing with turbulent flows over a surface mounted cube: Part 2 - high Reynolds number. *7th International Conference on CFD in the Mineral and Process Industries*. Melbourne, CSIRO.
- Assimakopoulos, V. D., ApSimon, H. M. & Moussiopoulos, N. (2003) A numerical study of atmospheric pollutant dispersion in different two-dimensional street canyon configurations. *Atmospheric Environment*, 37, 4037-4049.
- Baik, J. J. & Kim, J. J. (1999) A numerical study of flow and pollutant dispersion characteristics in urban street canyons. *Journal of Applied Meteorology*, 38, 1576-1589.
- Balczó, M., Gromke, C. & Ruck, B. (2009) Numerical modeling of flow and pollutant dispersion in street canyons with tree planting. *Meteorologische Zeitschrift*, 18, 197-206.
- Bhaskaran, R. & Collins, L. (2002) *Introductions to CFD Basics*. New York, Cornell University.

- Blackadar, A. K. (1962) The Vertical Distribution of Wind and Turbulent Exchange in a Neutral Atmosphere. *J. Geophys. Res.*, 67.
- Blocken, B., Carmeliet, J. & Stathopoulos, T. (2007a) CFD evaluation of wind speed conditions in passages between parallel buildings-effect of wall-function roughness modifications for the atmospheric boundary layer flow. *Journal of Wind Engineering and Industrial Aerodynamics*, 95, 941-962.
- Blocken, B., Stathopoulos, T. & Carmeliet, J. (2007b) CFD simulation of the atmospheric boundary layer: wall function problems. *Atmospheric Environment*, 41, 238-252.
- Blocken, B., Stathopoulos, T., Saathoff, P. & Wang, X. (2008) Numerical evaluation of pollutant dispersion in the built environment: Comparisons between models and experiments. *Journal of Wind Engineering and Industrial Aerodynamics*, 96, 1817-1831.
- Britter, R. & Schatzmann, M. (2007) Background and justification document to support the model evaluation guidance and protocol. COST Action 732.
- Britter, R. E. & Hanna, S. R. (2003) Flow and dispersion in urban areas. *Annual Review of Fluid Mechanics*, 35, 469-496.
- Buccolieri, R., Gromke, C., Di Sabatino, S. & Ruck, B. (2009) Aerodynamic effects of trees on pollutant concentration in street canyons. *Science of The Total Environment*, 407, 5247-5256.
- Buccolieri, R., Salim, S. M., Leo, L. S., Di Sabatino, S., Chan, A., Ielpo, P., de Gennaro, G. & Gromke, C. (2011) Analysis of local scale tree-atmosphere interaction on pollutant concentration in idealized street canyons and application to a real urban junction. *Atmospheric Environment*, 45, 1702-1713.

- Cai, X. M., Barlow, J. F. & Belcher, S. E. (2008) Dispersion and transfer of passive scalars in and above street canyons--Large-eddy simulations. *Atmospheric Environment*, 42, 5885-5895.
- Cebeci, T. & Smith, A. M. O. (1974) *Analysis of Turbulent Boundary Layers*, New York, Academic Press.
- Chan, T. L., Dong, G., Leung, C. W., Cheung, C. S. & Hung, W. T. (2002) Validation of a two-dimensional pollutant dispersion model in an isolated street canyon. *Atmospheric Environment*, 36, 861-872.
- Chang, C.-H. & Meroney, R. N. (2003) Concentration and flow distributions in urban street canyons: wind tunnel and computational data. *Journal of Wind Engineering and Industrial Aerodynamics*, 91, 1141-1154.
- Chang, C. H. (2006) Computational fluid dynamics simulation of concentration distributions from a point source in the urban street canyons. *Journal of Aerospace Engineering*, 19, 80-86.
- Cheng, Y., Lien, F. S., Yee, E. & Sinclair, R. (2003) A comparison of large Eddy simulations with a standard k- ϵ Reynolds-averaged Navier-Stokes model for the prediction of a fully developed turbulent flow over a matrix of cubes. *Journal of Wind Engineering and Industrial Aerodynamics*, 91, 1301-1328.
- Chung, T. J. (2002) *Computational Fluid Dynamics*, Cambridge, Cambridge University Press.
- CODASC (2008) Concentration Data of Street Canyons. Laboratory of Building- and Environmental Aerodynamics, IfH, Karlsruhe Institute of Technology.
- Coder, R. D. (1996) Identified Benefits of Community Trees and Forests. University of Georgia.
- COST (2005-2009) Quality Assurance and Improvement of Micro-Scale Meteorological Models. Hamburg.

- Di Sabatino, S., Buccolieri, R., Pulvirenti, B. & Britter, R. (2008) Flow and Pollutant Dispersion in Street Canyons using FLUENT and ADMS-Urban. *Environmental Modeling and Assessment*, 13, 369-381.
- Eliasson, I., Offerle, B., Grimmond, C. S. B. & Lindqvist, S. (2006) Wind fields and turbulence statistics in an urban street canyon. *Atmospheric Environment*, 40, 1-16.
- Ferziger, J. H. (1993) Simulation of complex turbulent flows: Recent advances and prospects in wind engineering. *Computational Wind Engineering*, 1.
- FLUENT (2005a) FLUENT 6.3 Documentation. Lebanon.
- FLUENT (2005b) Overview of Turbulence Modeling. Fluent User Services Centre: Advanced Fluent Training.
- Gao, Y. & Chow, W. K. (2005) Numerical studies on air flow around a cube. *Journal of Wind Engineering and Industrial Aerodynamics*, 93, 115-135.
- Gayev, Y. A. & Savory, E. (1999) Influence of street obstructions on flow processes within urban canyons. *Journal of Wind Engineering and Industrial Aerodynamics*, 82, 89-103.
- Gerdes, F. & Olivari, D. (1999) Analysis of pollutant dispersion in an urban street canyon. *Journal of Wind Engineering and Industrial Aerodynamics*, 82, 105-124.
- Germano, M., Piomelli, U., Moin, P. & Cabot, W. H. (1991) A dynamic subgrid-scale eddy viscosity model. *Physics of Fluids A*, 3, 1760-1765.
- Gromke, C., Buccolieri, R., Di Sabatino, S. & Ruck, B. (2008) Dispersion study in a street canyon with tree planting by means of wind tunnel and numerical investigations - Evaluation of CFD data with experimental data. *Atmospheric Environment*, 42, 8640-8650.

- Gromke, C., Denev, J. & Ruck, B. (2007) Dispersion of traffic exhausts in urban street canyons with tree plantings - Experimental and numerical investigations. *Int workshop on physical modeling of low and dispersion phenomena PHYSMOD 2007*. Orléans, France.
- Gromke, C. & Ruck, B. (2005) Die Simulation atmosphärischer Grenzschichten in Windkanälen. *13th GALA Fachtagung Lasermethoden in der Strömungsmechanik*. German Association for Laser Anemometry.
- Gromke, C. & Ruck, B. (2007) Influence of trees on the dispersion of pollutants in an urban street canyon-Experimental investigation of the flow and concentration field. *Atmospheric Environment*, 41, 3287-3302.
- Gromke, C. & Ruck, B. (2009) On the Impact of Trees on Dispersion Processes of Traffic Emissions in Street Canyons. *Boundary-Layer Meteorology*, 131, 19-34.
- Gross, G. (1987) A numerical study of the air flow within and around a single tree. *Boundary-Layer Meteorology*, 40, 311-327.
- Gross, G. (1997) ASMUS - A numerical model for simulations of wind and pollutant dispersion around individual buildings. Part II: Dispersion modelling and applications. *ASMUS - Ein numerisches Modell zur Berechnung der Strömung und der Schadstoffverteilung im Bereich einzelner Gebäude. II: Schadstoffausbreitung und Anwendung*, 6, 130-136.
- Hanna, S. R., Tehranian, S., Carissimo, B., Macdonald, R. W. & Lohner, R. (2002) Comparisons of model simulations with observations of mean flow and turbulence within simple obstacle arrays. *Atmospheric Environment*, 36, 5067-5079.
- Hinze, J. O. (1975) *Turbulence*, McGraw-Hill Companies.

- Hsieh, K.-J., Lien, F.-S. & Yee, E. (2007) Numerical modeling of passive scalar dispersion in an urban canopy layer. *Journal of Wind Engineering and Industrial Aerodynamics*, 95, 1611-1636.
- Hussein, H. J. & Martinuzzi, R. J. (1996) Energy balance for turbulent flow around a surface mounted cube placed in a channel. *Physics of Fluids*, 8, 764-780.
- Iaccarino, G., Ooi, A., Durbin, P. A. & Behnia, M. (2003) Reynolds averaged simulation of unsteady separated flow. *International Journal of Heat and Fluid Flow*, 24, 147-156.
- Kastner-Klein, P., Fedorovich, E. & Rotach, M. W. (2001) A wind tunnel study of organised and turbulent air motions in urban street canyons. *Journal of Wind Engineering and Industrial Aerodynamics*, 89, 849-861.
- Kastner-Klein, P. & Plate, E. J. (1999) Wind-tunnel study of concentration fields in street canyons. *Atmospheric Environment*, 33, 3973-3979.
- Kim, S. E. (2004) Large eddy simulation using unstructured meshes and dynamic subgrid-scale turbulence models. *34th AIAA Fluid Dynamics Conference and Exhibit*. Oregon, USA.
- Kolmogorov, A. N. (1941) local structure of turbulence in an incompressible fluid at very high Reynolds numbers. *Proceedings of the USSR Academy of Sciences*.
- Lakehal, D. & Rodi, W. (1997) Calculation of the flow past a surface mounted cube with 2 layer turbulence models. *J. Wind Eng. Aerodyn.*, 67-68, 66-78.
- Letzel, M. O., Krane, M. & Raasch, S. (2008) High resolution urban large-eddy simulation studies from street canyon to neighbourhood scale. *Atmospheric Environment*, 42, 8770-8784.

- Li, X.-X., Liu, C.-H. & Leung, D. Y. C. (2009) Numerical investigation of pollutant transport characteristics inside deep urban street canyons. *Atmospheric Environment*, 43, 2410-2418.
- Li, X. X., Liu, C. H., Leung, D. Y. C. & Lam, K. M. (2006) Recent progress in CFD modelling of wind field and pollutant transport in street canyons. *Atmospheric Environment*, 40, 5640-5658.
- Li, Y. & Stathopoulos, T. (1997) Numerical evaluation of wind-induced dispersion of pollutants around a building. *Journal of Wind Engineering and Industrial Aerodynamics*, 67-68, 757-766.
- Lilly, D. K. (1992) A proposed modification of the Germano subgrid-scale closure method. *Physics of Fluids A: Fluid Dynamics*, 4, 633-635.
- Louka, P., Belcher, S. E. & Harrison, R. G. (2000) Coupling between air flow in streets and the well-developed boundary layer aloft. *Atmospheric Environment*, 34, 2613-2621.
- Martinuzzi, R. & Tropea, C. (1993) Flow around surface-mounted, prismatic obstacles placed in a fully developed channel flow. *Journal of Fluids Engineering, Transactions of the ASME*, 115, 85-92.
- Meinders, E. R. & Hanjalić, K. (2002) Experimental study of the convective heat transfer from in-line and staggered configurations of two wall-mounted cubes. *International Journal of Heat and Mass Transfer*, 45, 465-482.
- Meinders, E. R., Hanjalić, K. & Martinuzzi, R. (1991) Experimental study of the local convective heat transfer from a wall mounted cube in turbulent channel flow. *Trans ASME J. Heat Transfer*, 113, 564-573.
- Meroney, R. N., Pavageau, M., Rafailidis, S. & Schatzmann, M. (1996) Study of line source characteristics for 2-D physical modelling of pollutant dispersion in street canyons. *Journal of Wind Engineering and Industrial Aerodynamics*, 62, 37-56.

- Mochida, A. & Lun, I. Y. F. (2008) Prediction of wind environment and thermal comfort at pedestrian level in urban area. *Journal of Wind Engineering and Industrial Aerodynamics*, 96, 1498-1527.
- Mochida, A., Tabata, Y., Iwata, T. & Yoshino, H. (2008) Examining tree canopy models for CFD prediction of wind environment at pedestrian level. *Journal of Wind Engineering and Industrial Aerodynamics*, 96, 1667-1677.
- N. Meroney, R., Leitl, B. M., Rafailidis, S. & Schatzmann, M. (1999) Wind-tunnel and numerical modeling of flow and dispersion about several building shapes. *Journal of Wind Engineering and Industrial Aerodynamics*, 81, 333-345.
- Pavageau, M. & Schatzmann, M. (1999) Wind tunnel measurements of concentration fluctuations in an urban street canyon. *Atmospheric Environment*, 33, 3961-3971.
- Pope, S. B. (2005) *Turbulent Flows*, New York, Cambridge University Press.
- Price, C. (2003) Quantifying the aesthetic benefits of urban forestry. *Urban Forestry & Urban Greening*, 1, 123-133.
- Richardson, L. F. (1922) *Weather Prediction by Numerical Process*, Cambridge, Cambridge University Press.
- Ries, K. & Eichhorn, J. (2001) Simulation of effects of vegetation on the dispersion of pollutants in street canyons. *Meteorologische Zeitschrift*, 10, 229-233.
- Rodi, W. (1997) Comparison of LES and RANS calculations of the flow around bluff bodies. *Journal of Wind Engineering and Industrial Aerodynamics*, 69-71, 55-75.
- Rossi, R. & Iaccarino, G. (2009) Numerical simulation of scalar dispersion downstream of a square obstacle using gradient-transport type models. *Atmospheric Environment*, 43, 2518-2531.

- Ruck, B. & Schmitt, F. (1986) Flow profile of single-tree boundary flow - Estimate of deposition probabilities for very fine droplets. *Forstwissenschaftliches Centralblatt*, 105, 178-196.
- Salim, S. M., Ariff, M. & Cheah, S. C. (2010) Wall y^+ approach for dealing with turbulent flows over a wall mounted cube. *Progress in Computational Fluid Dynamics*, 10, 341-351.
- Salim, S. M. & Cheah, S. C. (2009) Wall y^+ strategy for dealing with wall-bounded turbulent flows. *Lecture Notes in Engineering and Computer Science*, 2175, 2165-2170.
- Seeta Ratnam, G. & Vengadesan, S. (2008) Performance of two equation turbulence models for prediction of flow and heat transfer over a wall mounted cube. *International Journal of Heat and Mass Transfer*, 51, 2834-2846.
- Shah, K. B. & Ferziger, J. H. (1997) A fluid mechanics view of wind engineering: Large eddy simulation of flow past a cubic obstacle. *Journal of Wind Engineering and Industrial Aerodynamics*, 67-68, 211-224.
- Shi, R. F., Cui, G. X., Wang, Z. S., Xu, C. X. & Zhang, Z. S. (2008) Large eddy simulation of wind field and plume dispersion in building array. *Atmospheric Environment*, 42, 1083-1097.
- Smagorinsky, J. (1963) General Circulation Experiments With The Primitive Equations. *Monthly Weather Review*, 91, 99-164.
- Smirnov, A., Shi, S. & Celik, I. (2001) Random Flow Generation Technique for Large Eddy Simulations and Particle-Dynamics Modeling. *Journal of Fluids Engineering*, 123, 359-371.
- So, E. S. P., Chan, A. T. Y. & Wong, A. Y. T. (2005) Large-eddy simulations of wind flow and pollutant dispersion in a street canyon. *Atmospheric Environment*, 39, 3573-3582.

- Tominaga, Y. & Stathopoulos, T. (2009) Numerical simulation of dispersion around an isolated cubic building: Comparison of various types of k- ϵ models. *Atmospheric Environment*, 43, 3200-3210.
- Tominaga, Y. & Stathopoulos, T. (2010) Numerical simulation of dispersion around an isolated cubic building: Model evaluation of RANS and LES. *Building and Environment*, 45, 2231-2239.
- Tu, J. Y., Yeoh, G. H. & Liu, C. Q. (2008) *Computational Fluid Dynamics: A Practical Approach*, Oxford, Butterworth-Heinemann.
- Vardoulakis, S., Fisher, B. E. A., Pericleous, K. & Gonzalez-Flesca, N. (2003) Modelling air quality in street canyons: A review. *Atmospheric Environment*, 37, 155-182.
- Versteeg, H. K. & Malalasekera, W. (2007) *An Introduction to Computational Fluid Dynamics: The Finite Volume Method*, Harlow, Pearson Education Limited.
- Wilcox, D. C. (2006) *Turbulence Modeling for CFD*, DCW Industries, Incorporated.
- Xie, X., Huang, H. & Wang, J. (2006) The impact of urban street layout on local atmospheric environment. *Building and Environment*, 41, 1352-1363.
- Xie, Z.-T. & Castro, I. P. (2009) Large-eddy simulation for flow and dispersion in urban streets. *Atmospheric Environment*, 43, 2174-2185.
- Yakhot, A., Liu, H. & Nikitin, N. (2006) Turbulent flow around a wall-mounted cube: A direct numerical simulation. *International Journal of Heat and Fluid Flow*, 27, 994-1009.
- Zhou, X. H., Brandle, J. R., Takle, E. S. & Mize, C. W. (2002) Estimation of the three-dimensional aerodynamic structure of a green ash shelterbelt. *Agricultural and Forest Meteorology*, 111, 93-108.

APPENDICES

APPENDIX A – CODASC Database



CODASC
Concentration Data of Street Canyons
 Laboratory of Building- and Environmental Aerodynamics
 Karlsruhe Institute of Technology KIT
[homepage](#)













For whom is CODASC of interest?
 CODASC is addressing scientists working on urban air quality issues. It is of special interest for validation of numerical simulations or experimental investigations.

Where is CODASC from?
 CODASC data is from the [Laboratory of Building- and Environmental Aerodynamics](#) at the Institute for Hydromechanics (IfH) at the University of Karlsruhe/Germany. The Laboratory of Building Aerodynamics runs a number of wind tunnels, among them are several atmospheric boundary layer wind tunnels.

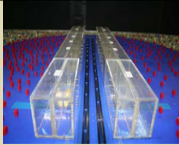
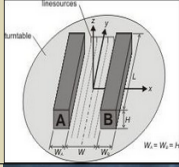
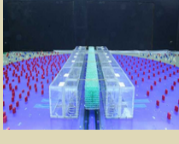
Atmospheric boundary layer wind tunnel: [wind tunnel boundary layer profile](#)

- Home
- Photo Gallery
- Wind Tunnel
- c* Data
- Tree Modeling
- Data Base
- References
- Terms & Conditions

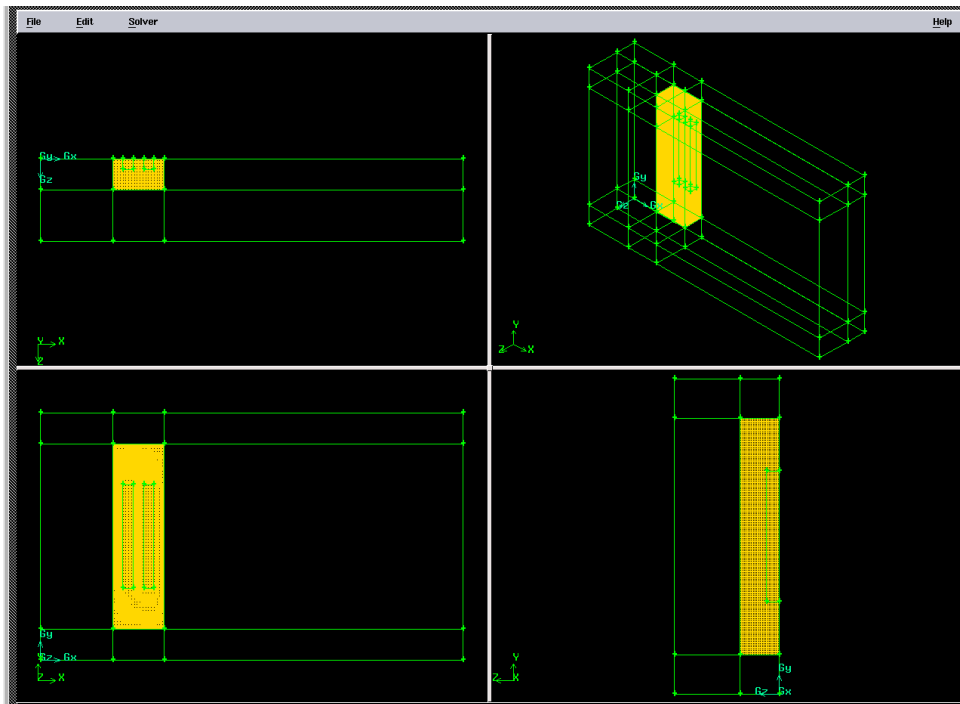
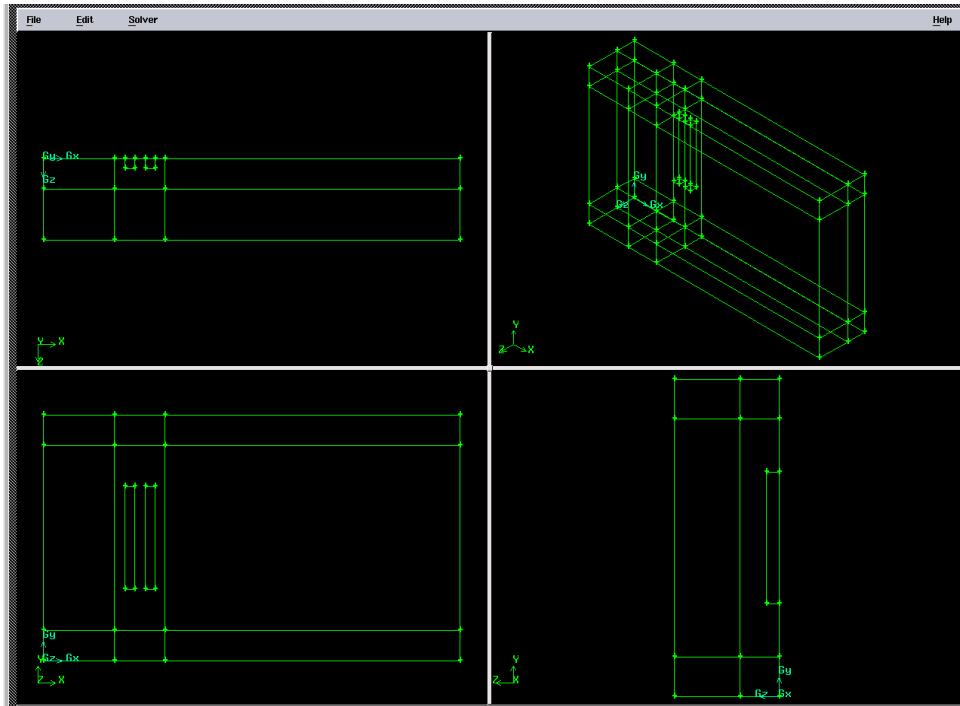
more information:
gromke@ifh.uka.de
ruck@uka.de

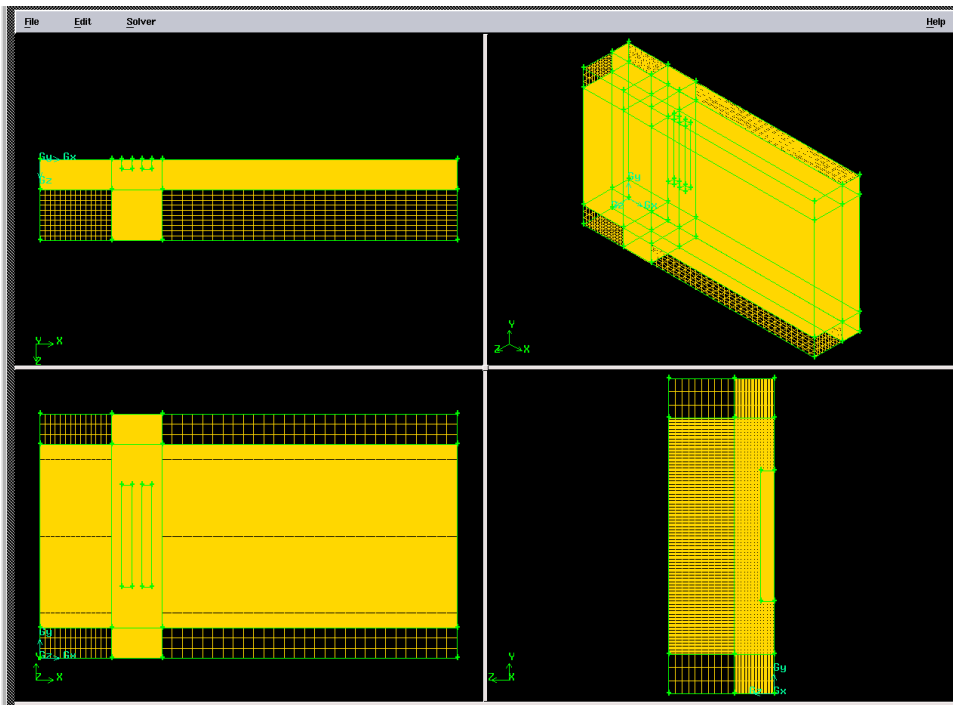
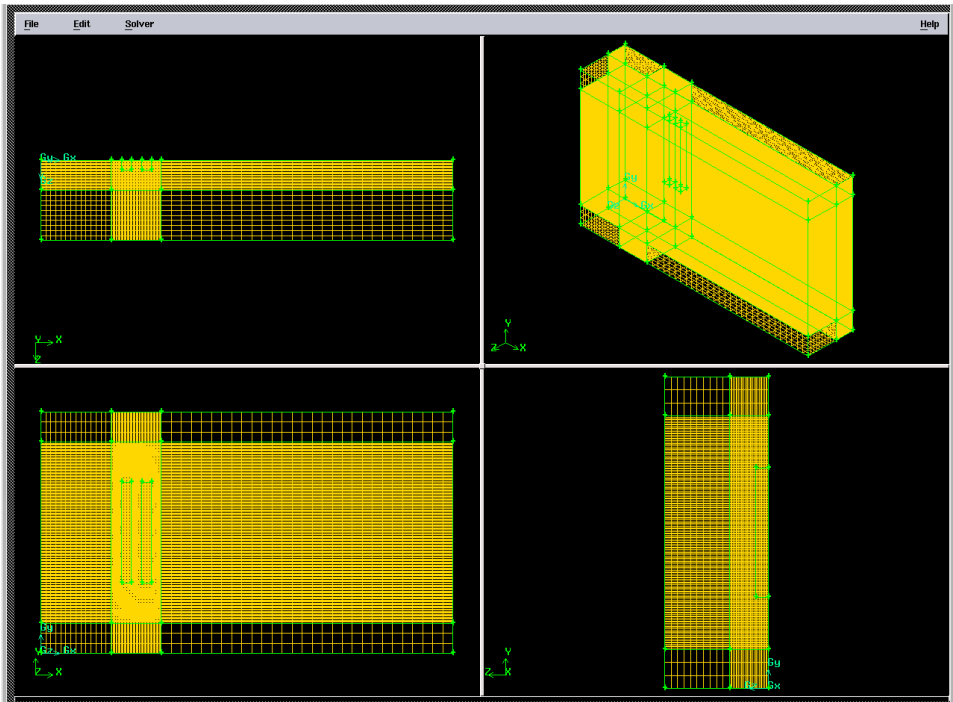
funded by:

 Project: Ru 345/28

$WH = 1$ (aspect ratio: street width W to building height H)	α	TREE PLANTING	normalized concentration data c^* file name = [WH]_[α]_[c_p]_[L]_[wall]	concentration contour plot (300 dpi)	
   (read how to model trees)	90°	tree-free (wind perpendicular to street)	1_90_0.0_000_A.txt 1_90_0.0_000_A.xls 1_90_0.0_000_B.txt 1_90_0.0_000_B.xls	 1_90_0.0_000.jpg	
	45°	tree-free (wind inclined to street)	1_45_0.0_000_A.txt 1_45_0.0_000_A.xls 1_45_0.0_000_B.txt 1_45_0.0_000_B.xls	1_45_0.0_000.jpg	
	0°	tree-free (wind parallel to street)	1_00_0.0_000_A.txt 1_00_0.0_000_A.xls 1_00_0.0_000_B.txt 1_00_0.0_000_B.xls	1_00_0.0_000.jpg	
	90°		stand density dense ($\rho_s = 1$)	1_90_1.0_080_A.txt 1_90_1.0_080_A.xls 1_90_1.0_080_B.txt 1_90_1.0_080_B.xls	1_90_1.0_080.jpg
			crown porosity $P_{Vol} = 97.5\%$ ($\lambda = 80m^{-1}$) $P_{Vol} = 96.0\%$ ($\lambda = 200m^{-1}$) (read how to model trees)	1_90_1.0_200_A.txt 1_90_1.0_200_A.xls 1_90_1.0_200_B.txt 1_90_1.0_200_B.xls	1_90_1.0_200.jpg
			stand density dense ($\rho_s = 1$)	1_45_1.0_080_A.txt 1_45_1.0_080_A.xls 1_45_1.0_080_B.txt 1_45_1.0_080_B.xls	1_45_1.0_080.jpg

APPENDIX B – Mesh Configuration

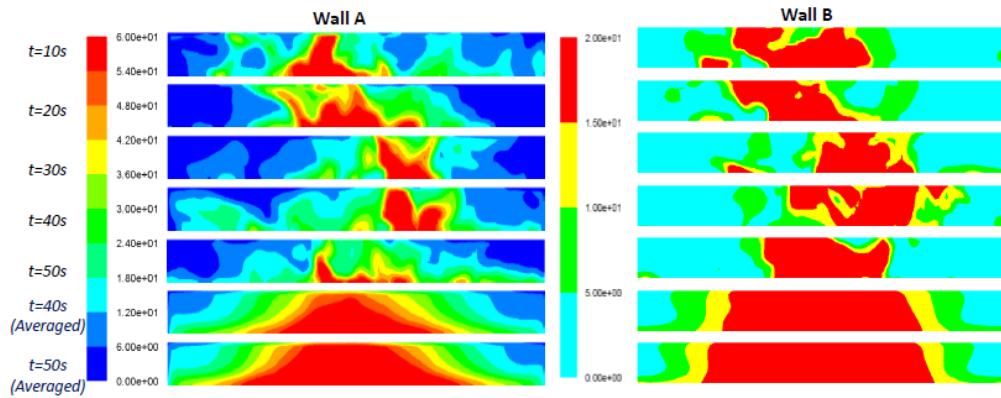




APPENDIX C – Mesh Independence Study

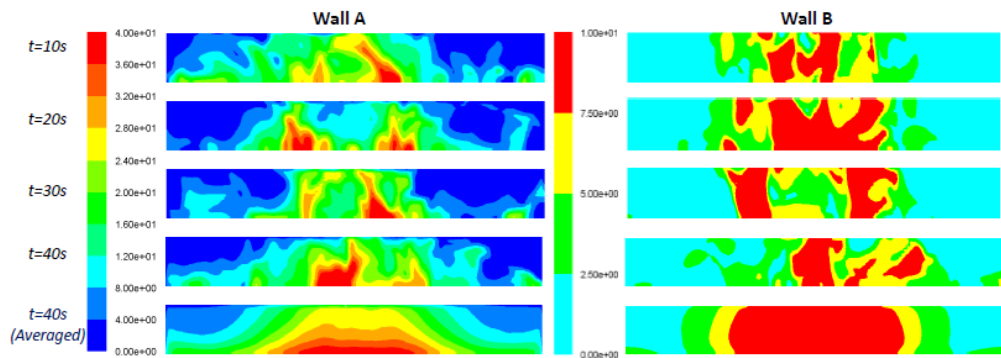
Case A – Empty Street Canyon

0.55 million cells, converged k-ε mean-flow solution, Dynamic Smagorinsky-Lilly LES, Default Sc_v , SIMPLEC, PRESTO, bounded-central differencing: momentum, 2nd order: Energy and SF6.



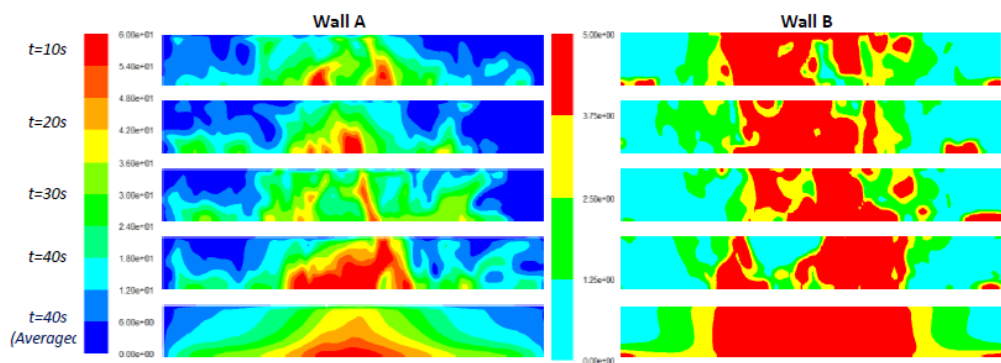
Case B – Empty Street Canyon

1.1 million cells, converged k-ε mean-flow solution, Dynamic Smagorinsky-Lilly LES, Default Sc_v , SIMPLEC, PRESTO, bounded-central differencing: momentum, 2nd order: Energy and SF6.



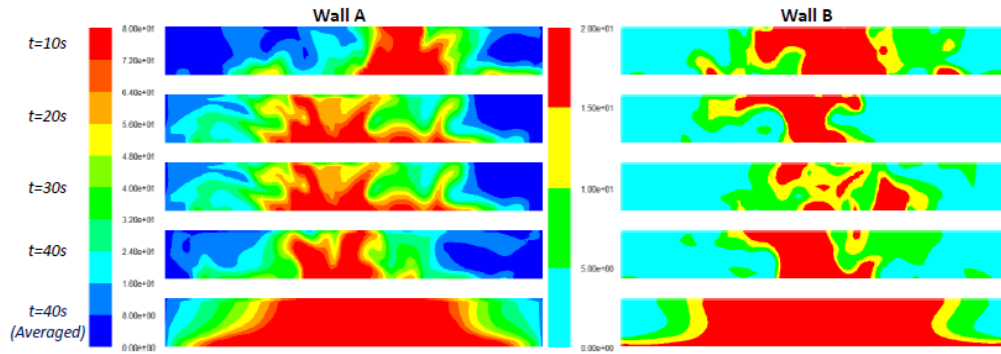
Case C – Tree lined Canyon ($\lambda=200$)

1.1 million cells, converged k-ε mean-flow solution, Dynamic Smagorinsky-Lilly LES, Default Sc_v , SIMPLEC, PRESTO, bounded-central differencing: momentum, 2nd order: Energy and SF6. Porous zone



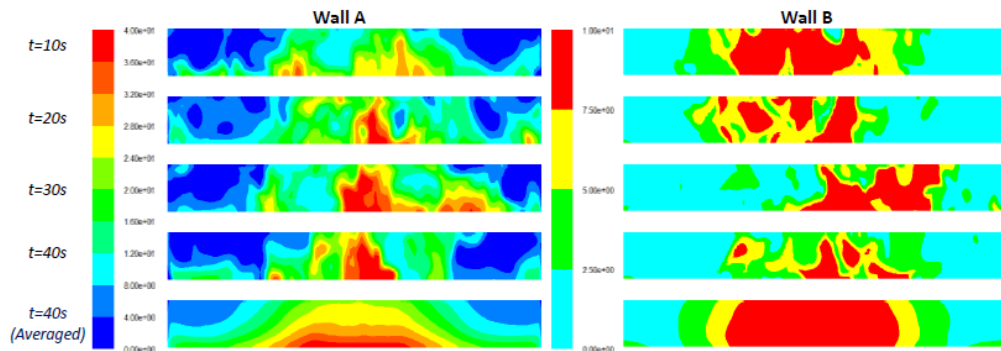
Case D – Tree lined Canyon ($\lambda=200$)

0.55 million cells, converged k- ϵ mean-flow solution, Dynamic Smagorinsky-Lilly LES, Default Sc_v , SIMPLEC, PRESTO, bounded-central differencing: momentum, 2nd order: Energy and SF6. Porous zone



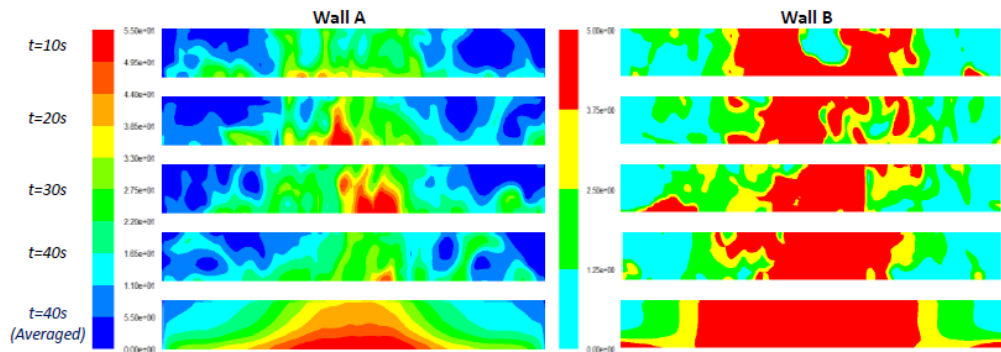
Case E – Empty Street Canyon

1.1 million cells, converged k- ϵ mean-flow solution, Dynamic Smagorinsky-Lilly LES, Default Sc_v , SIMPLEC, PRESTO, bounded-central differencing: momentum, 2nd order: Energy and SF6. Half the time-step (double the temporal resolution)

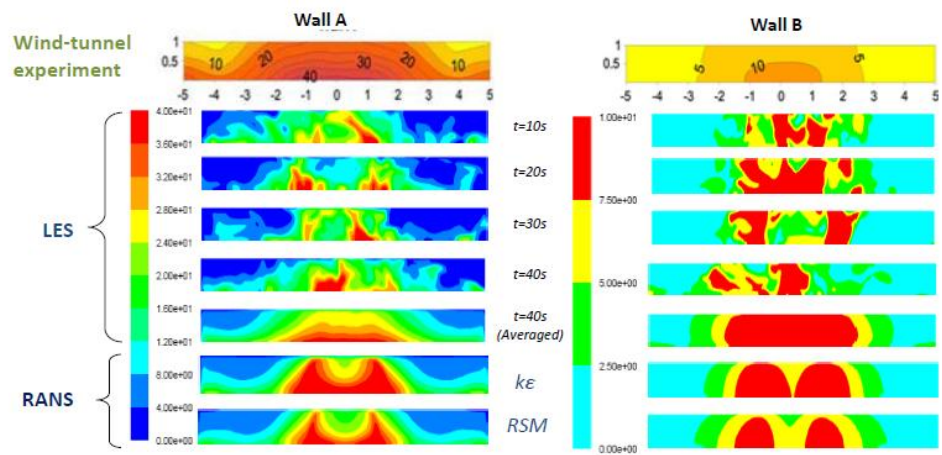


Case F – Tree lined Canyon ($\lambda=80$)

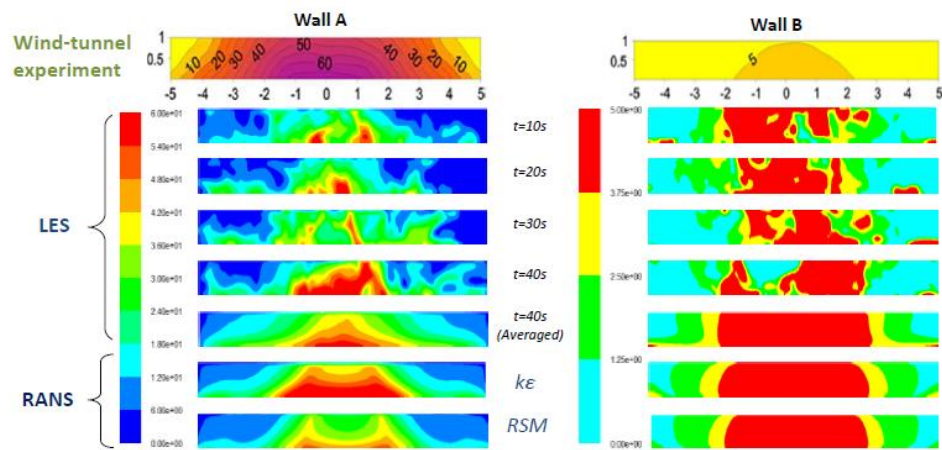
1.1 million cells, converged k- ϵ mean-flow solution, Dynamic Smagorinsky-Lilly LES, Default Sc_v , SIMPLEC, PRESTO, bounded-central differencing: momentum, 2nd order: Energy and SF6. Porous zone



Empty Street Canyon



Tree-lined Canyon ($\lambda=200$)



APPENDIX D – User Defined Function for Inlet Profiles

```
#include "udf.h"
#define ZMIN 0.0
#define ZMAX 0.96
#define UH 4.7
#define UMEAN 7.
#define ALPHA 0.3
#define CMU 0.09
#define USTAR 0.54
#define KCONST 0.23
#define K 0.4
#define ECONST 0.277

DEFINE_PROFILE(x_velocity,t,i)
{
    real z, HB, h, x[ND_ND], uref;
    face_t f;

    h = ZMAX - ZMIN;
    HB = 0.12;
    uref = UH;
    begin_f_loop(f,t)
    {
        F_CENTROID(x,f,t);
        z = x[1];
        if (z <= 0.5)
            F_PROFILE(f,t,i) = uref*pow(z/HB,ALPHA);
        else
            F_PROFILE(f,t,i) = UMEAN;
    }
    end_f_loop(f,t)
}

DEFINE_PROFILE(k_profile,t,i)
{
    real z, del, h, x[ND_ND], u;
    face_t f;

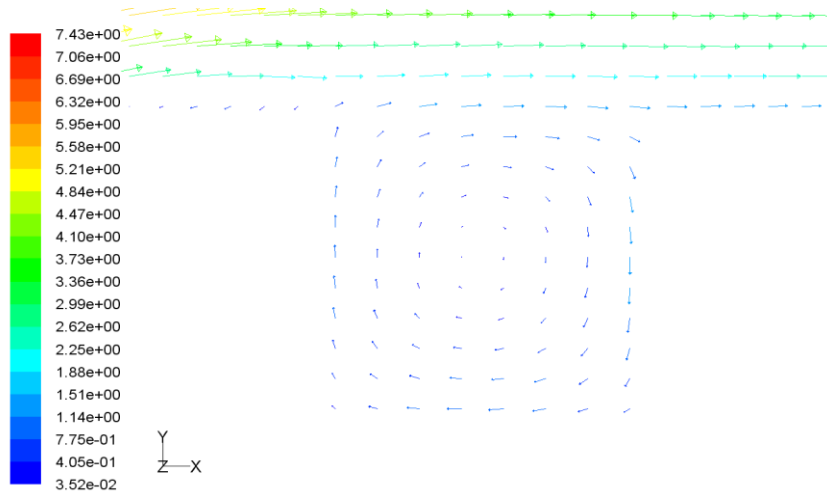
    del = 0.5;
    u = USTAR;
    begin_f_loop(f,t)
    {
        F_CENTROID(x,f,t);
        z = x[1];
        if (z <= 0.37)
            F_PROFILE(f,t,i) = u*u/pow(CMU,0.5)*(1-z/del);
        else
            F_PROFILE(f,t,i) = KCONST;
    }
    end_f_loop(f,t)
}

DEFINE_PROFILE(dissip_profile,t,i)
{
    real z, del, h, x[ND_ND], u;
```

```
face_t f;

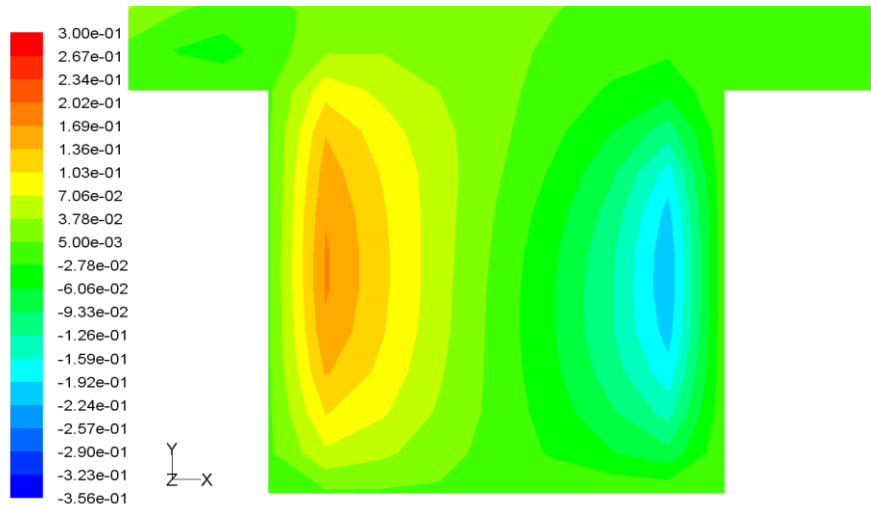
del = 0.5;
u = USTAR;
begin_f_loop(f,t)
{
    F_CENTROID(x,f,t);
    z = x[1];
    if (z <= 0.37)
        F_PROFILE(f,t,i) = u*u*u/(K*z)*(1-z/del);
    else
        F_PROFILE(f,t,i) = ECONST;
}
end_f_loop(f,t)
}
```

APPENDIX E – In-Canyon Velocity Vectors relationship to Velocity Contours



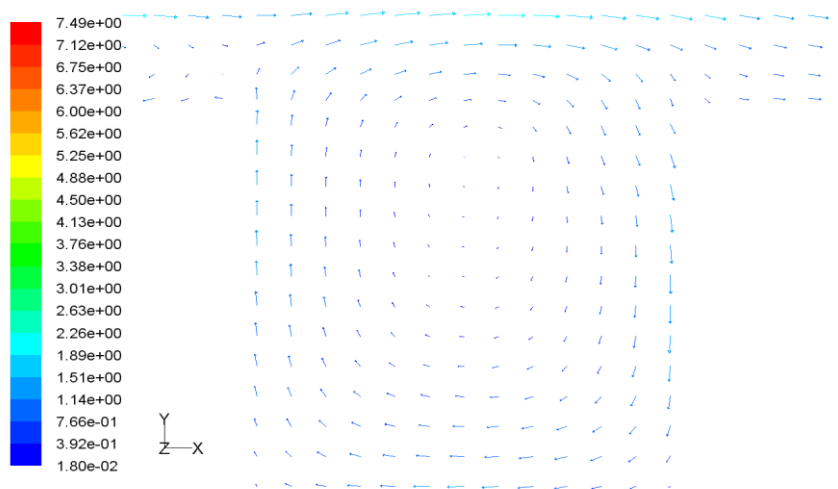
Velocity Vectors Colored By Velocity Magnitude (m/s)

Jun 18, 2009
FLUENT 6.3 (3d, dp, pbns, spe, ske)

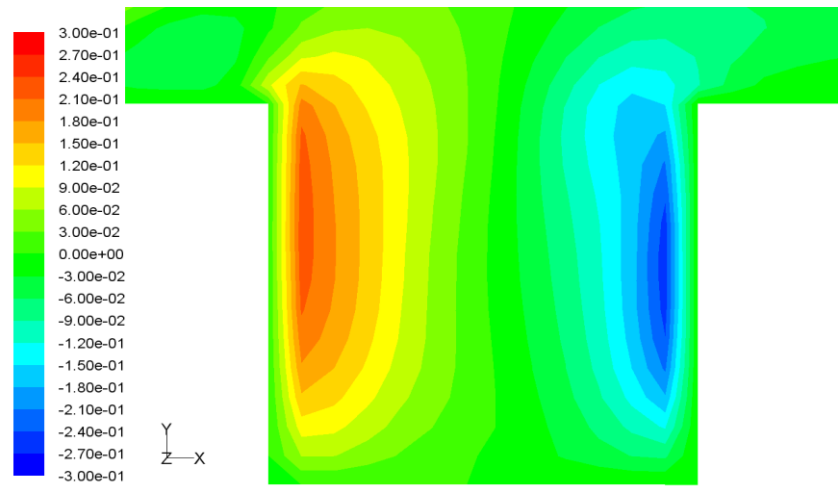


Contours of norm-velocity

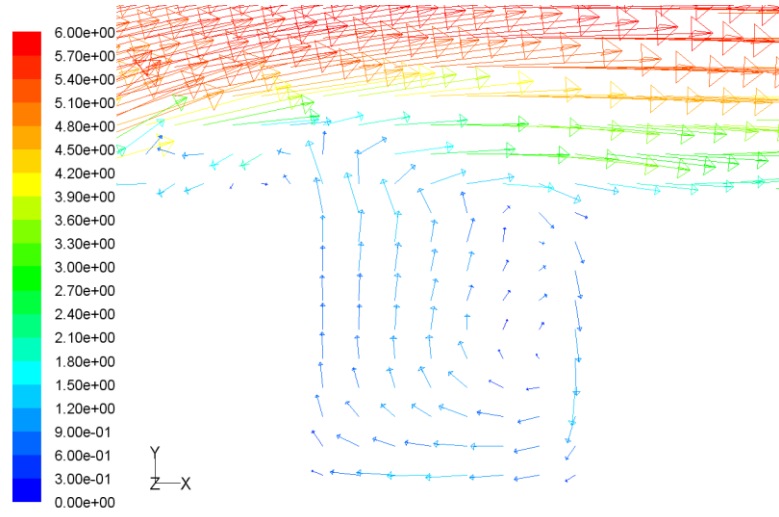
Jun 18, 2009
FLUENT 6.3 (3d, dp, pbns, spe, ske)



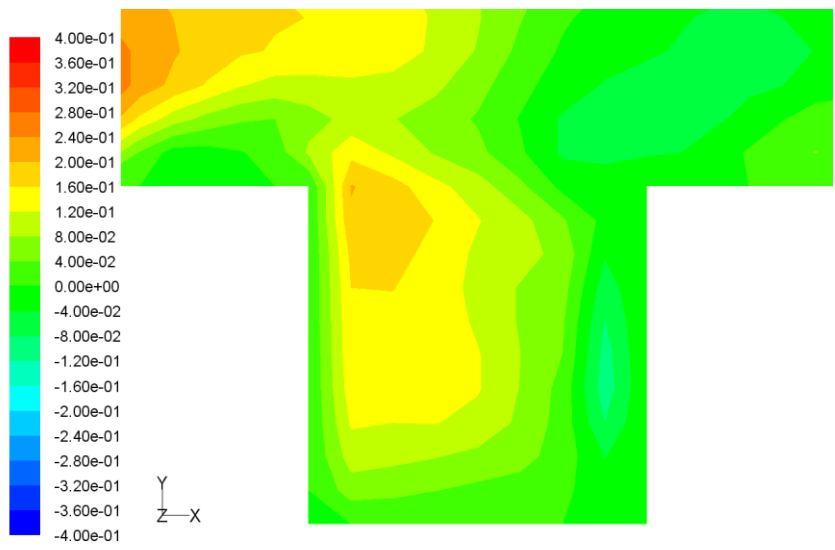
Velocity Vectors Colored By Velocity Magnitude (m/s) Jul 02, 2009
FLUENT 6.3 (3d, dp, pbns, spe, RSM)



Contours of norm-velocity Jul 02, 2009
FLUENT 6.3 (3d, dp, pbns, spe, RSM)



Velocity Vectors Colored By Velocity Magnitude (m/s) (Time=1.5000e+01) Sep 17, 2009
 FLUENT 6.3 (3d, dp, pbns, spe, LES, unsteady)



Contours of norm-velocity (Time=1.5000e+01) Sep 14, 2009
 FLUENT 6.3 (3d, dp, pbns, spe, LES, unsteady)